The Dissertation Committee for Camille R. Brightwell Certifies that this is the approved version of the following dissertation:

Aging Skeletal Muscle Plasticity in Exercise and Injury

Committee:

Christopher S. Fry, PhD, Supervisor, Chair

Stanley J. Watowich, PhD

Andrew Murton, PhD

Craig Porter, PhD

Charlotte A. Peterson, PhD

Aging Skeletal Muscle Plasticity in Exercise and Injury

by

Camille R. Brightwell, B.S., M.S

Dissertation

Presented to the Faculty of the Graduate School of

The University of Texas Medical Branch

in Partial Fulfillment

of the Requirements

for the Degree of

Doctor of Philosophy

The University of Texas Medical Branch

February, 2021

Dedication

This dissertation is dedicated to Benny.

$(-\infty,\infty)$

Acknowledgements

My journey through graduate school has been exciting, challenging, and largely unpredictable. I have learned a great deal and grown not only as a scientist but as a critical thinker; more importantly, I have formed relationships with some of the very best people. During this journey: I changed degree programs, transitioned to a new mentor, switched from a focus predominately on clinical studies to rodent work, moved with the lab from Texas to Kentucky to continue working with the very best mentor, altered my dissertation aims based on changes to institution-associated funding, not only survived but remained productive and continued to collect experimental data and publish throughout the COVID-19 global pandemic, and became pregnant with Ben's and my first child—a precious daughter, Zoe Hope Brightwell, to be born April 2021. My path to a PhD has looked nothing like I imagined when I began, with some difficult and some beautiful changes to original plans. I have been forced to learn flexibility, but any successes I have had are not my own but are shared with an amazing network of supportive people.

My mentor, Chris Fry, is not only an excellent scientist and teacher but is also a kind, thoughtful, and good person. He has been patient with me as I was introduced to many new techniques in his lab and has enabled my work on a myriad of projects outside of these dissertation studies, facilitating my prolific publishing record as a graduate student. In addition to his unwavering support in lab, Chris and his wife, Jean, have been dear friends to Ben and me as we moved away from all our family and friends in Texas. Most

graduate students are not so fortunate to have a mentor like Chris, and many are not blessed with people like the Fry family in their lives; I am so thankful to have been given both.

I'm also grateful to Blake Rasmussen, who allowed me to work on his clinical exercise studies before and during my Master's degree and then offered me a position in his lab, beginning my career as a graduate student in Rehabilitation Sciences at UTMB. Blake has always been supportive of me as a student, and I can confidently say that I would not have been successful in my graduate studies without his guidance and support. He is a kind and generous person with whom I'm grateful to have worked. I'm also thankful to Ted Graber and Maria Maroto in the Rasmussen Lab at UTMB for introducing me to the basics of *in vivo* muscle contractility experiments. Furthermore, I thank each of my committee members in addition to my committee Chair, Chris Fry: Stan Watowich, Andy Murton, Craig Porter, and Charlotte Peterson. Thank you to Stan for including me in multiple NNMT muscle studies; I have been so fortunate to get to know both Stan and Harshini Neelakantan through this work, both of whom are not only great scientists but also wonderful people. Thank you to Andy for the helpful insight you have provided after my TRAM presentations, Cell Biology Graduate Program poster presentations, and Forum on Aging poster presentations at UTMB, which strengthened multiple projects. Thank you to Craig for also providing insightful comments after my TRAM presentations and for setting aside your valuable time to teach me a citrate synthase enzyme activity assay which was included in my first first-author publication. Thank you to Charlotte for challenging me while also providing a welcoming environment in the Center for Muscle Biology during my transition to the University of Kentucky.

Cory Dungan and Kevin Murach in the Peterson Lab at University of Kentucky have been a bountiful source of insight and instruction. They developed the PoWeR protocol in young mice on which Chapter 3 of this dissertation is built, and worked alongside the Fry Lab to initiate PoWeR in old mice. Additionally, I am grateful to Cory and Kevin for their guidance and thought-provoking conversations on multiple rodent

projects. Members of the Fry Lab have also formed a team without which this work would not be possible: Christine Latham, Nick Thomas, Alex Keeble, and Alyaa Zagzoog.

I must also thank Tatiana Moro, who not only taught me basic lab techniques but also taught me how to truly enjoy science. Tatiana may be the most instrumental person regarding my entrance into science. She patiently taught me how to function in a lab and, along the way, became my best friend. There are few people with whom a connection is so easily and naturally formed, especially when communication is initially limited by a language barrier; however, Tatiana has been this person for me. Graduate school is difficult and often feels hopeless, but Tatiana consistently reoriented and encouraged me. She is a bright scientist, but more importantly, she is an unmatched friend and the most thoughtful, considerate person I know.

Most essentially, I thank my husband, Ben. He is quietly brilliant. He has supported me in my educational endeavors—with great sacrifice—and challenged me to continually grow, while also achieving educational excellence of his own as a clinician and scientist. More importantly, he is steadfast, patient, and genuinely good. He loves me well. I'm overwhelmingly thankful that he is my husband and that our daughter, Zoe, will also be blessed to learn from him and be supported and loved so truly by him. I'm proud of my accomplishments in graduate school, but all of that fades away as extraneous in comparison to my love and appreciation for Ben. Thank you, Benny.

Aging Skeletal Muscle Plasticity in Exercise and Injury

Publication No._____

Camille R. Brightwell, Ph.D.

The University of Texas Medical Branch, 2021

Supervisor: Christopher S. Fry

Sarcopenia—progressive loss of muscle mass and strength—diminishes quality of life and longevity. In addition to progressive atrophy, older adults exhibit impaired regeneration after muscular injury. Activity of muscle stem cells, termed satellite cells, is dysregulated with aging which impairs skeletal muscle remodeling and limits plasticity of aged muscle. Aim 1 (Chapter 2) of this dissertation seeks to clarify the debated requirement of satellite cells for overload-induced hypertrophy in aging muscle via a common surgical overload model, with the original hypothesis that while aging satellite cells contribute to overload-induced hypertrophy to mitigate sarcopenia, growth can occur in the absence of satellite cells via expansion of the myonuclear domain. In light of Aim 1 results demonstrating no overload-induced hypertrophy in aging skeletal muscle with surgical overload, Aim 2 (Chapter 3) examines the efficacy of a novel and translatable murine resistance exercise model to elicit satellite cell expansion with myonuclear accretion and hypertrophy in aging skeletal muscle, with the hypothesis that this novel exercise model would result in expansion of the satellite cell pool along with hypertrophy not observed in old mice with the surgical overload model. Indeed, PoWeR (Progressive Weighted wheel Running) elicited hypertrophy in old mice, likely supported by a robust angiogenic response in hind limb muscles. Lastly, Aim 3 (Chapter 4) examines the efficacy of a novel

NNMT inhibitor to enhance regeneration of aging skeletal muscle after injury by enhancement of satellite cell proliferation and fusion to myofibers, confirming the hypothesis that NNMT inhibition would rescue age-related deficits in satellite cell activity to promote superior regeneration of muscular injury of old mice.

TABLE OF CONTENTS

List of Tables

List of Figures

List of Abbreviations

1-MNA	1-methylnicotinamide
ADLs	Activities of Daily Living
AF	Alexa Fluor
ANOVA	Analysis of Variance
$BaCl_2$	Barium Chloride
BCA	Bicinchoninic Acid
BID	“bis in die”/Twice Daily Injections
CSA	Cross Sectional Area
DAPI	4’,6-diamidino-2-phenylindole
DTA	Diphtheria Toxin A
DXA	Dual Energy X-Ray Absorptiometry
ECM	Extracellular Matrix
EdU	5-ethynyl-2’-deoxyuridine
eMHC	Embryonic Myosin Heavy Chain
HRP	Horse Radish Peroxidase
IF	Immunofluorescence
IP	Intraperitoneal
IS	Internal Standard
IHC	Immunohistochemistry
MHC	Myosin Heavy Chain
MRI	Magnetic Resonance Imaging

mTORC1	Mammalian Target Of Rapamycin Complex 1
myostatin-I	Myostatin Inhibitor (Follistatin)
NA	Nicotinamide
NAD+	Nicotinamide Adenine Dinucleotide
NIA	National Institute of Aging
NMN	Nicotinamide Mononucleotide
NNMT	Nicotinamide N-Methyltransferase
NNMTi	Nicotinamide N-Methyltransferase Inhibitor
NR	Nicotinamide Riboside
Pax7	Paired Box 7
Pax7-DTA	$Pax7_{CreER/+}$; $Rosa26_{DTA/+}$
PFA	Paraformaldehyde
PoWeR	Progressive Weighted Wheel Running
PVDF	Polyvinylidene Fluoride
RE	Resistance Exercise
RET	Resistance Exercise Training
SAH	S-Adenosyl-L-homocysteine
SAM	S-(5′-Adenosyl)-L-methionine
SC	Subcutaneous
muSC	Satellite Cell
SC-Dep	Satellite Cell Depleted
SC-WT	Satellite Cell Wild Type
SDS-PAGE	Sodium Dodecyl Sulfate Polyacrylamide Gel Electerophoresis

SIRT1	Sirtuin 1
TA	Tibialis Anterior
TBSA	Total Body Surface Area
TGF	Transforming Growth Factor
TSA	Tyramide Signal Amplification
WGA	Wheat Germ Agglutinin

CHAPTER 1:

General Introduction

SKELETAL MUSCLE

Skeletal muscles are striated muscles under the voluntary control of the somatic nervous system. They are attached to bones by bundles of collagen called tendons. Through attachment to bone, skeletal muscle is primarily responsible for locomotion and force generation to support postural stability and all movement. Skeletal muscle cells are referred to as myofibers which are multi-nucleated and are most notably composed of myofibrils containing contractile units called sarcomeres that produce force via actin-myosin/myofilament crossbridges (Figure 1.1). An entire skeletal muscle is composed of thousands of myofibers of different types. Myofiber type is determined by predominant metabolism (myosin heavy chain type I- oxidative, myosin heavy chain type II- glycolytic). Myofibers may transition between fiber types as an adaptation to imposed demands, and hybrid fiber types do exist. In addition to transitions of myofiber type, myofibers respond to external stimuli with growth (hypertrophy) and size reduction (atrophy), further demonstrating the adaptability of this tissue. These changes are typically accompanied and supported by alterations of the extracellular matrix (ECM). Skeletal muscle readily adapts to pathological stimuli and demands of altered activity, and this capacity is termed skeletal muscle plasticity.

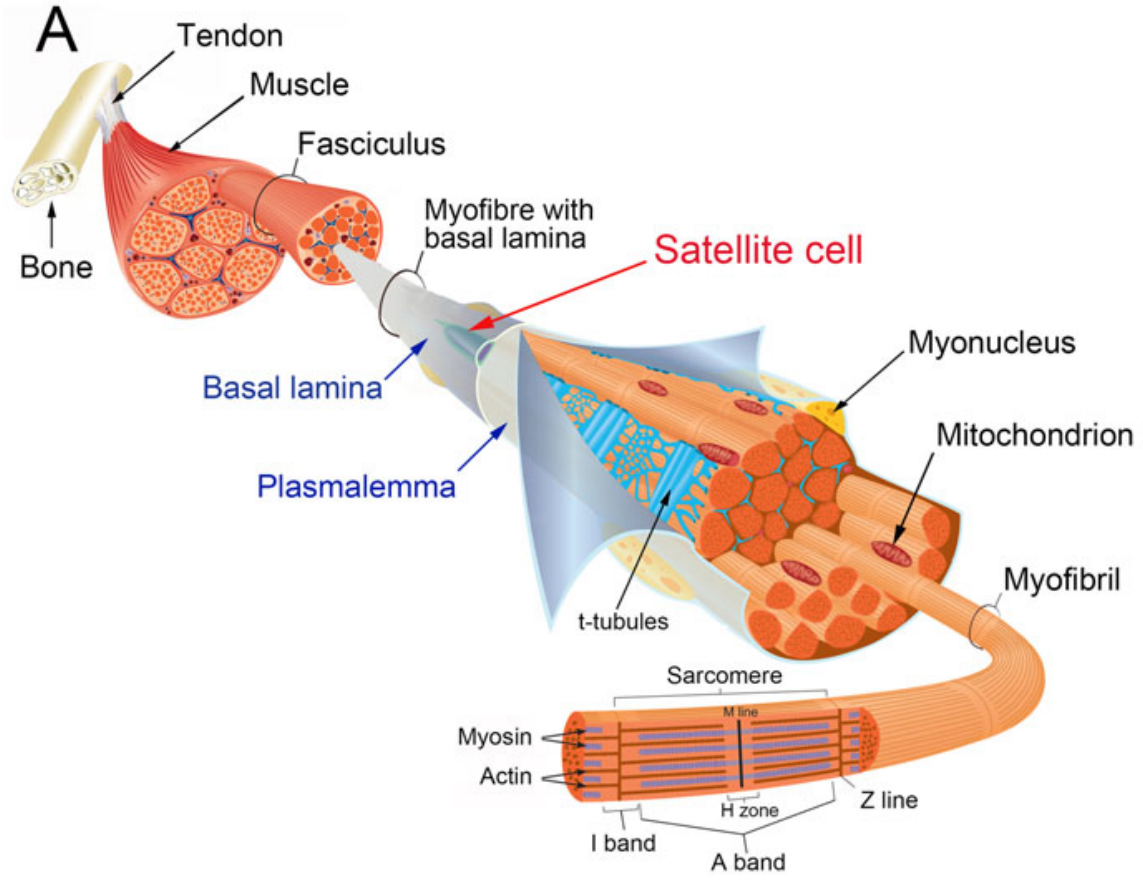

Figure 1.1: Skeletal muscle anatomy.

A skeletal muscle is composed of thousands of myofibers. Myofibers are comprised of many myofibrils which contain the contractile units, sarcomeres. Sarcomeres produce force via myofilaments/actin-myosin cross bridges. *Relaix & Zammit, Development 2012, doi: 10.1242/dev.069088.*

Skeletal muscle architecture and size largely regulate maximal force development (along with myofiber type distribution and neuromuscular factors), thus impacting performance and function.[1] Skeletal muscle size is most precisely measured in the laboratory as cross-sectional area (CSA) of individual myofibers, commonly analyzed by immunohistochemistry/immunofluorescence. This method can determine size of different myofiber types. In clinical settings, muscle mass may be determined by dual energy x-ray absorptiometry (DXA), ultrasound, computed tomography (CT), or magnetic resonance imaging (MRI).

AGE-RELATED ATROPHY OF SKELETAL MUSCLE

Skeletal muscle atrophy involves the loss of myofibers and of myofibrillar proteins in remaining myofibers . In aging, skeletal muscle progressively atrophies which contributes to muscular weakness and eventually sarcopenia (clinically relevant low muscle mass and strength with loss of function, increased likelihood of falls, and mortality).[2-4] Age-related atrophy occurs preferentially in glycolytic type II myofibers, impairing strength related activities of daily living (ADLs).[5, 6] In addition to progressive atrophy, older adults exhibit impaired regenerative capacity after muscular injury, further underwriting the decline into sarcopenia.[7]

Sarcopenia is closely associated with aging; beginning around 50 years of age, most older adults experience 1% and 3% annual declines in muscle mass and strength, respectively.[8] Approximately 30% of adults 60 years of age and over and 50% over 80 years are estimated to suffer from sarcopenia,[9-11] with muscle mass and function (e.g., gait speed, grip strength) below measurable healthy norms.[3] Sarcopenic older adults experience (i) significantly reduced muscle strength, function, and regenerative ability, (ii) serious comorbidities and health complications, (iii) a greatly diminished quality of life, and (iv) a 2- 5-fold increased risk of disability.

Age-related losses in skeletal muscle mass and quality and subsequent strength decline are well documented as integral contributors in the development of disability.[12] Atrophy associated with sarcopenia leads to reduced peak strength which causes difficulty with weight-bearing ADLs, such as carrying groceries or standing from a chair.[13] Furthermore, muscular power is reduced, impairing quick movements to catch oneself from a fall and leading to higher incidence of fall-related injuries. Muscular endurance also decreases which increases fatigue and difficulty with exercise, making endurance ADLs problematic. These functional deficits eventually lead to decreased physical activity and

disability. The compensatory decrease in physical activity then exacerbates the sarcopenic decline and further feeds into increased disability (Figure 1.2).[13]

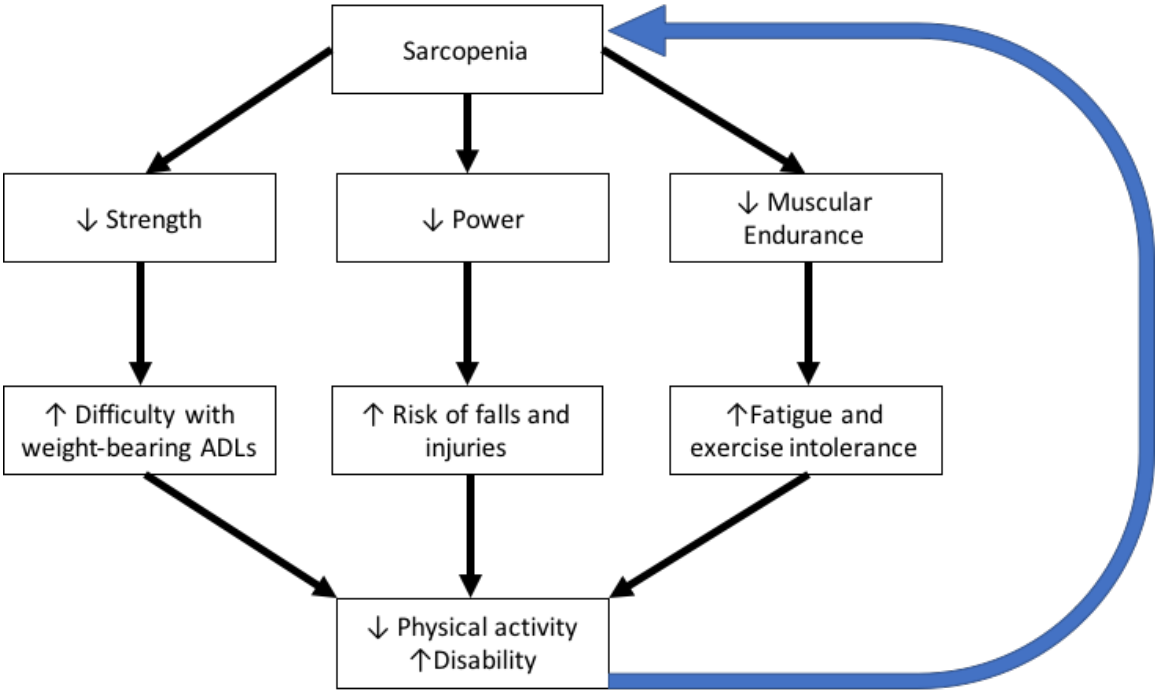

Figure 1.2: A model of functional consequences of sarcopenia leading to decreased physical activity and increased disability and the feedback loop in which decreased physical activity further contributes to the sarcopenic decline into disability.

Adapted from Hunter et al.[13]

Healthcare expenses in the US attributable to sarcopenic disability are estimated at $30 billion; these costs are predicted to be a large driver of burgeoning Medicare payments over the next decade.[14] Therapies to promote skeletal muscle hypertrophy and congruent strength gain are necessary to combat the sarcopenic deterioration into disability. Additionally, therapies to enhance recovery of aging skeletal muscle after injury will promote maintenance of existing muscle mass and further combat the sarcopenic decline.

SKELETAL MUSCLE HYPERTROPHY

The functional implications of the loss of skeletal muscle mass support the clinical relevance of skeletal muscle hypertrophy to mitigate disability, particularly in aging. Skeletal muscle hypertrophy is the process of increasing contractile elements (actin-myosin/myofilament cross bridges) and supporting structural proteins within muscle tissue resulting in a greater number of actin-myosin cross bridges for force development.[15] Strategies to promote skeletal muscle hypertrophy in both clinical and non-clinical populations include resistance exercise (RE), amino acid supplementation, hormone therapy, and various combinations of these. Resistance exercise training is the most effective countermeasure to attenuate the sarcopenic decline into frailty and eventually disability as it preserves, and in some scenarios increases, muscle mass.[16] Skeletal muscle hypertrophy resultant from resistance exercise training is termed overload-induced hypertrophy.

Although resistance exercise training is effective to promote overload-induced hypertrophy in older adults, both the acute and chronic anabolic response to resistance exercise is impaired in old compared to young.[17, 18] Anabolic resistance translates into an inability of older adults to achieve youthful levels of skeletal muscle mass and associated strength given the same resistance exercise training stimulus as young adults. The mechanisms of chronic anabolic resistance have not been clearly elucidated. However, decreased phosphorylation/activation of mTORC1 (mammalian target of rapamycin complex 1) in response to acute resistance exercise has been reported in older adults compared to young.[17] In addition to impaired anabolic signaling, it has been suggested that dysregulation of muscle stem cells may contribute to impaired overload-induced hypertrophy in older adults.[19-21] However, the role/requirement of muscle stem cells in overload-induced hypertrophy has remained controversial.[22, 23] Regardless of stem cell requirement, manipulation of stem cell activation in conjunction with an overload stimulus

may effectively enhance overload-induced hypertrophy in older adults to at least partially restore a youthful hypertrophic adaptation.

SKELETAL MUSCLE REGENERATION

In addition to impaired overload-induced hypertrophy, older adults exhibit progressively impaired muscle regenerative potential.[7, 24, 25] After physical trauma, skeletal muscle of older adults does not recover at the same rate or to the same extent as muscle of healthy young adults, contributing to sarcopenia. Instead of a rapid myogenic response to form new myofibers, the response is delayed and partial in aged muscle and is accompanied by fibrosis.[25] Muscle stem cells are indispensable for regeneration after sever muscle injury,[26-28] and deficits in muscle resident stem cell function likely drive impaired in recovery (muscle stem cells are discussed in detail in the following section). A model that exposes old mice to circulatory factors of young mice (heterochronic parabiosis) effectively enhances skeletal muscle regeneration of old mice through exposure to systemic factors that change with age, mediated by restoration of normal Notch signaling.[29]

Currently there are no effective therapies to significantly enhance post-injury muscle regeneration in older adult humans. Manipulation of muscle stem cell activity via parabiotic pairing effectively enhances muscle recovery in mice; however, this is not a practical treatment model for humans. Via parabiotic pairing, exposure to serum from young mice provides increased levels of the Notch ligand, Delta, which is decreased with aging.[30] Since muscle stem cell activation and differentiation are Notch-dependent, this strategy demonstrates that manipulation of a regulator of stem cells can be an effective method to promote muscle recovery in aging. Development of pharmacological therapies that can safely enhance muscle stem cell activity is needed to improve myofiber regenerative capacity and promote injury recovery.

THE ROLE OF SATELLITE CELLS IN HYPERTROPHY AND REGENERATION

Satellite cells are the resident stem cells in skeletal muscle that lie between the basal lamina and the myofiber plasma membrane/sarcolemma and account for nearly all regenerative capacity of myofibers.[31] Satellite cells are identified by location and discrete expression of various genes, most notably paired box 7 (Pax7).[32] During embryonic development and post-natal growth, satellite cells are active and contribute nuclei to growing myofibers. In adult skeletal muscle, satellite cells remain quiescent (in reversible cell cycle arrest) under resting conditions and are activated in response to mechanical overload and injury.[33] Upon activation, satellite cells proliferate and give rise to daughter cells that can either re-enter quiescence to maintain the satellite cell pool (self-renewal) or differentiate into myoblasts that will either fuse to existing myofibers or to other myoblasts to form new myofibers.[34] Satellite cell quiescence, activation, proliferation, and differentiation are regulated by factors in the surrounding milieu, or niche.[35] In response to resistance exercise/mechanical overload and injury, satellite cells differentiate into myoblasts and fuse with myofibers, contributing a myonucleus to promote myofiber hypertrophy and repair. Furthermore, satellite cells regulate activity of fibrogenic cells and control deposition of excessive extracellular matrix (ECM)/fibrosis.[36]

Historically, satellite cells have been thought to be required for overload-induced hypertrophy.[37-39] The myonuclear domain hypothesis postulates that myonuclear accretion is required to support expanding fiber volume to maintain a constant nucleus to sarcoplasm ratio, and myonuclear accretion only occurs via satellite cell differentiation and fusion.[40] However, Dr. Charlotte Peterson's group demonstrated that myofibers grow to the same extent with or without satellite cells in the short-term (2-week overload) with synergistic ablation surgery (removal of gastrocnemius and soleus facilitating overload of plantaris) of satellite cell-depleted mice.[41] These findings indicate that satellite cells are not necessary for the initial amount of overload-induced growth of skeletal muscle in healthy young adult

mice. However, her group more recently demonstrated that continued myofiber growth over eight weeks is attenuated in the absence of satellite cells.[32] Since satellite cells regulate fibrogenic cells, depletion of satellite cells also facilitated excessive ECM deposition which may inhibit myofiber hypertrophy, regenerative capacity, and contractile function. Seemingly conflicting findings regarding the requirement of satellite cells for overload-induced hypertrophy highlight the necessity of additional studies with different time points.[42, 43] Additionally, additional experiments are needed in old mice, as the requirement for satellite cells may be different between old and young animals since the satellite cell pool is depleted and increasingly dysfunctional in skeletal muscle of old mice and humans. Previous work has explored the requirement of satellite cells to induce hypertrophy with a surgical overload stimulus in old mice; however, the relatively short 2-week overload period was insufficient to produce myofiber hypertrophy in old mice, despite myonuclear accrual and a subsequent alteration to the myonuclear domain.[44] In the absence of myofiber hypertrophy, the 2-week surgical overload model was not able to clarify the requirement of satellite cells for overload-induced myofiber hypertrophy, but instead demonstrated that satellite cell fusion and subsequent myonuclear accrual alone is not sufficient to cause hypertrophy. A longer surgical overload period may be required to stimulate myofiber hypertrophy in old mice, if a hypertrophic response is delayed in old mice compared to young in which a 2-week surigical overload effectively induced muscle hypertrophy.[41] This knowledge gap is addressed in Aim 1 presented in Chapter 2 of this dissertation, with Chapter 2 results directly leading to characterization of an effective and translational aging murine hypertrophy model (recently validated in young mice[45, 46]) as Aim 2 presented in Chapter 3.

Divergent from overload-induced muscle hypertrophy, the requirement of satellite cells for myofiber regeneration after muscle injury has been well established.[26-28] Myofiber injury causes a complex signaling cascade that eventually results in formation of new/restored myofibers.[47-50] After muscle injury, quiescent satellite cells are activated and

proliferate, becoming myoblasts that are now capable of fusion to other myoblasts and existing myofibers. After injury and necrosis of existing myofibers, myoblasts align with one another and fuse, producing new multinucleated myofibers. Myoblasts also fuse to remaining myofibers in the injured muscle and contribute a myonucleus to promote recovery and growth.[25] Thus, satellite cells are required for muscle recovery from injury.[26-28] However, satellite cell activity is dysregulated in aging.

DYSREGULATION OF SATELLITE CELLS IN AGING SKELETAL MUSCLE

Sarcopenic muscle exhibits a decline in both satellite cell number and function.[51, 52] Satellite cells are quiescent under normal conditions and only become activated in response to stimuli (overload and injury). A reversible quiescence of satellite cells is necessary so that after proliferation, some satellite cells return to the quiescent state and maintain cell number. However, satellite cells of aged muscle lose the intrinsic capacity for reversible quiescence in homeostatic conditions,[53] at least partially explaining the depleted satellite cell pool in skeletal muscle of older adults. Furthermore, satellite cells in aged muscle increasingly switch to a dysfunctional state and are not activated by overload and injury stimuli, impeding proliferation, differentiation, and subsequent myoblast fusion.[53] In addition to intrinsic dysregulation of aged satellite cells, factors of the niche exhibit age-related deficits which impede satellite cell activation and contribute to dysregulation of satellite cells in aging.[54] Both the intrinsic and extrinsic regulators of satellite cells present promising therapeutic targets, and the manipulation of an intrinsic factor to enhance satellite cell activity is explored in Aim 3 presented in Chapter 4 of this dissertation. Restoring youthful levels and/or function of regulators of satellite cells may then partially restore satellite cell activity.

Loss of satellite cell function in aging does not contribute to age-associated muscle atrophy in sedentary mice, but does cause age-related skeletal muscle fibrosis;[55] however, satellite cell depletion does impair the muscle hypertrophic response to lifelong wheel

running.[56] The impact of satellite cell loss on overload-induced skeletal muscle hypertrophy with aging remains inconclusive, meriting further study. However, it has been well established that satellite cell loss drastically compromises the regenerative capacity of sarcopenic skeletal muscles after injury.[53] After injury, fewer myoblasts are formed in muscle of old compared to young, resulting in formation of fewer myofibers and grossly impaired recovery of skeletal muscle.[30, 57] Restoration of youthful/healthy satellite cell function in aging will promote enhanced regeneration and recovery after skeletal muscle injury and may partially restore a youthful hypertrophic response to overload/resistance exercise.

THERAPEUTIC REGULATION OF SATELLITE CELL ACTIVITY IN AGING

As discussed above, physiological factors that regulate satellite cell function are commonly altered in aging. Regulators of satellite cells offer promising therapeutic targets to enhance satellite cell activity and promote both growth and regeneration in aging skeletal muscle. One noted regulator of satellite cell activity is nicotinamide N-methyltransferase (NNMT).[58, 59]

NNMT is an enzyme upregulated in aged skeletal muscle (Figure 1.3) and newly discovered to regulate cellular metabolic pathways, particularly NAD+ biosynthesis via the NAD+ salvage pathway (Figure 1.4), which is highly compromised in aged muscle.[58] NNMT is the fourth most differentially upregulated gene in skeletal muscle between old and young,[60] and NNMT protein expression levels are inversely correlated with intracellular levels of NAD+.[58] Sirtuin 1 (SIRT1) is an NAD+-dependent deacetylase; SIRT1 activity closely correlates with intracellular levels of NAD+[61] and also decreases with age.[62, 63] In the absence of SIRT1 (SIRT1 muscle-specific knockout), mice have downregulated expression of developmental genes of muscle, reduced myofiber size, and impaired muscle regeneration capacity.[64] Moreover, decreased NAD+ content in satellite cells leads to a SIRT1-mediated metabolic switch (fatty acid oxidation to glycolysis) that

induces premature differentiation of satellite cells and ultimately a loss of regenerative capacity.[64]

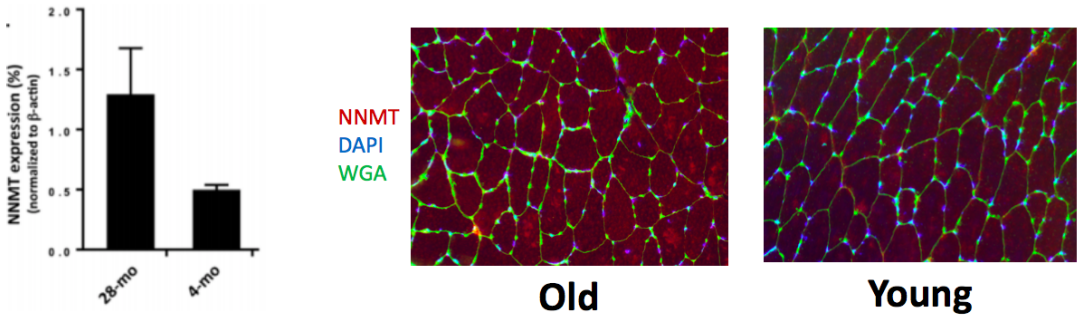

Figure 1.3: Comparison of NNMT expression in old and young skeletal muscle.
Our preliminary data showed that NNMT protein expression is elevated in old muscle. Data/images from the Fry laboratory.

Although the etiology of age-related dysfunction of satellite cells is unknown, the NAD+/SIRT1 results described above suggest the model that at least partially contributes to impaired regenerative capacity in aging[65] (Figure 1.4): As muscles age, they progressively develop increased expression and/or activity of NNMT, which results in lowered intracellular NAD+ levels, reduced SIRT1 activity, and increased premature differentiation of satellite cells that ultimately interferes with satellite cell activity and muscle repair/growth.[64, 66] Support for this model comes, in part, from recent studies showing nutraceutical supplements that elevated intracellular NAD+ levels also improved muscle function and accelerated muscle regeneration in aged mice. However, these supplements required high doses.[64, 67-70] An inhibitor of NNMT that can effectively enhance satellite cell activity and promote skeletal muscle recovery and overload-induced hypertrophy at much lower, more clinically feasible doses is needed. A novel inhibitor of NNMT was developed by Dr. Stan Watowich.[58] Chapter 4 of this dissertation proposes the use of the novel NNMT inhibitor (NNMTi, 5-Amino-1-methylquinolinium) to promote

myogenesis through upregulated satellite cell activity at doses that may be translatable to clinical use.

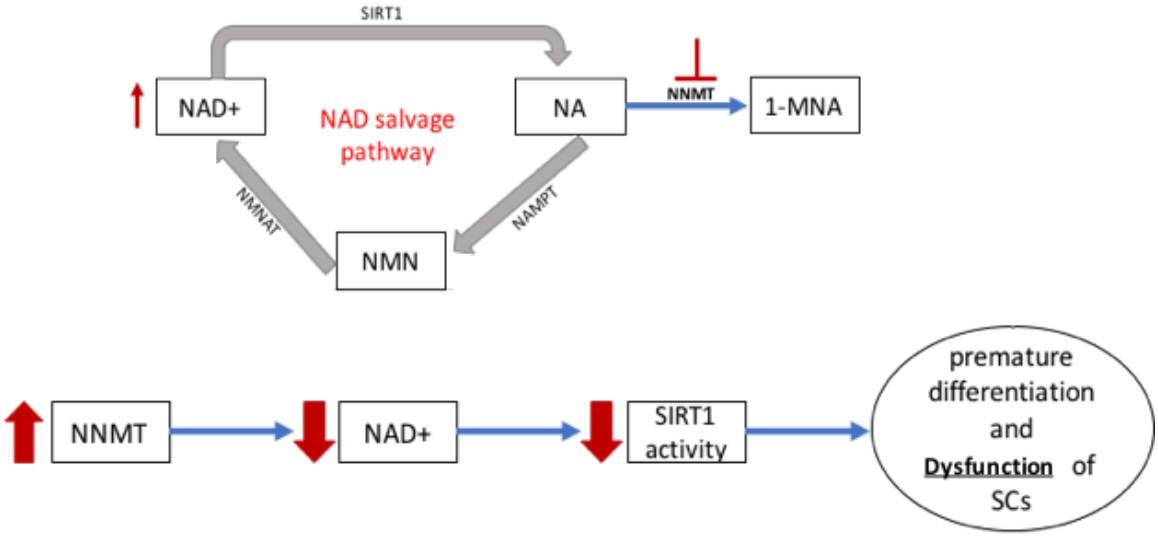

Figure 1.4: Schematic of the NAD+ salvage pathway and the progression from elevated NNMT to impaired SC function.

SIRT1 activity is NAD+-dependent, converting NAD+ to NA. NA is converted back to usable NAD+ by the NAD salvage pathway. However, NNMT can convert NA to 1-MNA, eventually depleting NAD+ levels. When NNMT is inhibited, NAD+ levels increase and facilitate SIRT1 activity. Conversely, elevated NNMT results in low NAD+ levels. Low NAD+ levels cause reduced SIRT1 activity which causes premature differentiation and senescence of SCs. NA (nicotinamide), NAMPT (nicotinamide phosphoribosyltransferase), NMN (nicotinamide mononucleoside), NMNAT (nicotinamide adenylyltransferase), NNMT (nicotinamide Nmethyltransferase), SIRT1 (NAD-dependent deacetylase sirtuin 1), 1-MNA (1-Methylnicotinamide).

SPECIFIC AIMS

Sarcopenia diminishes quality of life and longevity. In addition to progressive atrophy, older adults exhibit impaired regeneration after muscular injury. Satellite cells are dysregulated in aging which impairs skeletal muscle remodeling in response to exercise and injury, contributing to the progressive sarcopenic decline into disability. Aim 1 (Chapter 2) of this dissertation seeks to elucidate the debated requirement of satellite cells for overload-induced hypertrophy in aging muscle via a common surgical overload model,

with the original hypothesis that while aging satellite cells contribute to overload-induced hypertrophy to mitigate sarcopenia, growth can occur in the absence of satellite cells via expansion of the myonuclear domain. In light of Aim 1 results, Aim 2 (Chapter 3) examines the efficacy of a novel and translatable murine exercise model to elicit satellite cell expansion and overload-induced hypertrophy in aging skeletal muscle, with the hypothesis that this novel exercise model will result in expansion of the satellite cell pool and corresponding overload-induced hypertrophy not observed in old mice with the surgical overload model. Lastly, Aim 3 (Chapter 4) examines the efficacy of a novel NNMT inhibitor to enhance regeneration of aging skeletal muscle after injury by enhancement of satellite cell proliferation and fusion to myofibers, with the hypothesis that NNMT inhibition will rescue age-related deficits in satellite cell activity to promote superior regeneration of muscular injury of old mice.

CHAPTER 2:

Aged muscle is resistant to surgical overload-induced hypertrophy regardless of satellite cell abundance or satellite cell fusion to myofibers

INTRODUCTION

Sarcopenia is highly prevalent and imposes deleterious effects on quality of life and longevity.[4, 9, 71-74] The progressive loss of muscle mass and strength which defines sarcopenia contributes to the decline in physical function commonly associated with aging. This loss of functional independence due to weakness and impaired mobility dramatically impacts physical and mental well-being of older adults.[71, 75] However, resistance exercise training provides an overload stimulus to promote growth (overload-induced hypertrophy) and partially restore muscle mass and physical function in older adults, combatting the sarcopenic decline into disability.[18, 76, 77]

Satellite cells are the principle stem cell population in skeletal muscle and are activated in response to mechanical overload—such as resistance exercise—and injury which require myofiber hypertrophy and regeneration to support remodeling.[36] Satellite cells modulate muscle plasticity by fusion to myofibers, facilitating myonuclear accretion to support transcriptional demands of growth.[36, 78] It had previously been proposed and accepted that myonuclear domain (the volume of sarcoplasm transcriptionally regulated by a myonucleus) remains constant, requiring satellite cell fusion to contribute a myonucleus to facilitate myonuclear accretion and subsequent myofiber growth.[79, 80] However, the traditional myonuclear domain theory has been challenged.[32, 41, 44, 81]

A 2-week surgical overload stimulus in older animals has been reported to successfully activate satellite cells and induce fusion-dependent myonuclear accretion, with no increase in myofiber size.[44] Thus, satellite cells are required to add a myonucleus in response to overload, but are insufficient on their own to drive growth in aged muscle.

Although it was established that satellite cell fusion alone is insufficient to stimulate hypertrophy in skeletal muscle of older mice, the alternative possibility of hypertrophy without satellite cell fusion is more controversial. Normal overload-induced hypertrophy in the absence of satellite cells has been reported.[41] Yet, attenuated overload-induced myofiber hypertrophy has also been reported with satellite cell depletion.[32] Furthermore, the requirement for satellite cells in overload-induced skeletal muscle hypertrophy has primarily been studied in young mice, limiting translation to aging skeletal muscle in which satellite cells along with their microenvironment are altered.[24, 25, 30, 54] Satellite cell fusion and myonuclear accretion occur in the absence of hypertrophy during a short 2-week overload in older mice,[44] demonstrating that satellite cell fusion to myofibers is insufficient to promote growth in aging skeletal muscle and indicating that myonuclear domain is plastic even in aging skeletal muscle, challenging the myonuclear domain theory. Myonuclear domain plasticity suggests that hypertrophy in aged muscle may not be dependent on satellite cell-mediated myonuclear accrual, if the myonuclear domain not only contracts but may also expand in aging skeletal muscle.

The aim of this study was to elucidate the requirement of satellite cells for overload-induced hypertrophy in aging skeletal muscle given an extended overload period (4 weeks compared to the previously reported 2-week overload period), as elucidation of contributors to hypertrophy in aging skeletal muscle may identify future therapeutic targets to mitigate sarcopenia. A transgenic mouse model in which satellite cells are conditionally depleted was utilized to mechanistically approach this aim. The original hypothesis was that 1) an extended 4-week surgical overload would effectively elicit hypertrophy in the plantaris muscle of old mice, demonstrating a delayed growth response compared to young mice subjected to surgical overload[41, 44] and 2) while satellite cells contribute to overload-induced skeletal muscle hypertrophy, myofiber growth can occur with overload in the absence of satellite cells via expansion of the myonuclear domain.

MATERIALS AND METHODS

Ethical approval

Animal procedures were approved by the Institutional Animal Care and Use Committees at the University of Texas Medical Branch (1411059) and the University of Kentucky (2019-3241). All mice were housed in temperature and humidity controlled rooms on a 12h:12h light-dark cycle. Mice were given ad libitum access to food and water and were euthanized by cervical dislocation under deep anesthesia.

Experimental design

The $Pax7^{CreER/+}$; $Rosa26^{DTA/+}$ (Pax7-DTA) mouse model was utilized. The Pax7-DTA mouse strain is an innovative approach for the effective and specific depletion of satellite cells in skeletal muscle, as Pax7 is only expressed in satellite cells in muscle. Treatment of Pax7-DTA mice with tamoxifen activates *Pax7* promoter–driven *Cre* recombinase through a modified estrogen receptor only in satellite cells[82], which activates diphtheria toxin A (DTA) gene through recombination of the floxed stop codon between the constituitive Rosa26 promoter and the DTA gene and causes apoptosis of satellite cells, resulting in satellite cell depletion.[41] Tamoxifen treatment results in the depletion of >90% of satellite cells in skeletal muscle, which is irreversible.[32] Tamoxifen treatment does not have apparent long-term effects on non-transgenic mouse muscle physiology.[32]

Six-week-old Pax7-DTA mice were randomized into 1 of 2 different groups (SC-WT/satellite cell replete or SC-Dep/satellite cell depleted). Following 5 days of vehicle (SC-WT; saline) or tamoxifen (SC-Dep; 0.1 mg/kg/day) treatment, mice were aged to 23 months. At 23 months of age, both SC-WT and SC-Dep mice were further randomized into 2 additional groups (n=4-9 mice/group). One group was subjected to synergist ablation surgery as an overload stimulus for a 4-week period (SA/synergist ablation). The other group did not undergo synergist ablation surgery (Sham). Synergist ablation surgery was

performed on mice in the SA groups as previously described.[83] Briefly, mice were anesthetized with 2.5% isoflurane vaporized in oxygen flowing at 1 L/min, and surgery was performed under sterile conditions. Gastrocnemius and soleus muscles were removed from both hind limbs, leaving only the plantaris to generate plantar flexion movements, resulting in a functional mechanical overeload. The experimental design resulted in the following 4 groups: SC-WT Sham, SC-Dep Sham, SC-WT SA, and SC-Dep SA.

To track satellite cell proliferation and fusion, 5-Ethynyl-2´-deoxyuridine (EdU), a thymidine analog, was injected intraperitoneally (150 µg/mouse in saline) every other day during the 4-week overload period. Upon completion of the 4-week period, 24-month-old mice underwent in vivo contractile function assessment (SC-WT SA and SC-Dep SA mice only) before being euthanized for tissue collection (SC-WT Sham, SC-Dep Sham, SC-WT SA, and SC-Dep SA). Figure 2.1 illustrates a schematic of the study.

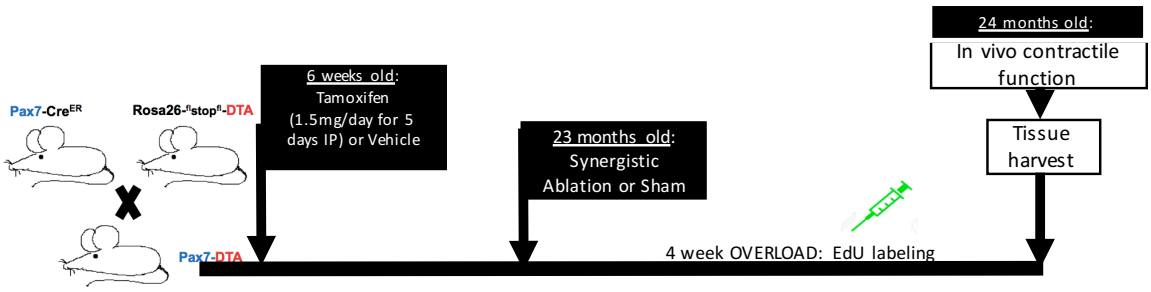

Figure 2.1: Study Schematic.

Immunohistochemistry

Immunohistochemical (IHC) analyses were performed on the plantaris muscle from the right hind limb for all mice. The plantaris was covered in Tissue Tek (O.C.T. Compound, Sakura Finetek, Torrance, CA, USA) at resting length and frozen in liquid nitrogen-cooled 2-methylbutane. Samples were stored at -80°C prior to analysis. Using a cryostat (HM525-NX, Thermo Fisher Scientific, Waltham, MA, USA), 7µm-thick sections

were cut and air dried for 1 h on slides. Slides were stored at -20°C until commencement of IHC staining.

For identification of satellite cells, Pax7 immunostaining was performed given it is a transcription factor uniquely expressed in satellite cells. Laminin was used to denote myofiber borders and confirm sub-laminar location of Pax7+ satellite cells. For Pax7/EdU/laminin staining, sections were fixed in 4% paraformaldehyde (PFA). Following washes in phosphate buffered saline (PBS), antigen retrieval was performed with sodium citrate (10mM, pH 6.5) at 92°C for 20 minutes. Slides were washed again in PBS, and endogenous peroxidases were blocked using 3% hydrogen peroxide for 7 min, followed by another blocking step in mouse-on-mouse IgG blocking reagent (cat#MKB-2213, Vector Laboratories). Sections were then blocked for 1 h at room temperature in 1% blocking reagent included in a commercially available tyramide signal amplification kit (Life Technologies/Thermo Fisher Scientific), followed by overnight incubation at 4°C in primary antibodies against Pax7 (mouse IgG, 1:100; Developmental Studies Hybridoma Bank) and laminin (rabbit IgG, 1:200; L9393, Millipore Sigma) in the 1% blocking reagent. The following day, slides were washed in PBS and incubated for 1 h at room temperature in goat anti-mouse biotinylated secondary antibody (1:1000; #115-065-205, Jackson Immuno Research) and goat anti-rabbit secondary antibody directly conjugated to Alexa Fluor 647 (1:500; #A11034, Invitrogen). Slides were again washed in PBS and incubated for 1 h at room temperature in streptavidin conjugated to horse radish peroxidase included in a commercially available tyramide signal amplification kit (SA-HRP, Life Technologies/Thermo Fisher Scientific). Following an additional PBS wash, Pax7 was amplified by incubation for 20 min at room temperature in TSA-Alexa Fluor 488 (1:100 in amplification diluents; #T30955, Invitrogen). After Pax7-laminin staining, sections were permeabilized in 0.1% Triton-X100 in PBS and incubated with Click-iT EdU Cell Proliferation Kit for Imaging (C10338, ThermoFisher Scientific) per manufacturer's instructions. Slides were washed in PBS, incubated for 10 min in 4′,6-diamidino-2-

phenylindole (DAPI; 10 nM, Life Technologies/Thermo Fisher Scientific), washed again in PBS, and mounted using Vectashield fluorescence mounting media (Vector Laboratories, Burlingame, CA, USA).

For IHC assessment of fiber type distribution and fiber type-specific cross sectional area (CSA) to assess hypertrophy, sections were blocked for 1 h at room temperature in a mouse-on-mouse Ms IgG blocking solution (cat#MKB-2213, Vector Laboratories) followed by a PBS wash. Slides were incubated overnight at 4°C in primary antibodies against dysrophin (rabbit IgG, 1:100; #sc-15376, Santa Cruz) and myosin heavy chain (MHC) type I (mouse IgG2b, 1:100; BA.D5 concentrate, Developmental Studies Hybridoma Bank) in myosin heavy chain type IIa supernatant (mouse IgG1; SC.71, Developmental Studies Hybridoma Bank). The next day, slides were washed in PBS and incubated for 1 h at room temperature in goat anti-mouse IgG1 AF488 secondary antibody (1:500; #A21121, Invitrogen), goat anti-mouse IgG2b AF647 secondary antibody (1:250; #A21242, Invitrogen), and goat anti-rabbit IgG AF555 secondary antibody (1:500; #A21428, Invitrogen) in PBS. Slides were washed in PBS and incubated in DAPI (10nM, Life Technologies/Thermo Fisher Scientific) followed by post-fixation in methanol and another wash in PBS. Slides were mounted using Vectashield fluorescence mounting media (Vector Laboratories, Burlingame, CA, USA).

Image acquisition and analysis

Images were captured at 100-200x magnification with a Zeiss upright microscope (AxioImager M1; Zeiss, Oberkochen, Germany). Zen Blue (v 3.1) software was used to manually determine satellite cell abundance, proliferation, and fusion by the same assessor in a blinded manner. MyoVision software was used for automated analysis of fiber type distribution and fiber type-specific CSA, as previously reported.[84]

Satellite cells were identified as Pax7+/DAPI+ within the laminin border. Myofibers were manually counted, and satellite cell number was normalized per myofiber

number. Proliferating satellite cells were identified as Edu+/Pax7+/DAPI+ within the laminin border and were normalized to myofiber number. Satellite cell fusion was determined by the number of myofibers with a sublaminar EdU+/Pax7-/DAPI+ myonucleus relative to the total number of myofibers, which may underestimate total satellite cell fusion in the event that some satellite cells fuse without prior division; however, the EdU+/Pax7-/DAPI+ myonuclei method does facilitate comparable measurement between groups as all groups are treated in the same manner.

Plantar flexion peak torque

Upon completion of the 4-week overload period (SA), strength of the plantaris muscle was assessed as *in vivo* isometric peak tetanic torque, modified from our prior publication.[45] In an anesthesia induction chamber, mice were anesthetized with 2.5% isoflurane vaporized in 1.5 L/min oxygen (VetEquip vaporizer). Mice were then transferred to a secure nose cone with a continuous flow of anesthesia. The right hind limb was analyzed for all mice. Fur was trimmed (Wahl Bravmini, Wahl Corporation) to ensure an unobstructed view to optimized electrode placement. Mice were placed in the supine position on a 37°C temperature regulated platform (809c in-situ mouse apparatus, Aurora Scientific, Aurora, ON, Canada), and the hind limb was secured using a clamp at the knee with the foot placed in a footplate on a dual-mode lever and motor (300D-300C-LRFP, Aurora Scientific). Surgical tape was wrapped around the foot secured inside the footplate to prevent movement of the heel. The footplate and motor arm was adjusted to place the tibia parallel with the platform with a 90-degree angle at the ankle. Teflon-covered needle electrodes were positioned percutaneously lateral to the knee to maximally stimulate the tibial nerve using an electrical stimulator (High Power Bi-Phase Stimulator, Aurora Scientific). Using repeated twitches with the Instant Stimulation function with Live View in Dynamic Muscle Control LabBook (DMC v6.000), placement of needle electrodes was adjusted to generate maximum isometric torque and eliminate antagonistic dorsiflexion

activation. Amperage to produce maximal torque was determined by a progressive series of twitch experiments (0.05 s stimulus duration) beginning with 10 mA and increasing in small increments until the maxim torque stimulated by the minimum amperage was recorded. The amperage then remained constant throughout the force-frequency experiment (10 Hz, 40 Hz, 80 Hz, 120 Hz, 150 Hz, 180 Hz, and 200 Hz, 0.25s stimulus duration with a 2 min rest period between each stimulus) from which isometric peak tetanic torque was recorded. Data was collected using DMC v6.000 and analyzed with Dynamic Muscle Analysis software (DMA v5.501). Plantaris isometric peak tetanic torque is reported as peak torque normalized to body mass (mN*m/g) and normalized to plantaris wet weight (mN*m/mg).

Statistical analysis

All statistical analyses were performed using GraphPad Prism version 7.00 for Mac OS X (GraphPad Software, La Jolla, CA). Two-way ANOVA was utilized to detect statistically significant differences with factors being satellite cell status (SC-WT/SC-Dep) and overload status (Sham/SA). Tukey's post hoc analysis was used to determine differences between individual groups (SC-WT Sham, SC-WT SA, SC-Dep Sham, SC-Dep SA). For plantar flexor peak torque data, an unpaired t-test was used as contractile function was only assessed on the 2 SA groups (SC-WT SA and SC-Dep SA). All data are reported as mean ± standard error of the mean (SEM). For all analyses, $p<0.05$ was considered statistically significant.

RESULTS

Body weight

Body weight was not different between Sham SC-WT and SC-Dep mice; however, there was an effect of overload on body weight ($p=0.0019$) (Fig 2.2A). Plantaris wet weight normalized to body weight was not different between Sham SC-WT and SC-Dep mice;

however there was an effect of overload ($p<0.0001$), and post hoc analyses revealed a difference between SC-WT Sham and SC-WT SA ($p<0.0001$) and between SC-Dep Sham and SC-Dep SA ($p<0.0001$) (Fig 2.2B).

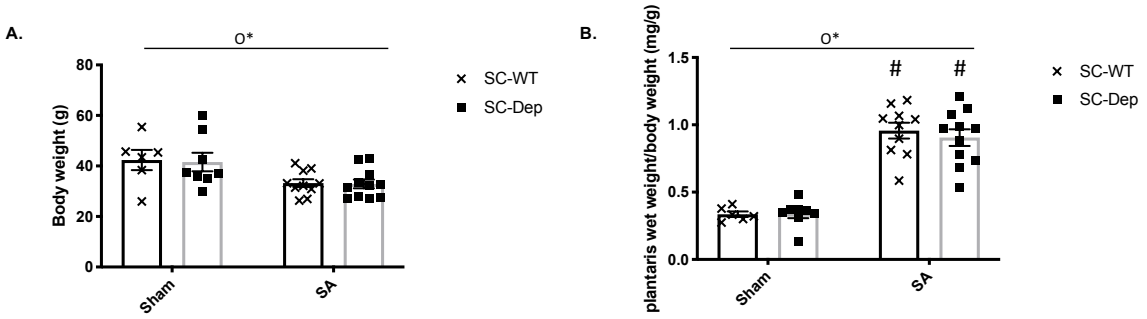

Figure 2.2: Lifelong satellite cell depletion does not alter body weight or overload-induced plantaris wet weight.

A. Body weight is not different between SC-WT and SC-Dep mice without overload (Sham), but there is an effect of overload. B. Plantaris wet weight normalized to body weight is not different between SC-WT and SC-Dep mice without overload (Sham), but there is an effect of overload. # denotes $p<0.05$ compared to Sham with post hoc analysis. O* denotes significant effect of overload ($p<0.05$). Error bars represent standard error of the mean (SEM).

Satellite cell abundance, proliferation, and fusion

There was a significant interaction for Pax7+ satellite cell abundance ($p=0.0230$), with a significant effect of overload status ($p=0.0109$) and satellite cell status ($p<0.0001$). Pax7+ satellite cell abundance was elevated in SC-WT Sham mice compared to SC-Dep Sham mice ($p=0.0074$), confirming effective depletion of satellite cells with tamoxifen treatment. Satellite cells were effectively depleted with tamoxifen treatment, evidenced by 89.01% depletion among Sham mice and 87.10% depletion in overloaded mice (Fig 2.3A). Pax7+ satellite cell abundance did not change with overload in SC-Dep mice ($p=0.9955$), but was significantly greater than baseline/Sham in response to overload in SC-WT mice ($p=0.0082$) (Fig 2.3A). Regarding Edu+/Pax7+ satellite cell abundance—indicative of satellite cell proliferation—there was a significant interaction ($p=0.0029$) with an effect of overload ($p=0.0004$) and satellite cell status ($p=0.0029$). Satellite cell proliferation was not

elevated with overload in SC-Dep mice (p=0.9532) but was significantly elevated with overload in SC-WT mice (p=0.0002) (Fig 2.3B). There was also a significant interaction for EdU+ myonuclei (p=0.0005)—indicative of satellite cell fusion into myofibers—with an effect of overload (p<0.0001) and satellite cell status (p=0.0005). Frequency of fibers with EdU+ myonuclei was not elevated subsequent to overload in SC-Dep mice (p=0.2468) but was increased in SC-WT mice with overload (p<0.0001) (Fig 2.3C). A representative image of Pax7/EdU/laminin/DAPI IHC staining is shown in Figure 2.3D. Collectively, these data indicate that expansion of the satellite cell pool, satellite cell proliferation, and fusion of satellite cells into myofibers occurred predominately in the SC-WT mice in response to overload—indicating that satellite cells remain responsive to an overload stimulus in old skeletal muscle. However, depletion of satellite cells severely impaired myonuclear accrual, suggesting that satellite cells alone contribute new myonuclei during overload.

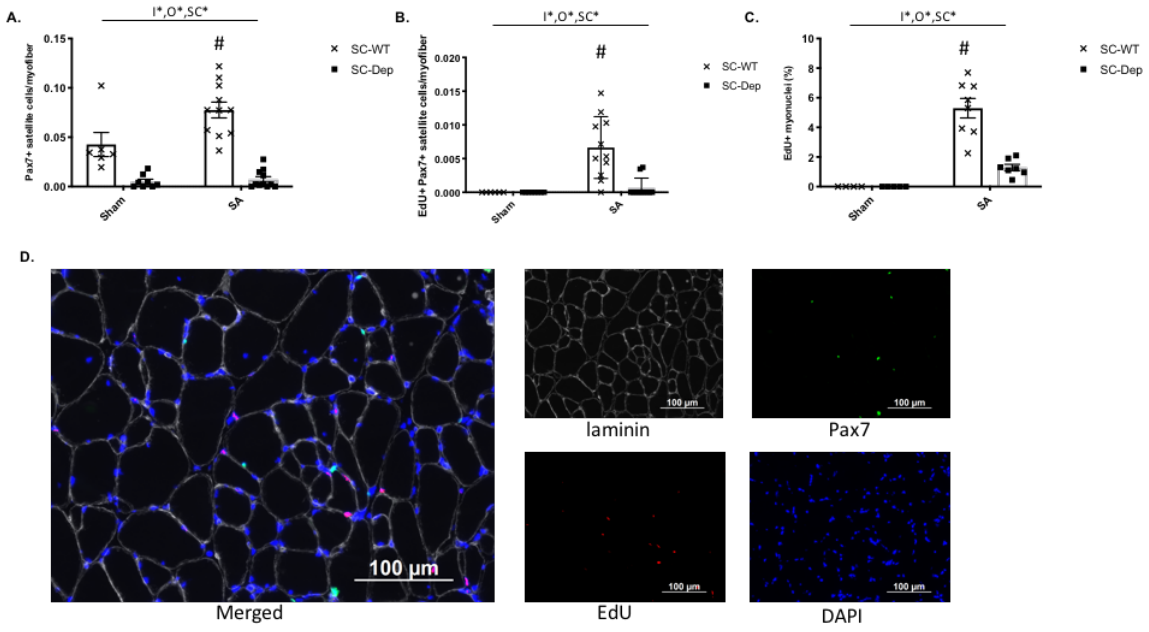

Figure 2.3: Satellite cell abundance, proliferation, and fusion is altered by surgical overload in old SC-WT mice.

A. Satellite cell abundance is different between SC-WT and SC-Dep mice without overload (Sham), confirming effective depletion of satellite cells in SC-Dep mice. Expansion of

satellite cell abundance occurs in SC-WT mice with overload (SA). B. Satellite cell proliferation occurs in SC-WT mice with overload (SA). C. Satellite cell fusion to myofibers occurs in SC-WT mice with overload (SA). D. Representative image of Pax7/EdU/laminin/DAPI immunohistochemical staining.
# denotes $p<0.05$ compared to Sham with post hoc analysis. I* denotes significant interaction ($p<0.05$). O* denotes significant effect of overload ($p<0.05$). SC* denotes significant effect of satellite cell status ($p<0.05$). Error bars represent standard error of the mean (SEM).

Fiber type distribution and fiber type-specific cross sectional area

There was no significant interaction, effect of overload or satellite cell status, or significant post hoc comparison for any fiber type (MHC type I, MHC type IIa, MHC type I/IIa hybrid, and pooled unstained MHC type IIx & IIb), demonstrating no difference in fiber type distribution between SC-WT and SC-Dep mice and no shift in fiber type distribution with surgical overload (Fig 2.4A). Likewise, there were no significant findings regarding pooled or fiber type-specific CSA (Fig 2.4B-F). Additionally, no significant differences existed in any binned fiber CSA distributions (Fig 2.4G), demonstrating a lack of the rightward shift (defined as increased frequency of fibers throughout the 1200-2000 μm^2 range) characteristic of overload-induced hypertrophy in young mice subjected to synergist ablation in conjunction with elevated mean fiber CSA.[32, 41] There was a statistically significant effect of overload on plantaris myofiber number ($p=0.0418$) (Fig 2.4H), supportive of fiber branching and/or splitting which has previously been reported with the extreme loading associated with synergist ablation.[85] A representative image of MHC I/MHC IIa/dystrophin/DAPI IHC staining is shown in Figure 2.4I. For all fiber types, CSA was not different between SC-WT and SC-Dep mice at baseline/Sham, supportive of the previous report that lifelong satellite cell depletion does not exacerbate sarcopenia.[55] Importantly, for all fiber types, there was no significant increase in CSA in SC-WT mice with overload, despite greater plantaris wet weight compared to Sham and superior satellite cell abundance, satellite cell proliferation, and satellite cell fusion in response to surgical overload—indicating that satellite cell proliferation and subsequent fusion to myofibers

was insufficient to support overload-induced hypertrophy with this extended surgical overload period.

Plantar flexion peak torque

Maximal strength, measured as isometric peak tetanic torque in plantar flexion normalized to body weight, did not differ between SC-WT SA and SC-Dep SA mice ($p=0.4785$) (Fig 2.5A). Similarly, peak torque normalized to plantaris wet weight did not differ between SC-WT SA and SC-Dep SA mice ($p=0.9421$) (Fig 2.5B). These data reveal no functional advantage offered by satellite cells with the 4-week surgical overload.

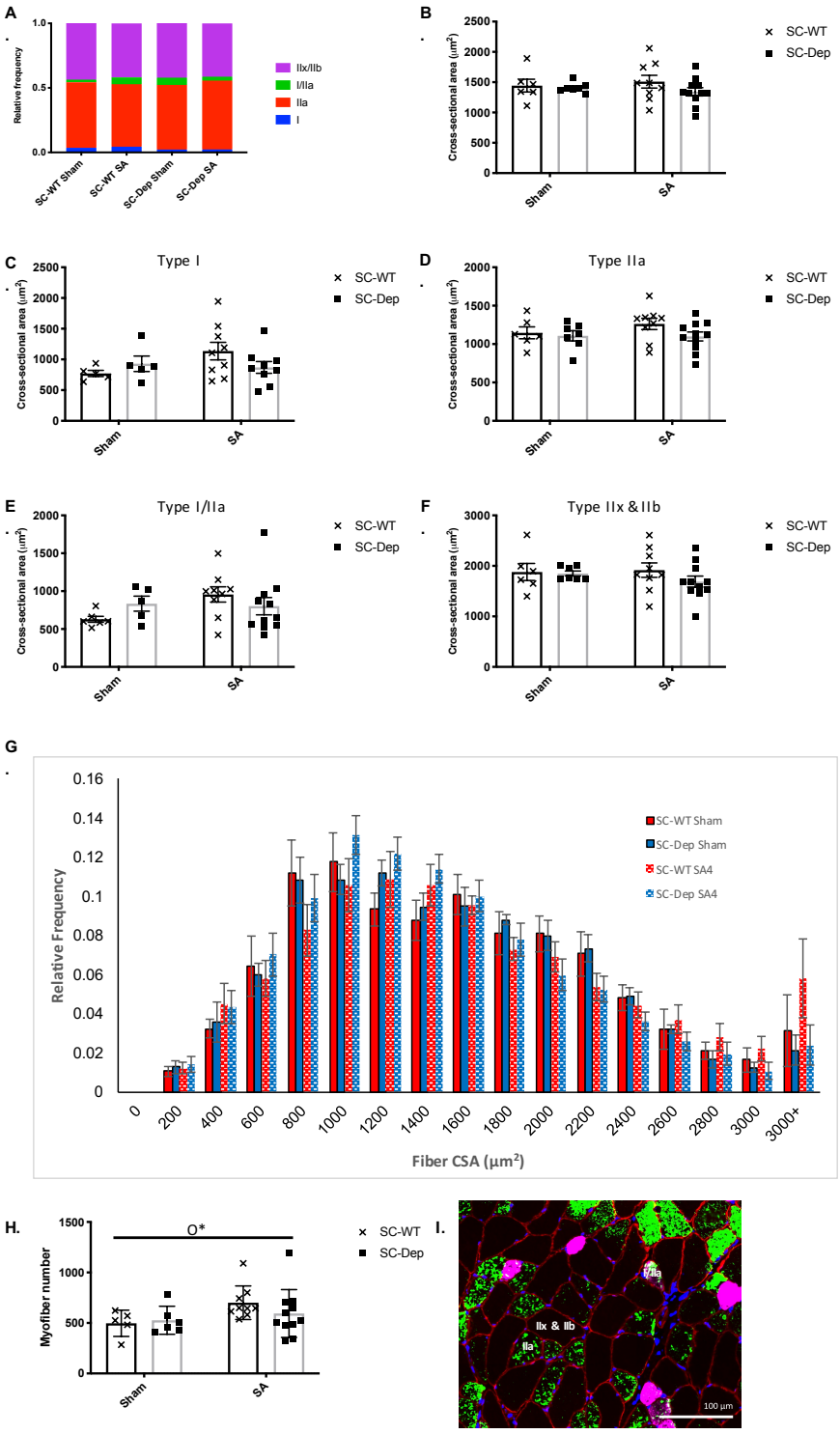

Figure 2.4: Fiber type distribution and fiber type-specific cross sectional area are not altered in old mice subjected to a 4-week surgical overload, independent of satellite cell status.

A. No fiber type shift occurs in SC-WT or SC-Dep mice with overload. B. Hypertrophy of myofibers irrespective of fiber type does not occur in SC-WT or SC-Dep mice with

overload. C. Hypertrophy of type I myofibers does not occur in SC-WT or SC-Dep mice with overload. D. Hypertrophy of type IIa myofibers does not occur in SC-WT or SC-Dep mice with overload. E. Hypertrophy of type I/IIa hybrid myofibers does not occur in SC-WT or SC-Dep mice with overload. F. Hypertrophy of pooled type IIx and IIb myofibers does not occur in SC-WT or SC-Dep mice with overload. G. No hypertrophy occurs in SC-WT or SC-Dep mice with overload, as evidenced by the lack of significant rightward shift in myofiber CSA distribution. H. Myofiber number in SC-WT and SC-Dep mice with overload. I. Representative image of fiber type immunohistochemical staining with dystrophin to denote myofiber borders. O* denotes significant effect of overload ($p<0.05$). Error bars represent standard error of the mean (SEM).

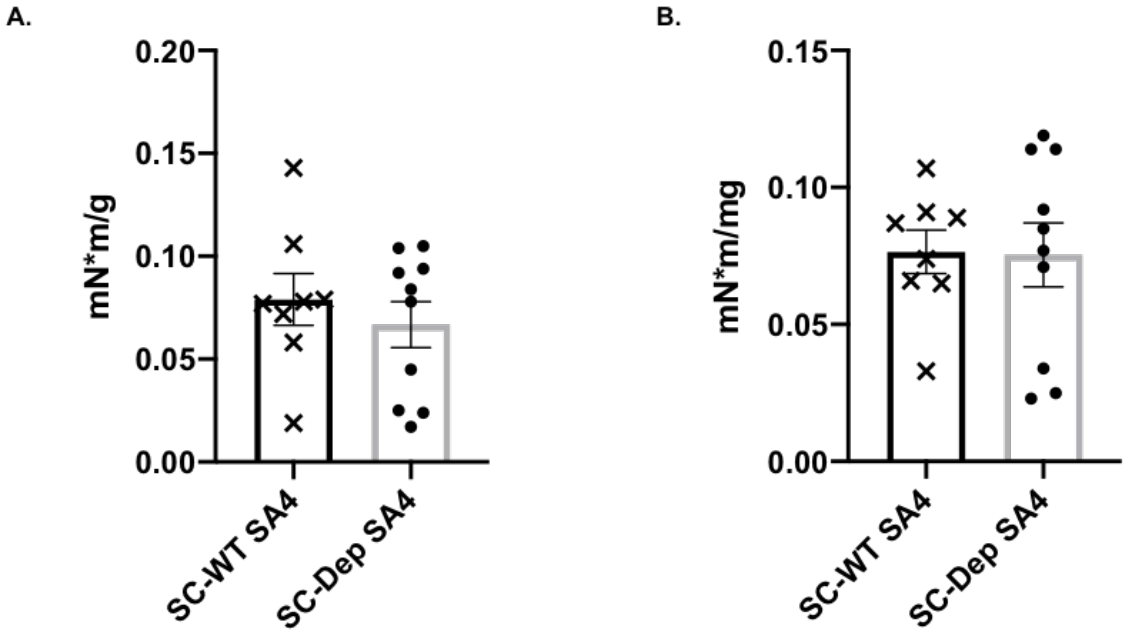

Figure 2.5: Plantaris contractile function does not differ between SC-WT and SC-Dep mice subjected to a 4-week surgical overload.

A. *in vivo* Peak tetanic torque normalized to body weight is not impacted by satellite cell status with overload. B. *in vivo* Peak tetanic torque normalized to plantaris wet weight is not impacted by satellite cell status with overload. Error bars represent standard error of the mean (SEM).

DISCUSSION

The old mice in the current study failed to mount a hypertrophic response to an extended 4-week surgical overload, despite expansion of the satellite cell pool and satellite cell proliferation with subsequent fusion to myofibers in SC-WT mice. Although wet

weight of the plantaris was elevated in response to surgical overload independent of satellite cell status, this did not translate to elevated myofiber CSA and is likely explained by the observed effect of surgical overload to increase myofiber number in both SC-WT and SC-Dep old mice, likely representative of fiber splitting which has previously been reported with extreme loading models in animals.[85] Additionally, accumulation of extracellular matrix products—which have already been shown to expand with synergist ablation in old mice[44]—may further contribute to altered plantaris wet weight. Previously, a shorter duration 2-week overload period was reported to also not produce hypertrophy in old mice determined by myofiber CSA, independent of satellite cell status.[44] Similar to the current findings, muscle wet weight was elevated by a 2-week surgical overload in old satellite cell replete and deplete mice[44], but to a lesser extent compared to the 4-week overload performed in this study—suggesting that potential contributors to the enlarged wet muscle weight continue to accumulate past the initial 2-week overload period. However, the same short 2-week surgical overload period was sufficient to produce hypertrophy in young mice with and without satellite cells,[41] underscoring the blunted hypertrophic response to overload in old compared to young skeletal muscle which was also reported with a direct comparison of young and old C57BL/6 mice subjected to a 6-week overload.[21] Due to the lack of overload-induced hypertrophy in old mice with this common surgical overload model—despite the extended 4-week overload period—the original hypothesis regarding the requirement of satellite cells to support overload-induced hypertrophy specifically in aging skeletal muscle could not be directly tested. Instead, this work importantly highlights the need for a more effective murine model to induce overload-induced hypertrophy specifically in old mice to study mechanisms of hypertrophy in aging skeletal muscle. Clearly, the surgical synergist ablation model of overload-induced myofiber hypertrophy, which has been well documented as effective to elicit muscle growth in young mice,[32, 41] is not an appropriate or translational model to mimic and

mechanistically study overload-induced hypertrophy in aging skeletal muscle that occurs in humans with resistance exercise.[77]

The observation of a lack of overload-induced hypertrophy despite expansion of the satellite cell pool, elevated satellite cell proliferation, and satellite cell fusion to myofibers in SC-WT SA mice aligns with the previous finding of myonuclear accretion without concurrent growth in response to the shorter 2-week overload in old mice, again highlighting plasticity of the myonuclear domain.[44] However, others have reported synergist ablation-induced fiber type adaptations independent of satellite cell status in the absence of hypertrophy in old mice.[44] Although the current findings also demonstrate no hypertrophy regardless of satellite cell status, no significant fiber type adaptations were observed with the 4-week surgical overload. Lee et al reported a significant shift toward increased expression of type IIa and IIb fibers with a concomitant decrease of IIx fibers, restoring a fiber type distribution similar to that observed in plantaris muscles of young mice compared to the age-associated loss of IIb with an increase in IIx fibers.[55] However, with a 6-week surgical overload in C57BL/6 mice, Ballak et al reported blunted overload-induced hypertrophy in old mice compared to young with a decrease in type IIb fiber frequency,[21] contrasting the fiber type adaptations observed by Lee et al. In the current study, IIx and IIb fibers were not separately distinguished immunohistochemically, so overload-induced adaptations could not be assessed individually but only on a pooled basis for IIx and IIb fibers, limiting identification of subtle fiber type distribution adaptations.

In addition to a lack of overload-induced hypertrophy, surgical overload did not produce a functional advantage in the mice with satellite cells (SC-WT SA) compared to those in which satellite cells were depleted (SC-Dep SA). The current findings are unique in that *in vivo* isometric peak tetanic torque was assessed following overload, leaving neuromuscular anatomy and blood flow fully intact. Others have demonstrated with *in situ* contractile force measurement that maximal tetanic force of the plantaris is not altered with a 7-week surgical overload in old C57BL/6 mice.[86] However, the current study is the first

to report the inability of synergist ablation to stimulate an *in vivo* functional adaptation in old mice.

One group has reported significant, albeit blunted, overload-induced hypertrophy in plantaris muscles of old mice subjected to a surgical overload stimulus.[21, 86] However, the surgical intervention utilized in these studies differs from the current study with the gastrocnemius and soleus muscles not being partially removed but instead denervated by cutting the medial and lateral branches of the tibial nerve. The difference in surgical approach may contribute to the contrasting findings relative to the current study, along with the duration of the overload period. The aforementioned studies utilized 6-week and 7-week overload periods following surgical denervation of agonists of the plantaris muscle, so a much longer overload period may be necessary to generate overload-induced hypertrophy in old mice compared to the sufficient 2-week period for young mice.[41] This denervation model of surgical overload requires a high level of technical skill likely requiring extensive training, which may limit use as a practical murine model of overload-induced hypertrophy. Furthermore, synergist ablation via denervation of the tibial nerve was performed unilaterally, in contrast to the bilateral approach of surgical overload used in the current study and in the majority of reported surgical overload studies. A unilateral surgical intervention facilitates use of the alternate hind limb as an internal control but may impair normal gait biomechanics in an unbalanced manner, and thus confound interpretation of results dependent on mechanical overload.

In summary, surgical overload offers inadequate capacity to induce hypertrophy in skeletal muscle of old mice, limiting translational use of this model to study mechanisms of hypertrophy in aging skeletal muscle. A murine overload model including an aerobic exercise component to concurrently enhance muscle capillarization may prove more effective to stimulate hypertrophy in old mice—since adequate muscle capillarization supports the hypertrophic response to resistance exercise in older adults[87]—and thus present a novel pre-clinical model to optimally examine aging skeletal muscle hypertrophy.

Based upon these findings, a novel murine model addressing this need is proposed in Chapter 3 of this dissertation.

CHAPTER 3:

Progressive weighted wheel running stimulates satellite cell expansion, myonuclear accrual, and overload-induced hypertrophy concurrently with capillarization in skeletal muscle of aging mice to support functional adaptation

INTRODUCTION

Age-related atrophy of skeletal muscle and concurrent decline in muscle strength and physical function, termed sarcopenia, directly contribute to development of progressive disability with aging.[12, 14] To combat the sarcopenic decline into disability, clinical exercise studies have long sought to optimize overload-induced skeletal muscle hypertrophy in older adults, primarily through variations of resistance exercise. Many modes of exercise have proven effective to elicit a hypertrophic response with improved muscle strength, albeit blunted perhaps, in older adults.[13, 77, 87, 88] However, exercise studies in humans are limited regarding the capacity to explore cellular and molecular mechanisms mediating or limiting overload-induced hypertrophy, strength gain, and other exercise-induced adaptations.

In conjunction with human exercise studies, pre-clinical translational mouse models offer the opportunity to more deeply investigate mediators of exercise adaptations, specifically hypertrophy and subsequent strength gain. Multiple approaches have been successfully employed to generate overload-induced hypertrophy in young healthy mice;[89] however, old mice have been resistant to hypertrophy in previously reported models,[44, 90] obscuring mechanistic examination of overload-induced hypertrophy to optimize exercise interventions for mitigation of sarcopenia.

A novel and practical exercise model utilizing progressive weighted wheel running (PoWeR) was recently reported to elicit substantial but not supraphysiological hypertrophy, expansion of the satellite cell pool, and myonuclear accretion in young mice, comparable to typical results from resistance exercise training studies in humans.[46] PoWeR is promising compared to other murine hypertrophy models as it requires simple modification of running wheels, does not require exposure to anesthetic gas and recovery from surgery, and is easily reversible for the study of detraining effects. Furthermore, in addition to offering a novel murine hypertrophy model, PoWeR includes a significant endurance training component with metabolic adaptions also reported in young mice,[46] akin to concurrent exercise training.

In the current study, we examine the efficacy of PoWeR as a pre-clinical exercise model to produce a hypertrophic response with satellite cell expansion and increased muscle strength in old mice, comparable to that previously observed in older adults with resistance exercise training. Since adequate muscle capillary density may be essential to facilitate overload-induced hypertrophy in older adutlts,[87] we also explore alterations to muscle capillarization induced by PoWeR that may facilitate a hypertrophic response not observed in other hypertrophy models in old mice.

MATERIALS AND METHODS

Ethical approval

Animal procedures were approved by the Institutional Animal Care and Use Committee at the University of Kentucky. All mice were singly housed in the same temperature and humidity controlled room on a 12h:12h light-dark cycle. Mice were given ad libitum access to food and water and were euthanized by cervical dislocation under deep anesthesia.

Experimental design

Twenty-two-month-old female C57BL/6 mice were obtained from the Charles River Laboratories National Institute of Aging research colony. Mice were randomly assigned to the PoWeR or sedentary control group. Mice in the PoWeR group were singly housed in cages with running wheels to allow for monitoring of individual running volume using ClockLab software, and mice in the sedentary group were singly housed in cages without running wheels. Following an introductory week with an unweighted wheel, 8 weeks of PoWeR training commenced with the following weight progression: 2 g in week 1, 3 g in week 2, 4 g in week 3, and 5 g in weeks 4-8. One g magnets (product no. B661, K&J Magnetics, Pipersville, PA) were affixed to one side of the wheel to allow for the progressive increase in weight. As previously described,[46] the asymmetrical loading pattern of the weight produced an unbalanced wheel, resulting in frequent stopping and restarting of running which forced the mice to overcome the weight of the wheel repeatedly instead of relying on momentum after the initial starting effort. Mice were 24 months old upon completion of the experiment. The PoWeR protocol was modified based upon the PoWeR protocol previously reported to be effective to elicit hypertrophy in young mice.[46] Following 8 weeks of PoWeR or sedentary control, contractile function of plantar flexors was assessed on the right hind limb, and mice were humanely euthanized by cervical dislocation under deep anesthesia. Plantar flexor muscles (soleus, plantaris, and gastrocnemius) were rapidly dissected. Muscle from the right hind limb was processed for immunohistochemical analyses, and muscle from the left leg was processed for RNA isolation. Figure 3.1 illustrates the study design.

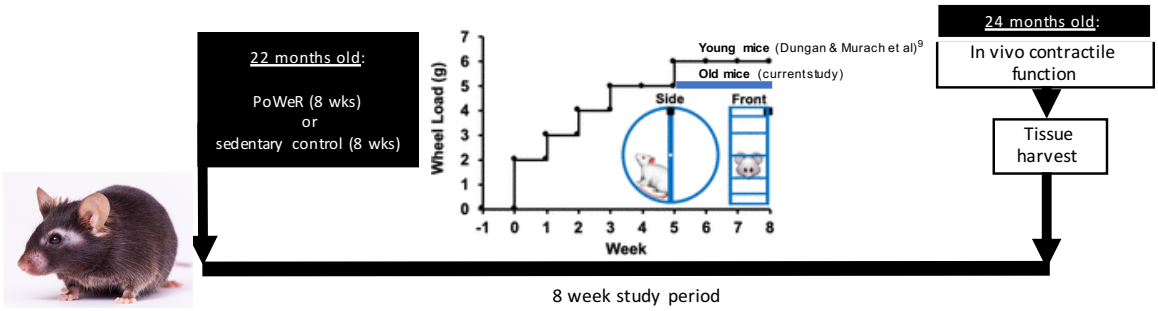

Figure 3.1: Study Schematic.

Immunohistochemistry

Immunohistochemistry (IHC) analyses were performed on soleus, plantaris, and gastrocnemius muscles—comprising the entire plantar flexor complex. Each muscle from the right hind limb was covered in Tissue Tek (O.C.T. Compound, Sakura Finetek, Torrance, CA, USA) at resting length and frozen in liquid nitrogen-cooled 2-methylbutane on a foil-covered cork. Samples were stored at -80°C until analysis. Using a cryostat (HM525-NX, Thermo Fisher Scientific, Waltham, MA, USA), 7µm-thick sections were cut from each muscle and air dried for 1 h on slides. Slides were stored at -20°C prior to IHC staining.

For immunofluorescent detection of satellite cells and myonuclei, sections were fixed in 4% paraformaldehyde (PFA) for 7 min at room temperature followed by washes with phosphate buffered saline (PBS, pH 7.5). Antigen retrieval was performed with sodium citrate (10mM, pH 6.5) in a 92°C water bath for 20 min. Slides were allowed to cool to room temperature and washed in PBS followed by blocking of endogenous peroxidases with 3% hydrogen peroxide for 7 min. Slides were then washed in PBS and blocked for 1 h in a mouse-on-mouse Ms IgG blocking solution (cat#MKB-2213, Vector Laboratories). Slides were washed again in PBS and blocked for 1 h in 1% blocking reagent included in a commercially available tyramide signal amplification kit (Life Technologies/Thermo Fisher Scientific), followed by overnight incubation at 4°C in primary antibodies against Pax7 (mouse IgG, 1:100; Developmental Studies Hybridoma

Bank) and laminin (rabbit IgG, 1:200; L9393, Millipore Sigma) in the 1% blocking reagent. On the following day, slides were washed in PBS and incubated for 90 min at room temperature in goat anti-mouse biotinylated secondary antibody (1:1000; #115-065-205, Jackson Immuno Research) and goat anti-rabbit secondary antibody directly conjugated to Alexa Fluor 488 (1:500; #A11034, Invitrogen). Slides were washed in PBS and incubated for 1 h at room temperature in streptavidin conjugated to horse radish peroxidase included in a commercially available tyramide signal amplification kit (SA-HRP, Life Technologies/Thermo Fisher Scientific). Following another wash in PBS, Pax7 was amplified by incubation for 20 min at room temperature in TSA-Alexa Fluor 555 (1:100 in amplification diluents; #T30955, Invitrogen). Slides were washed in PBS, incubated for 10 min in 4′,6-diamidino-2-phenylindole (DAPI; 10 nM, Life Technologies/Thermo Fisher Scientific), washed again in PBS, and mounted using Vectashield fluorescence mounting media (Vector Laboratories, Burlingame, CA, USA).

For immunofluorescent assessment of muscle fiber type distribution and fiber type-specific cross sectional area (CSA), sections were blocked for 1 h at room temperature in a mouse-on-mouse Ms IgG blocking solution (cat#MKB-2213, Vector Laboratories) followed by a wash in PBS. Slides were incubated overnight at 4°C in primary antibodies against dystrophin (rabbit IgG, 1:100; #sc-15376, Santa Cruz) and myosin heavy chain (MHC) type I (mouse IgG2b, 1:100; BA.D5 concentrate, Developmental Studies Hybridoma Bank) in myosin heavy chain type IIa supernatant (mouse IgG1; SC.71, Developmental Studies Hybridoma Bank). On the following day, slides were washed in PBS and incubated for 90 min at room temperature in goat anti-mouse IgG1 AF488 secondary antibody (1:500; #A21121, Invitrogen), goat anti-mouse IgG2b AF647 secondary antibody (1:250; #A21242, Invitrogen), and goat anti-rabbit IgG AF555 secondary antibody (1:500; #A21428, Invitrogen) in PBS. Slides were washed in PBS and incubated in DAPI (10nM, Life Technologies/Thermo Fisher Scientific) followed by post-

fixation for 3 min in methanol and another wash in PBS. Slides were mounted using Vectashield fluorescence mounting media (Vector Laboratories, Burlingame, CA, USA).

For immunofluorescent detection of muscle capillaries, sections were fixed in acetone for 10 min at -20°C and washed in PBS. Slides were blocked for 1 h in 2.5% normal horse blocking solution (#S-2012, Vector Laboratories) at room temperature and incubated overnight in primary antibodies against CD31 (rat IgG, 1:100; #550274, BD Biosciences) and laminin (rabbit IgG, 1:200; L9393, Millipore Sigma) in 2.5% normal horse serum at 4°C. The following day, slides were washed in PBS and incubated for 1 h in goat anti-rabbit secondary directly conjugated to Alexa Fluor 488 (1:500; #A11034, Invitrogen) and goat anti-rat Cy3 secondary (1:250; #550274, BD Biosciences) in PBS. Slides were washed again in PBS followed by incubation in DAPI for 10 min (10nM, Life Technologies/Thermo Fisher Scientific), additional washing in PBS, and mounting with Vectashield fluorescence mounting media (Vector Laboratories, Burlingame, CA, USA).

Image acquisition and analysis

Images were captured at 100-200x magnification with a Zeiss upright microscope (AxioImager M1; Zeiss, Oberkochen, Germany). Image analysis was performed in a blinded manner by the same assessor using Zen Blue software for manual counting of satellite cells. Satellite cells were identified as Pax7+/DAPI+ within the laminin border. Myofibers were manually counted, and satellite cell number was normalized per 100 myofibers. Myovision software was used for automated analysis of myonuclear density normalized to myofiber number, fiber type distribution, and fiber type-specific CSA. Unstained myofibers were counted as MHC IIx/IIb fibers. Zen Blue was used for manual analysis of all capillary indices which were calculated as previously reported by our laboratory.[87] Briefly, capillary contacts were counted as the total number of capillaries in contact with the myofiber. The capillary-to-fiber ratio was calculated as the number of capillaries divided by a sharing factor (the number of myofibers sharing the same

capillary). The capillary-to-fiber-perimeter-exchange index was measured as the supply of capillaries relative to the myofiber perimeter (capillary-to-fiber ratio/perimeter of the myofiber). The index of the capillary to fiber interface was calculated as the percentage of the capillary in contact with the myofiber.

Plantar flexor peak torque

Upon completion of 8 weeks of PoWeR training or the sedentary control period, strength of the plantar flexor muscle complex was assessed in the 24-month-old mice by *in vivo* isometric peak tetanic torque. In an induction chamber, mice were anesthetized with 2.5% isoflurane vaporized in 1.5 L/min oxygen (VetEquip vaporizer). Mice were then transferred to a secure nose cone with a continuous flow of isoflurane in oxygen. The right hind limb was analyzed for all mice, and fur was trimmed (Wahl Bravmini, Wahl Corporation) to ensure unobstructed electrode placement. Mice were placed in the supine position on a 37°C temperature regulated platform (809c in-situ mouse apparatus, Aurora Scientific, Aurora, ON, Canada), and the hind limb was secured using a clamp at the knee with the foot placed in a footplate on a dual-mode lever and motor (300D-300C-LRFP, Aurora Scientific). Surgical tape was wrapped around the foot secured to the footplate to prevent movement of the heel of placement shifting, and the footplate and motor arm was adjusted to place the tibia parallel with the platform with a 90-degree angle at the ankle. Needle electrodes were positioned percutaneously slightly lateral to the knee to maximally stimulate the tibial nerve using an electrical stimulator (High Power Bi-Phase Stimulator, Aurora Scientific). Using repeated twitches with the Instant Stimulation function with Live View in Dynamic Muscle Control LabBook (DMC v6.000), placement of needle electrodes was adjusted to optimize location to generate maximum isometric torque and eliminate antagonistic dorsiflexion. Optimal amperage to produce maximal torque was determined by a progressive series of twitch experiments (0.05 s stimulus duration) beginning with 10 mA and increasing in small increments until the maxim torque stimulated by the minimum

amperage was recorded. The amperage then remained constant throughout the force-frequency experiment (10 Hz, 40 Hz, 80 Hz, 120 Hz, 150 Hz, 180 Hz, and 200 Hz, 0.25s stimulus duration with a 2 min rest period between each stimulus) from which isometric peak tetanic torque was recorded. Data was collected using DMC v6.000 and analyzed with Dynamic Muscle Analysis software (DMA v5.501). Plantar flexor isometric peak tetanic torque is reported as peak torque normalized to body mass (mN*m/g).

RNA isolation and RNA-seq

Muscle from the left hind limb was flash frozen in liquid nitrogen and stored at -80°C. Soleus and plantaris muscles were homogenized (n: Control=5, PoWeR=4 for both plantaris and soleus; samples were not pooled) in TRI Reagent (R2050-1-200, Zymo Research). RNA was isolated using the Direct-zol RNA Miniprep kit (R2051, Zymo Research) per manufacturer's instructions. RNA concentration and quality (RIN>8.1) was assessed with an RNA Nano chip kit on a bioanalyzer by the University of Kentucky Genomics Core Laboratory. Isolated RNA was sent to Novogene for library construction, sequencing, and preliminary bioinformatic analyses. Preliminary downstream analysis was performed by Novogene using a combination of programs: STAR, HTseq, Cufflink, and proprietary wrapped scripts. Alignments were parsed with Tophat and differential expression was determined using the edgeR R package (3.16.5). P values were adjusted using the Benjamini and Hochberg method, and a corrected p value of 0.05 and absolute fold change of 1 were considered the threshold for significantly differential expression. Gene ontology (GO) enrichment analysis of differentially expressed genes was performed using the clusterProfiler R package. GO terms with a corrected p value less than 0.05 were classified as significantly enriched by differentially expressed genes.

Statistical analysis

All statistical analyses were performed using GraphPad Prism version 7.00 for Mac OS X (GraphPad Software, La Jolla, CA). For each outcome, unpaired t-tests were utilized to detect statistically significant differences between PoWeR and control groups. All data are reported as mean ± standard error of the mean (SEM).

RESULTS

Voluntary wheel running activity, body weight, and plantar flexor muscle weights

Voluntary activity was measured as kilometers run on the wheel per day (km/day), reported as a weekly average for each mouse. Over the 8 week period, old mice ran on average 6.35 ± 0.72 km/day. This remained consistent each week, except for a slight peak of 8.20 ± 1.04 km/day at Week 2 (Fig 3.2A).

Old mice tended to have lower body weight with PoWeR ($p=0.0625$; Fig 2B). Soleus wet weight was elevated in old mice subjected to PoWeR ($p=0.0108$; Fig 3.2C). Plantaris and gastrocnemius wet weights were not altered (Fig 3.2D-E).

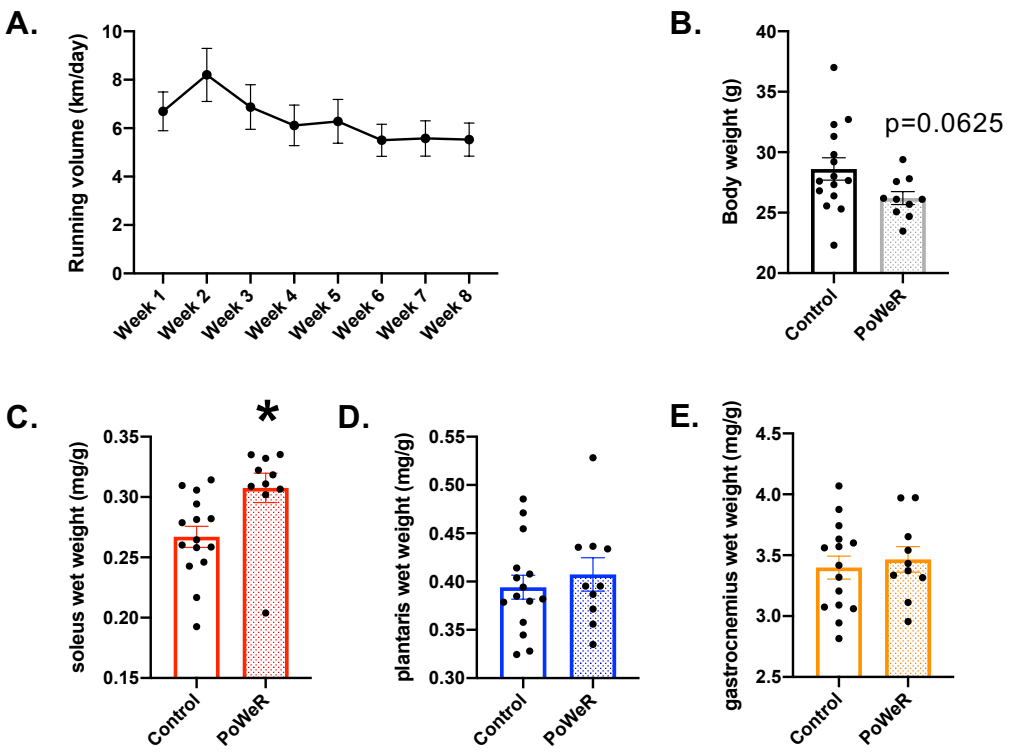

Figure 3.2: Voluntary running volume, body weight, and plantar flexor wet weight adaptations to progressive weighted wheel running in old mice.

A. Voluntary running volume is maintained by old mice throughout 8 weeks of PoWeR. B. Body weight tends to decrease in old mice subjected to PoWeR. C. Soleus wet weight normalized to body weight is elevated in old mice with PoWeR. D-E. Plantaris and gastrocnemius wet weights normalized to body weight are not altered in old mice with PoWeR. *p<0.05. Error bars represent standard error of the mean (SEM).

Satellite cell abundance and myonuclear density adaptions to PoWeR in aging skeletal muscle

Satellite cell abundance (number of satellite cells normalized to 100 myofibers) was elevated in PoWeR mice compared to sedentary control mice in soleus ($p<0.0001$; Fig 3.3A). Myonuclear density (number of myonuclei normalized to myofiber number) was elevated in the soleus muscles of PoWeR mice, irrespective of fiber type ($p=0.0036$; Fig 3.3B). Likewise, PoWeR resulted in increased myonuclear density of the soleus in type I fibers expressing myosin heavy chain I ($p=0.0194$; Fig 3.3C), type IIa fibers expressing myosin heavy chain IIa ($p=0.0018$; Fig 3.3D), and unstained type IIx and IIb fibers

(p=0.0369; Fig 3.3E). A representative image of Pax7, laminin, and DAPI immunohistochemical staining in soleus is shown in Figure 3.3F.

Plantaris satellite cell abundance was similarly elevated in old mice with PoWeR (p=0.0005: Fig 3.3G). Overall myonuclear density in the plantaris was not significantly impacted by PoWeR (Fig 3.3H), with similar lack of myonuclear accrual in type I fibers (Fig 3.3I) and type IIx and IIb fibers (Fig 3.3K); however, myonuclear content of type IIa fibers demonstrated elevation with PoWeR (p=0.0242; Fig 3.3J). A representative image of immunohistochemical staining in plantaris is shown in Figure 3.3L.

Gastrocnemius demonstrated a non-significant elevation in satellite cell abundance (p=0.1406; Fig 3.3M). Myonuclear density irrespective of fiber type was not impacted by PoWeR (Fig 3.3N) and similarly was not elevated in any specific fiber type (Fig 3.3O-Q). A representative image of immunohistochemical staining in gastrocnemius is shown in Figure 3.3R.

Collectively, these data indicate efficacy of PoWeR to expand the satellite cell pool and stimulate myonuclear accrual in aging skeletal muscle, particularly in the soleus and plantaris muscles.

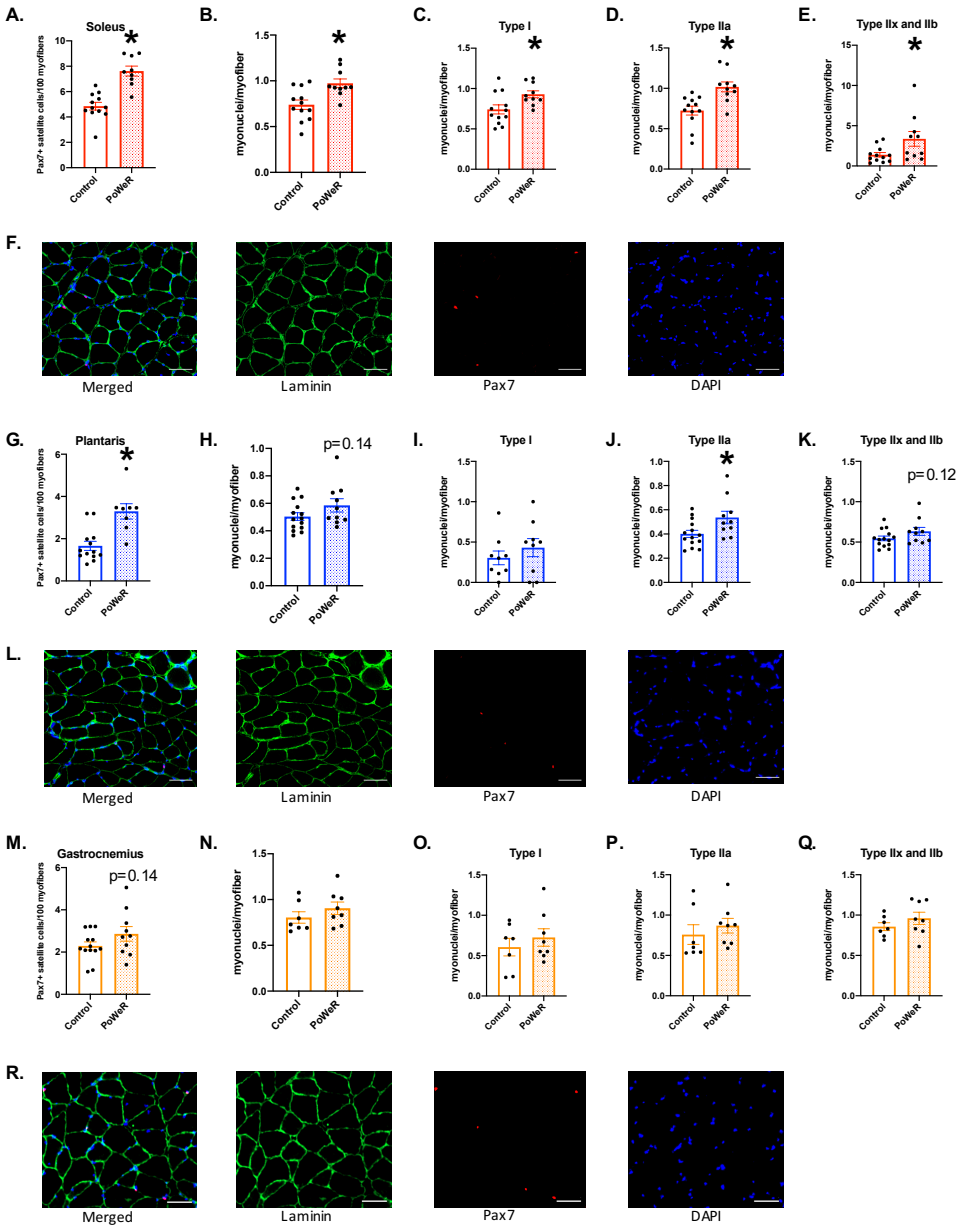

Figure 3.3: Satellite cell abundance and myonuclear density adaptations to progressive weighted wheel running in old mice.

A. Satellite cell abundance is increased in soleus muscles of old mice subjected to PoWeR. B-E. Myonuclear content is elevated in myofibers of the soleus in old mice subjected to PoWeR, irrespective of fiber type (B) and specifically in each fiber type (C-E). F. Representative immunohistochemical image of laminin/Pax7/DAPI in the soleus of a PoWeR old mouse. G. Satellite cell abundance is increased in plantaris muscles of old mice subjected to PoWeR. H-K. Myonuclear content demonstrates a trend toward elevation in myofibers of the plantaris in old mice with PoWeR (H) with no change in fiber type I myonuclear content (I), elevation in fiber type IIa myonuclear content (J), and a trend toward elevated fiber type IIx and IIb myonuclear content (K). L. Representative

immunohistochemical image of laminin/Pax7/DAPI in the plantaris of a PoWeR old mouse. M. Satellite cell abundance may be elevated in the gastrocnemius muscles of old mice subjected to PoWeR. N-Q. Myonculear content is not significantly altered in myofibers of the gastrocnemius in old mice with PoWeR. R. Representative immunohistochemical image of laminin/Pax7/DAPI in the gastrocnemius of a PoWeR old mouse. *$p<0.05$. Scale bars= 50μm. Error bars represent standard error of the mean (SEM).

Muscle fiber type and size adaptations to PoWeR in aging skeletal muscle

Oxidative fiber type adaptations were observed in response to PoWeR. In soleus muscles of PoWeR mice compared to sedentary control mice, there was a significant shift toward elevated abundance of type I fibers ($p=0.001$) with a concomitant decrease in type IIa fibers ($p=0.001$) and no change in relative frequency of IIx and IIb fibers ($p=0.185$; Fig 3.4A). In soleus muscles, PoWeR resulted in elevated overall mean myofiber CSA ($p=0.0111$; Fig 3.4B). Soleus type I fibers demonstrated higher CSA with PoWeR ($p=0.0432$; Fig 3.4C), and significant growth was observed in type IIa ($p=0.0086$; Fig 3.4D) with no change in size of the infrequent highly glycolytic type IIx and IIb fibers (Fig 3.4E). A representative image of dystrophin and myosin heavy chain isoform immunohistochemical staining in soleus is shown in Figure 3.4F.

Plantaris muscles of PoWeR mice demonstrated significantly elevated abundance of type IIa fibers ($p<0.0001$) with a decrease in type IIx and IIb fibers ($p<0.0001$) and no change in relative frequency of type I fibers ($p=0.206$; Fig 3.4G). A statistical trend toward elevation of overall mean myofiber CSA was observed in plantaris muscles of PoWeR mice ($p=0.0765$; Fig 3.4H). CSA was not altered with PoWeR in the low abundance type I fibers of the plantaris (Fig 3.4I); however, CSA was elevated by PoWeR in type IIa ($p<0.0001$; Fig 3.4J) and type IIx and IIb fibers ($p=0.0426$; Fig 3.4K). A representative image of immunohistochemical staining in plantaris is shown in Figure 3.4L.

Gastrocnemius muscles of PoWeR mice exhibited decreased frequency of the predominant glycolytic type IIx and IIb fibers ($p=0.001$) with elevated frequency of type IIa fibers ($p<0.001$) and non-significant doubling of type I fibers ($p=0.137$; Fig 3.4M).

Gastrocnemius overall mean CSA was not significantly altered by PoWeR (Fig 3.4N) with CSA of the relatively low abundance type I fibers remaining unchanged (Fig 3.40); however, CSA was elevated in the more abundant type IIa (p=0.047; Fig 3.4P) but not the predominant highly glycolytic type IIx and IIb fibers (p=0.266; Fig 3.4Q). A representative image of immunohistochemical staining in gastrocnemius is shown in Figure 3.4R.

Unlike the extreme loading model of synergist ablation reported in Chapter 2 of this Dissertation, PoWeR did not alter fiber number in any of the plantar flexor muscles. Collectively, these data highlight the efficacy of PoWeR to elicit oxidative fiber type adaptations along with fiber type-specific overload-induced myofiber hypertrophy in aging skeletal muscle.

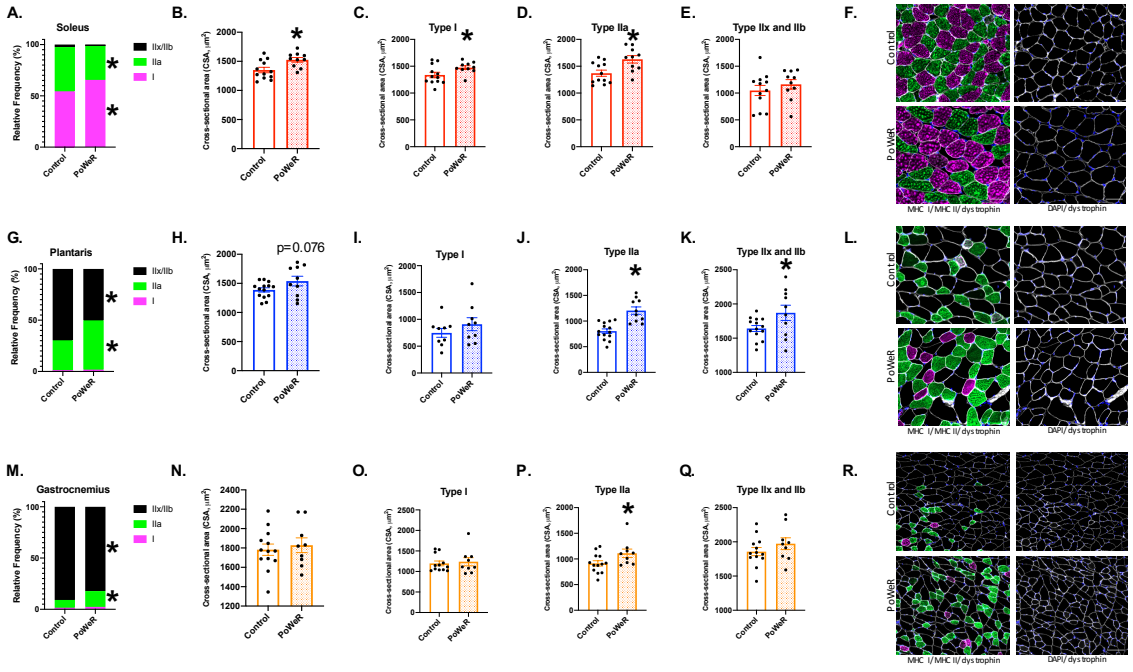

Figure 3.4: Skeletal muscle fiber type and size adaptation to progressive weighted wheel running in old mice.

A. An oxidative fiber type shift occurs in soleus muscles of old mice subjected to PoWeR. B-E. Cross-sectional area of myofibers in the soleus muscles of old mice is elevated with PoWeR, regardless of fiber type (B) and specifically in type I fibers (C) and type IIa fibers (D) but not type IIx and IIb fibers (E). F. Representative immunohistochemical images of MHC I/MHC II/dystrophin/DAPI in soleus muscles of Control and PoWeR old mice. G. An oxidative fiber type shift occurs in plantaris muscles of old mice with PoWeR. H-K.

Cross-sectional area of myofibers in the plantaris muscles of old mice demonstrate a trend toward elevation with PoWeR (H) with no change in type I fibers (I) and significant increase in type IIa (J) and type IIx and IIb fibers (K). L. Representative immunohistochemical images of MHC I/MHC II/dystrophin/DAPI in plantaris muscles of Control and PoWeR old mice. M. An oxidative fiber type shift occurs in gastrocnemius muscles of old mice with PoWeR. N-Q. Pooled cross-sectional area of myofibers in the gastrocnemius muscles of old mice is not altered by PoWeR (N) with no change in type I fibers (O), significant elevation in type IIa fibers (P), and no change in type IIx and IIb fibers (Q). R. Representative immunohistochemical images of MHC I/MHC II/dystrophin/DAPI in gastrocnemius muscles of Control and PoWeR old mice. MHC= myosin heavy chain. *$p<0.05$. Scale bars= 50μm for soleus and plantaris and 100μm for gastrocnemius. Error bars represent standard error of the mean (SEM).

Muscle capillary adaptations to PoWeR in aging skeletal muscle

Capillary density measured as capillary contacts per fiber and capillary to fiber ratio (C:Fi) was elevated in soleus muscles of PoWeR mice ($p<0.0001$; Fig 3.5A and $p=0.0412$; Fig 3.5B, respectively), as was capillary to fiber perimeter exchange (CFPE) ($p=0.0489$; Fig 3.5C) and capillary to fiber interface (LCPF) ($p=0.0048$; Fig 3.5D). A representative image of CD31, laminin, and DAPI immunohistochemical staining in soleus is shown in Figure 3.5E.

In plantaris muscles of PoWeR mice, capillary contacts and C:Fi were increased ($p=0.0002$; Fig 3.5F and $p=0.0001$; Fig 3.5G, respectively), along with CFPE ($p=0.0056$; Fig 3.5H) and LCPF ($p=0.0175$; Fig 3.5I). A representative image of immunohistochemical staining in plantaris is shown in Figure 3.5J.

Likewise, capillary contacts in gastrocnemius muscles of PoWeR mice demonstrated a statistical trend toward elevation ($p=0.0940$; Fig 3.5K) with significant elevation of C:Fi ($p=0.0338$; Fig 3.5L), CFPE ($p=0.0147$; Fig 3.5M), and LCPF ($p=0.0450$; Fig 3.5N). A representative image of immunohistochemical staining in gastrocnemius is shown in Figure 3.5O.

Collectively, these data demonstrate the efficacy of PoWeR to stimulate robust angiogenic adaptations in aging skeletal muscle.

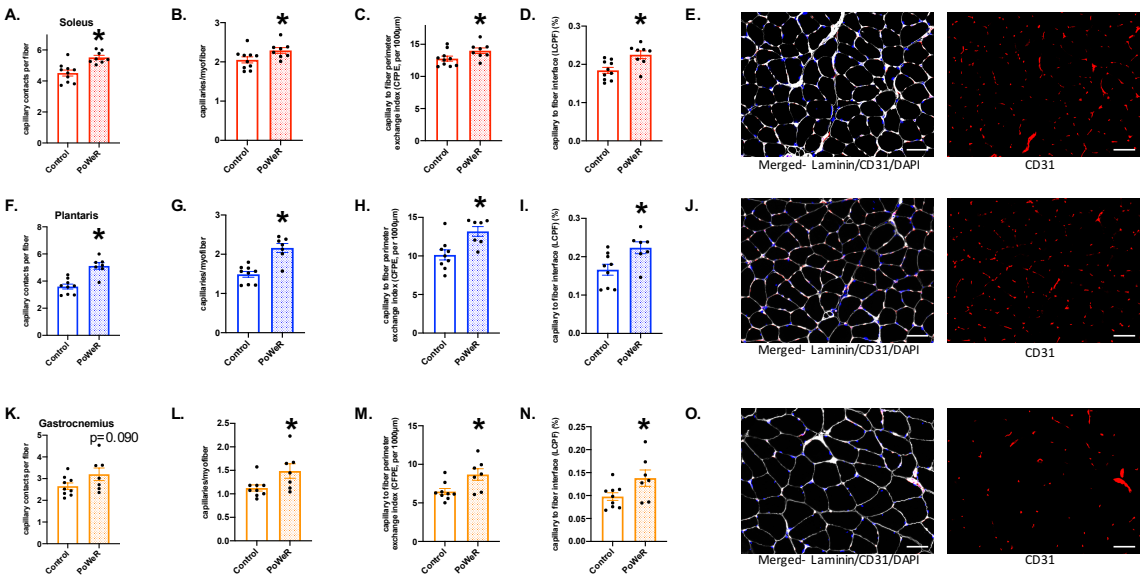

Figure 3.5: Skeletal muscle capillary adaptations to progressive weighted wheel running in old mice.

A. Capillary contacts are elevated in soleus muscles of old mice subjected to PoWeR. B. Capillary density normalized to fiber number is elevated in the soleus with PoWeR. C. CFPE is elevated in the soleus with PoWeR. D. LCPF is elevated in the soleus with PoWeR. E. Representative immunohistochemical image of CD31/laminin/DAPI in the soleus. F. Capillary contacts are elevated in plantaris muscles of old mice subjected to PoWeR. G. Capillary density normalized to fiber number is elevated in the plantaris with PoWeR. H. CFPE is elevated in the plantaris with PoWeR. I. LCPF is elevated in the plantaris with PoWeR. J. Representative immunohistochemical image of CD31/laminin in the plantaris. K. Capillary contacts are elevated in the gastrocnemius muscles of old mice subjected to PoWeR. L. Capillary density normalized to fiber number is elevated in gastrocnemius with PoWeR. M. CFPE is elevated in gastrocnemius with PoWeR. N. LCPF is elevated in gastrocnemius with PoWeR. O. Representative immunohistochemical image of CD31/laminin in the gastrocnemius. CFPE: capillary to fiber perimeter exchange index. LCPF: capillary to fiber interface. *$p<0.05$. Scale bars= 50μm. Error bars represent standard error of the mean (SEM).

Contractile function adaptations to PoWeR in aging skeletal muscle

Isometric peak tetanic torque of the plantar flexors was numerically greater, but not statistically significant, in PoWeR mice compared to sedentary control mice when normalized to both body weight ($p=0.0745$; Fig 3.6A) and wet weight of the plantar flexor complex ($p=0.0702$; Fig 3.6B). These data suggest that in addition to effective overload-

induced myofiber hypertrophy in aging muscle, PoWeR may also elicit a functional adaptation in old mice.

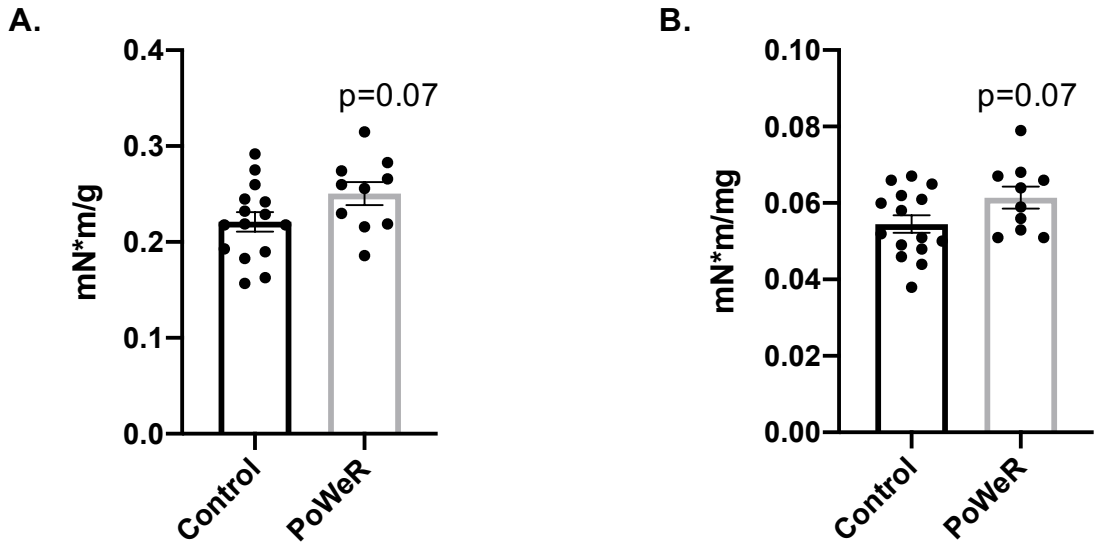

Figure 3.6: Plantar flexion peak torque adaptation to progressive weighted wheel running in old mice.

A. Isometric peak tetanic torque of plantar flexors normalized to body weight is elevated in old mice subjected to PoWeR. B. Isometric peak tetanic torque of plantar flexors normalized to combined plantar flexor wet muscle weights is elevated in old mice subjected to PoWeR. Error bars represent standard error of the mean (SEM).

Differential transcriptional regulation by PoWeR in aging skeletal muscle

Soleus muscles of mice subjected to 8 weeks of PoWeR exhibited upregulation of 1211 genes and downregulation of 1244 genes (Fig 3.7A). Preliminary pathway analysis revealed differential regulation of genes associated with the myogenic program, mRNA transcription, inner mitochondrial membrane protein complex, the mitochondrial inner membrane, the mitochondrial protein complex, and others listed in Figure 3.7B and Figure 3.7C.

Plantaris muscles of mice subjected to PoWeR expressed upregulation of 806 genes and downregulation of 634 genes (Fig 3.7D). Preliminary pathway analysis highlighted

differential regulation of genes associated with angiogenesis, regulation of vascular development, regulation of angiogenesis, and others listed in Figure 3.7E and Figure 3.7F.

DISCUSSION

PoWeR is a practical, non-surgical murine exercise model now demonstrated to generate robust overload-induced hypertrophy with concurrent functional adaptation in skeletal muscle of old mice. Old mice exposed to 8 weeks of PoWeR compared to sedentary control mice exhibited 11% significantly larger myofibers in soleus, 10% significantly larger myofibers in plantaris, and 3% non-significantly larger myofibers in gastrocnemius muscles of the hind limb (irrespective of fiber type), with significantly larger type IIa myofibers in all three plantar flexor muscles. These data contrast the lack of overload-induced hypertrophy observed with surgical overload models in old mice[44] and offer a novel pre-clinical model to effectively study hypertrophy in aging skeletal muscle. Furthermore, PoWeR facilitates overload-induced hypertrophy of the entire intact plantar flexor complex—in juxtaposition to synergist ablation surgical overload to target only the plantaris which is largely considered a poorly characterized vestigial muscle in humans,[91] highlighting the translational relevance of PoWeR compared to synergist ablation in both young and old mice. In addition to muscle morphological adaptations, PoWeR stimulates beneficial functional alterations accompanied by differential transcriptomic regulation.

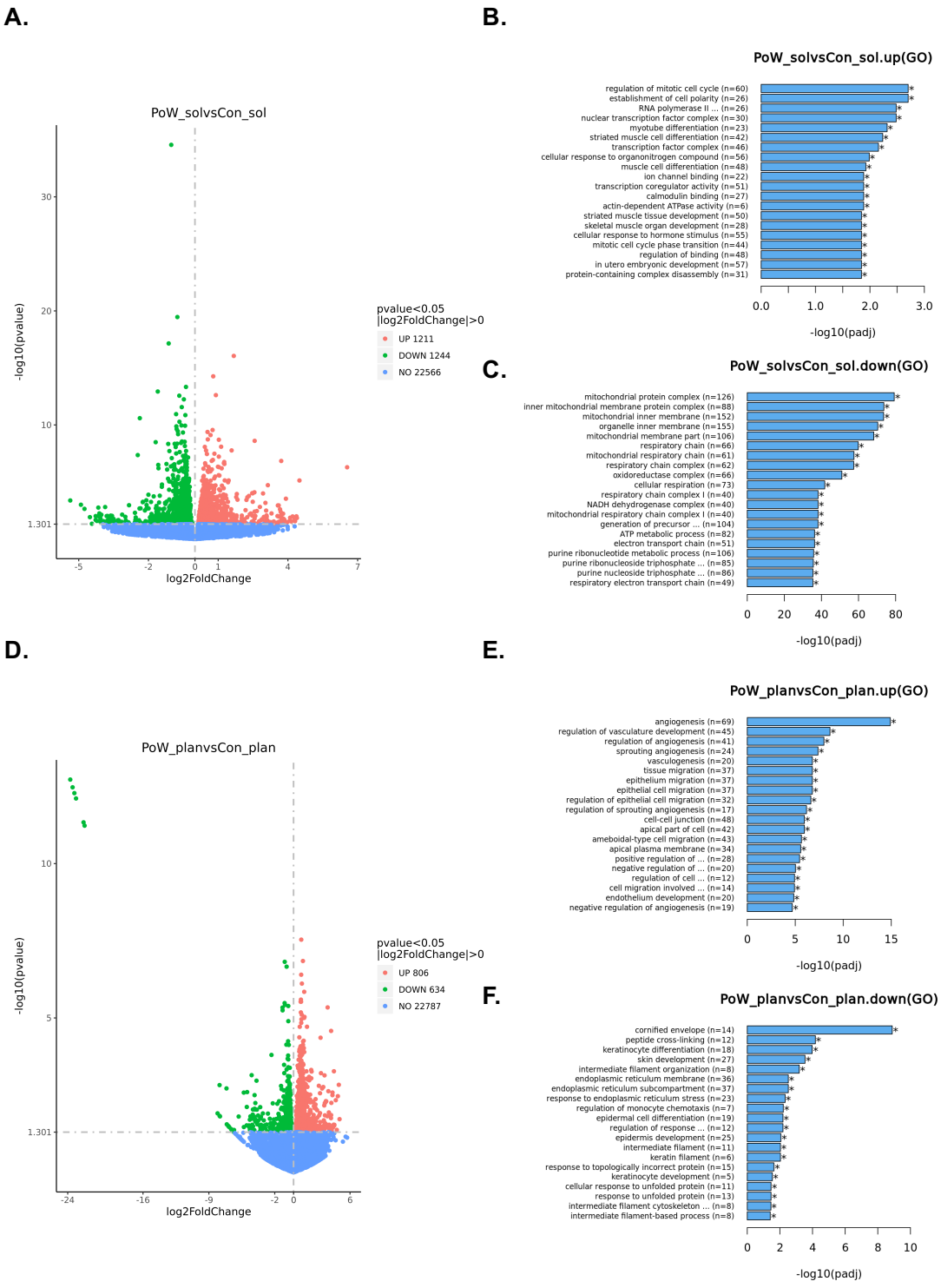

Figure 3.7: Transcriptomic impact of PoWeR.

A. 1211 genes are upregulated and 1244 genes are downregulated in soleus muscles of old mice subjected to PoWeR compared to sedentary control mice. B. Upregulated pathways in soleus muscles of old mice subjected to PoWeR compared to sedentary control mice. C.

Downregulated pathways in soleus muscles of old mice subjected to PoWeR. D. 806 genes are upregulated and 634 genes are downregulated in plantaris muscles of old mice subjected to PoWeR compared to sedentary control mice. E. Upregulated pathways in plantaris muscles of old mice subjected to PoWeR compared to sedentary control mice. F. Downregulated pathways in plantaris muscles of old mice subjected to PoWeR.

PoWeR resulted in myofiber hypertrophy along with an oxidative fiber type shift and improved contractile function in old mice, similar to observations in older adult clinical studies utilizing cycling with a resistance component or concurrent (aerobic and resistance exercise) training.[92-96] The observed hypertrophy and shift toward a more oxidative phenotype is supported by upregulated transcriptional regulation of the myogenic program and mRNA translation in the soleus (which demonstrated more robust hypertrophy compared to the plantaris and gastrocnemius) and angiogenic pathways in the plantaris muscles of old mice subjected to PoWeR; however, a caveat of the gene ontology data that should be considered is that it does not reveal the relationship between the differentially expressed genes and their function in the identified pathways. Running volume was lower in the old mice compared to young mice previously subjected to PoWeR;[45, 46, 97] however, the progressive intensity of PoWeR was sufficient to elicit morphological and functional adaptations in old mice. Additionally, the PoWeR model supported relatively consistent running volume throughout the 8 week period, in contrast to previous wheel loading strategies which precluded sustained exercise[98, 99] and merely attenuated age-related atrophy but not did not produce overt muscle hypertrophy in old mice.[90]

Myofiber hypertrophy—particularly in the intermediate type IIa myofibers, which occurred in all 3 plantar flexor muscles—and the oxidative fiber type shift of the old mice subjected to 8 weeks of PoWeR are consistent with previous reports of young mice undergoing a similar PoWeR protocol.[45, 46, 97] However, myofiber hypertrophy in the current study is blunted compared to that reported in young mice[45, 46, 97]—potentially partially attributable to lower absolute intensity (maximum of 5 g resistance on the wheel, compared to 6 g in young mice) and lower running volume. Although, overload-induced hypertrophy has previously been reported to be blunted in aged mice given the same surgical overload

stimulus as young mice in association with lower satellite cell abundance compared to young[21] and in older adult humans with comparable resistance exercise training.[18] Impaired satellite cell abundance and activity with aging[25, 35, 54, 100] may contribute to the blunted hypertrophic response to PoWeR in old mice compared to young, as satellite cell depleted young mice also demonstrate blunted PoWeR-induced hypertrophy compared to satellite cell replete young mice.[45]

Similar to observations in older adult exercise training,[101] an expansion of the satellite cell pool occurred in plantar flexor muscles subsequent to PoWeR and was accompanied by myonuclear accretion evidenced by an elevated number of myonuclei relative to myofiber number. Myonuclear accretion was also comparable to that observed in young mice with PoWeR in the plantar flexor muscles,[45,46,97] with the type IIa myofibers demonstrating a hypertrophic response in soleus, plantaris, and gastrocnemius muscles along with congruent myonuclear accrual (excluding the gastrocnemius with inclusion of 2 apparent outliers with elevated myonuclei/fiber in the sedentary Control group). These findings align with the myonuclear accretion reported in plantaris muscles of old mice subjected to the classical surgical overload model of synergist ablation.[44] Although, with synergist ablation in old mice, myonuclear accretion did not support myofiber hypertrophy,[44] further highlighting the novel capacity of PoWeR to not only induce satellite cell expansion and myonuclear accretion but also hypertrophy in old mice.

PoWeR stimulated a robust angiogenic response in plantar flexor muscles of old mice—evidenced by immunohistochemical measures in the soleus, plantaris and gastrocnemius and preliminary molecular analysis in the plantaris. The observed muscle capillarization resultant from PoWeR in old mice is consistent with enriched capillarization signaling pathways in young satellite cell replete mice subjected to a similar PoWeR protocol.[45] However, angiogenesis supporting expanded muscle capillarization occurs in young but not old mice following synergist ablation surgical overload.[86] Importantly, increased capillarization in young mice with synergist ablation corresponds to robust

overload-induced hypertrophy, while old mice (in which expansion of capillary supply does not occur with synergist ablation) are resistant to myofiber growth resultant from surgical overload with previous reports of both blunted[86] and a complete lack of hypertrophy.[44] Angiogenesis induced by PoWeR likely supported the concurrent hypertrophic response observed in old mice in the current study. Furthermore, findings from older adult resistance exercise training indicate that sufficient capillary density is a key factor to facilitate overload-induced hypertrophy, with low muscle capillarization at the onset of resistance exercise training limiting the hypertrophic response.[87] These results align with our finding of more pronounced hypertrophy induced by PoWeR in the soleus and plantaris muscles which demonstrated higher indices of muscle capillarization compared to the gastrocnemius muscle in aged sedentary control mice.

Capillary supply is impaired in older skeletal muscle compared to young muscle with age-associated apoptosis of CD31+ endothelial cells,[102] and is effectively increased in older adults by aerobic exercise.[103, 104] An interference effect of aerobic exercise performed concurrently with resistance exercise has been proposed to exist, limiting overload-induced hypertrophy resultant from resistance exercise; however, evidence from multiple clinical exercise studies contradict this dogma.[105] Recent work in middle-aged mice has supported the absence of an interference effect with a combination of endurance exercise and hypertrophic stimuli producing unaltered overload-induced hypertrophy,[106] although duration of endurance exercise with overload should be considered as longer aerobic bouts concurrent with surgical overload may increase ubiquitinated proteins and oxidative stress in skeletal muscle that may limit hypertrophy.[107] We postulate that the aerobic component of PoWeR facilitates the observed angiogenic adaptations which support overload-induced hypertrophy in aging skeletal muscle elicited by the resistive component, comparable to concurrent training.

PoWeR is an effective and practical tool to stimulate exercise adaptations in both primarily oxidative (soleus) and glycolytic (plantaris) muscles in old mice, and thus

provides a novel method to study hypertrophy of aging skeletal muscle in murine models. Compared to common models of overload-induced hypertrophy—like mechanical overload by surgical synergist ablation—which effectively produce hypertrophy and functional adaptation in young but not old mice,[41, 44, 86] PoWeR offers superior utility to mechanistically investigate aging skeletal muscle plasticity in response to mechanical overload and is translationally relevant to exercise interventions in older adults to mitigate sarcopenia and the associated functional decline.

CHAPTER 4:

Small molecule nicotinamide N-methyltransferase inhibitors activate senescent muscle stem cells and improve regenerative capacity of aged skeletal muscle[100]

(PMID: 30753815)

INTRODUCTION

The population of older (60+ years of age) adults is rapidly expanding in the United States and throughout the world, placing ever-increasing strains on health care resources and an urgent need for improved approaches to elder care.[109] One of the most significant impacts of aging is the progressive decline in skeletal muscle mass and strength,[8, 110] with concomitant deteriorations in physical function and mobility that are strongly associated with numerous chronic diseases and increased mortality.[75, 111] While all older individuals experience muscle degeneration, approximately 30% of adults over 60 years of age and 50% of adults over 80 years of age develop sarcopenia, a geriatric disease characterized by significant and objective defects in muscle mass, strength, and function.[9, 10, 112] Sarcopenic elderly individuals are at a 2- to 5-fold increased risk for permanent disability and greatly diminished quality of life arising from progressive muscle degeneration, decreased muscle function, and poor muscle quality that predispose them to debilitating falls and substantial disease burden.[111] Furthermore, as muscle regenerative capacity of older adults becomes increasingly compromised, it leads to delayed and impaired recovery following muscle injury,[7, 24, 25] decreased mobility and independence, increased hospitalization costs [113], and higher mortality rates.[114]

Muscle stem cells (muSCs; also termed satellite cells) are responsible for mediating skeletal muscle repair by proliferating and differentiating into fusion-competent myoblasts

and facilitating myofiber regeneration following injury.[26, 27, 115] The major driving factor for delayed and impaired recovery of aged muscle following injury appears to be a significant decrease in satellite cell regenerative capacity and function.[24, 25, 116] These events occur independent of sarcopenia,[55] resulting in the formation of dysfunctional senescent satellite cells that are no longer activated by muscle injury or turnover stimuli and present compromised ability to proliferate, differentiate, fuse, and promote the repair and replacement of myofibers.[53, 100] Additionally, satellite cell abundance has been observed to decline in some aged skeletal muscle tissues[51] as satellite cells develop diminished intrinsic capacity for reversible quiescence, which further reduces the population of satellite cells supporting the post-injury repair cascade.[53] Applications of satellite cells in promoting muscle repair have been preclinically investigated;[115] however, there are no approved pharmacological therapeutics that can safely and effectively enhance satellite cell activation and regenerative capacity to promote recovery from injury among aging adults.

Nicotinamide adenine dinucleotide (NAD^+) is a fundamental cellular regulator of energy metabolism, mitochondrial function, and bioenergetics[117, 118] that declines with age.[63, 119, 120] Age-related diminished NAD^+ contributes to altered skeletal muscle metabolism and mitochondrial function,[120, 121] progressive muscle degeneration and loss of function, [122] which further link to increased satellite cell senescence, reduced satellite cell function, dysfunctional muscle regeneration, and impaired muscle repair.[70, 123] Recently, several studies have observed that nutraceutical supplements such as nicotinamide mononucleotide (NMN), nicotinamide riboside (NR), and nicotinamide analogues (e.g., acipimox), which increase intracellular NAD^+ levels and stimulate muscle NAD^+ biosynthetic pathways (e.g., NAD^+ salvage pathway), can improve muscle metabolic, mitochondrial, and satellite cell function, and accelerate muscle regeneration in aged mice.[68-70] Thus, pharmacologically enhancing NAD^+ levels in aging skeletal muscle tissues may provide a viable approach to improve the regenerative function of aged satellite cells.

The cytosolic enzyme nicotinamide N-methyltransferase (NNMT) has been newly discovered to modulate the levels of nicotinamide precursors required for NAD^+ biosynthesis, and thus plays a crucial role in regulating the NAD^+ salvage pathway and cellular metabolism.[124] NNMT is expressed in skeletal muscle, with progressively greater expression associated with aging in muscle tissues.[125, 126] Importantly, NNMT is a dominant component of the gene expression signature for sarcopenia,[60] overexpression of which could lead to significantly reduced levels of NAD^+ and associated declines in muscle mass, strength, and function that accompany aging.[127, 128] We recently discovered and developed first-in-class small molecule inhibitors of NNMT that have amenable drug-like properties and selectively inhibit NNMT activity in vivo.[128, 129] In the present study, we generated proof-of-concept data demonstrating the efficacy of a novel NNMT small molecule inhibitor to accelerate muscle regeneration in an aged mouse muscle injury model. Our results indicated that treatment of aged mice with a lead small molecule NNMT inhibitor (NNMTi) enhanced proliferation, fusion, and regenerative capacity of satellite cells, increased functional performance of skeletal muscle, and altered NAD^+ salvage pathway-related cellular metabolites. To the best of our knowledge, this is the first study to convincingly demonstrate that NNMT inhibition rescues age-related satellite cell deficits and serves as a suitable therapeutic approach to reactivate skeletal satellite cells and accelerate NAD^+ turnover in the salvage pathway in aging skeletal muscle, thus mitigating age-associated impaired muscle regeneration and improving skeletal muscle remodeling and function following injury.

MATERIALS AND METHODS

Chemicals

NNMT inhibitor (NNMTi), 5-amino-1-methylquinolium was synthesized by a previously established synthetic method.[129]

Quantitative measurement of NNMT expression in young and aged muscle tissue

20-40 mg of tibialis anterior (TA) muscle tissue were collected from young (4-month-old) and aged (24-month-old) C57Bl/6 mice, pulverized on ice, added to RIPA buffer (Cell Signaling Technology, product #9806) containing protein phosphatase inhibitor cocktail (P-5726, Sigma Aldrich, St. Louis, MO) (1:10 w/v), and homogenized using a hand-held tissue homogenizer (Tissue-Tearor™, Model 985370, BioSpec Products, Inc., OK, USA). Homogenized samples were centrifuged at 10,000 g for 10 min at 4°C. Supernatants were collected and stored at -20°C until further processing. Protein concentration in samples were determined using the bicinchoninic acid (BCA) protein assay (Pierce™ BCA Protein Assay Kit, Thomas Scientific, NJ, USA). Briefly, 40 μg of tissue homogenates from young and aged TA muscle samples were separated using sodium dodecyl sulfate polyacrylamide gel electerophoresis (SDS-PAGE). Separated proteins were transferred onto a polyvinylidene fluoride (PVDF) membrane and probed for NNMT protein expression using anti-NNMT primary antibody (ab58743, rabbit polyclonal; Abcam, Cambridge, MA) and HRP-conjugated polyclonal goat anti-rabbit secondary antibody (ab205718; Abcam) via western blotting. Membrane was striped and re-probed for β-actin using anti-β-actin primary antibody (ab101173, monoclonal mouse) as the loading control. Western blots were analyzed for NNMT and β-actin expression using ImageJ software (NIH). NNMT protein expression (bands detected at ~27 kDa) was normalized to β-actin expression (bands detected at ~42 kDa) and compared between young and aged TA muscle tissues. Samples were run and analyzed in technical duplicates.

Efficacy of NNMTi to activate and improve regenerative capacity of satellite cells in an aged mouse muscle injury model

Aged, 24-month-old (N=48), male C57Bl/6 mice were obtained from the National Institute of Aging (NIA). Upon arrival, mice were single-housed and allowed to acclimate to the controlled environment vivarium maintained at a constant temperature (21-23°C)

and humidity (40-50%) on a 12-hour light-dark cycle (lights on 0600-1800 h) for at least 7 days prior to initiation of experiments. Food and water were available ad libitum. All experiments were carried out in accordance with the Guide for the Care and Use of Laboratory Animals and with approval from the Institutional Animal Care and Use Committee at the University of Texas Medical Branch.

Short-term treatment effects of NNMTi on muscle regeneration after injury

Following acclimation, mice were randomized into control (saline; n=13), low dose NNMTi (5 mg/kg; n=10), and high dose NNMTi (10 mg/kg; n=13) treatment groups, ensuring similar mean average body weights across the three cohorts. Mice received twice daily (BID) subcutaneous (SC) injections of saline or NNMTi for 2 weeks (1 week pre-injury and 1 week post-injury). Mice were weighed and the body weights were recorded every other day. On day 8 (following 1 week of treatment), mice were briefly anesthetized using isoflurane and 30 ul of barium chloride ($BaCl_2$) toxin (1.2% concentration) was injected locally into the TA muscle of one hindlimb to induce muscle injury, followed by carprofen for analgesia. Starting on the day of the injury (day 8) and on days 10, 12, and 14, mice received a single intraperitoneal (IP) injection of 5-ethynyl-2´-deoxyuridine (EdU) (150 ug in saline) to track satellite cell proliferation and fusion into regenerating TA muscle fibers. All groups of mice continued to receive BID, SC injections of saline or NNMTi on days 8 through 14. At the terminal end of the study, a sub-cohort of mice from the 3 treatment groups (n=6/group) were deeply anesthetized using ketamine/xylazine cocktail anesthetic (IP injection) and the blood was drawn by cardiac puncture procedure, following which muscle tissues were harvested for additional processing. Remaining mice (n=7/group in control and high dose groups) were subject to TA contractile function measurements (measures described in detail below) under isoflurane-induced anesthesia to assess muscle strength. Terminal bleeds were performed on all remaining mice and the tissues harvested and flash frozen for ex-vivo analyses as described below.

Long-term treatment effect of NNMTi on complete muscle recovery after injury

A separate cohort of 24-month-old, aged mice were randomized into control (saline; n=6) and high dose NNMTi (10 mg/kg; n=6) treatment groups, ensuring similar mean average body weights across the two cohorts. In contrast to the short-term treatment regimen (1-week post-injury treatment) described above, mice received twice daily (BID) subcutaneous (SC) injections of saline or NNMTi for 4 weeks; pretreatment for 7 days prior to $BaCl_2$ injury to one TA muscle, followed by 3 weeks of post-injury treatment to examine a more complete muscle recovery. Muscle tissues were harvested and flash frozen for ex-vivo analyses as described below.

Effect of NNMTi on in vivo contractile physiology determined by dorsiflexor torque measurement

This protocol was adapted and modified from previously published literature.[130, 131] Briefly, mice were anesthetized with isoflurane (3-4% for induction and ~2.5% for maintenance of anesthesia via a nose cone; oxygen maintained at ~1.5 l/min with a VetEquip vaporizer), the $BaCl_2$ injured leg trimmed (Wahl Bravmini), and set on a platform (Aurora Scientific 809c in situ testing apparatus) heated to 37°C (with an Anova Industries Model 10 water circulator). The leg was then mounted into a clamp to hold it static at the knee, with the tibia perpendicular to the femur and the foot perpendicular to the tibia. The foot was secured in a mount connected to the force transducer, with the ankle wedged in place and with a piece of tape holding the foot to the mount. Platinum needle electrodes were set percutaneously, approximately near the top of the knee and halfway down TA, between the TA and the gastrocnemius (needles were adjusted to find the optimal placing for maximum force production with minimum current and minimal antagonistic muscle response). With an Aurora Physiology system (Model 6650LR Force Transducer, Dual Mode lever System, Hi power Bi-Phase Stimulator, Signal Interface, and software: Dynamic Muscle Control v5.500 and Dynamic muscle Analysis version 5.300), the proper

maximal current used to stimulate muscle contraction was determined by eliciting a twitch (pulse duration 0.2 s) with the stimulus starting at 5 mA and increased incrementally to ~50 mA until the maximum twitch torque at the minimum amperage needed to stimulate this torque was recorded. This minimum current was then maintained throughout a torque-frequency curve to find the maximum torque output ($twitch_1$, 10 Hz, 40 Hz, 80 Hz, 100 Hz, 120 Hz, 150 Hz, 180 Hz, 200 Hz, 250 Hz and a final $twitch_2$). A $twitch_1$/$twitch_2$ minimum ratio of 90% determined muscle integrity post-procedure (<90% may indicate extreme muscle fatigue or damage). No mice failed the $twitch_1$/$twitch_2$ test. Peak torque per gram of body mass and peak torque normalized to CSA (average cross-sectional area of fibers) per animal were recorded as outcomes, group averaged, and compared between control and high dose NNMTi (10 mg/kg)-treated mice. Data from one treated mouse was not included in analysis since torque could not be reliably measured above background levels.

Immunohistochemistry

For all immunohistochemical analyses, dissected muscles from mice were mounted in Tissue Tek (O.C.T. Compound, Sakura Finetek, Torrance,CA, USA) at resting length and frozen in liquid nitrogen-cooled 2-methylbutane and stored at −80°C until analysis. 7 μm-thick sections were cut with a cryostat (HM525-NX, Thermo Fisher Scientific, Waltham, MA, USA) and allowed to air dry for 1 h prior to storage at -20 °C.

NNMT expression in 4-month old young and 24-month old aged tibialis anterior (TA) muscle

For NNMT immunohistochemical staining, sections were fixed in 4% paraformaldehyde (PFA). Slides were blocked for 1 h in 1% TSA blocking reagent and incubated overnight at 4 °C in primary antibody against NNMT (ab58743, Abcam, Cambridge, MA; 1:100). The following day, slides were incubated for 1 h at room temperature with IgG anti-rabbit secondary conjugated to AF555 (no. A21428, Life

Technologies/Thermo Fisher Scientific; 1:500) and AF488-cojugated wheat germ agglutinin (WGA) (no. W11261, Life Technologies/Thermo Fisher Scientific) to denote myofiber borders. Slides were incubated in 4′,6-diamidino-2-phenylindole (DAPI; 10 nM, LifeTechnologies/Thermo Fisher Scientific) for 10 min and washed and mounted with Vectashield fluorescence mounting media (Vector Laboratories).

Satellite cell immunohistochemical analyses

Pax7 is a transcription factor unique to satellite cells and a routinely used marker to identify satellite cells; laminin is routinely used to denote muscle fiber borders. For Pax7-EdU-laminin staining, sections were fixed in 4% PFA followed by antigen retrieval using sodium citrate (10mM, pH 6.5) at 92°C for 20 min. Slides were then placed in 3% hydrogen peroxide in PBS for 7 min to block endogenous peroxidase activity followed by a second blocking step in Mouse-on-Mouse Blocking Reagent (Vector Laboratories, Burlingame, CA). Sections were incubated overnight at 4 °C in primary antibodies against Pax7 (DSHB, Iowa City, IA, USA; 1:100) and laminin (L9393, Sigma-Aldrich, St Louis, MO, USA; 1:100). Next, slides were incubated with biotinylated anti-mouse IgG secondary antibody for Pax7 (no. 115-065-205, Jackson ImmunoResearch, West Grove, PA, USA; 1:500) and anti-rabbit IgG secondary antibody for laminin (Alexa Fluor 647, no. A11034, Life Technologies/Thermo Fisher Scientific; 1:500) followed by incubation with streptavidin-horseradish peroxidase (HRP) included with a commercially available tyramide signal amplification kit (TSA, Life Technologies/Thermo Fisher Scientific). TSA-Alexa Fluor 488 was used to visualize Pax7 antibody binding. Following all Pax7-laminin steps, slides were permeabilized in 0.1% Triton-X100 in phosphate-buffered saline and incubated with the Life Technologies Click-iT Kit per manufacturer's instructions, with EdU visualized with Alexa Fluor 555. Slides were incubated in 4′,6-diamidino-2-phenylindole (DAPI; 10 nM, LifeTechnologies/Thermo Fisher Scientific) for 10 min,

washed, and mounted using Vectashield fluorescence mounting media (Vector Laboratories).

Image acquisition and quantification

Immunohistochemical images were captured at 200X total magnification room temperature with a Zeiss upright microscope (AxioImager M1; Zeiss, Göttingen, Germany). muSC abundance was evaluated by Pax7 staining along with laminin and DAPI; only cells that were $Pax7^+$ /$DAPI^+$ within the laminin border were counted. Proliferating satellite cells included only those that were $Pax7^+/EdU^+/DAPI^+$ within the laminin border. Satellite cell fusion to myofibers was determined by newly acquired myonuclei classified as $Pax7^-/EdU^+/DAPI^+$. Mean myofiber cross-sectional area (CSA) was measured by manually tracing myofiber area using the laminin border. Only injured myofibers (fibers with central myonucleation) were included in CSA analysis.

Image analysis was performed in a blinded manner using AxioVision Rel software (v4.9). To assess the reliability, accuracy, and reproducibility of the image quantification procedures, three blinded raters assessed images from six mice; two mice were randomly selected from each treatment group for validation of counts of satellite cell abundance, proliferating satellite cells, and satellite cell fusion (saline: n=2, low dose NNMTi: n=2, high dose NNMTi: n=2). Intraclass correlation coefficients (ICCs) were calculated for each variable to determine reliability of the data. ICC estimates and 95% confidence intervals were calculated using SPSS statistical software (IBM Corp. IBM SPSS Statistics for Windows, Version 25. Armonk, NY) based on a mean-rating, consistency, 2-way mixed-effects model with 3 raters across 6 mice. ICC values below 0.5 indicate poor reliability, 0.5 to 0.75 indicate moderate reliability, 0.75 to 0.9 indicate good reliability, and values greater than 0.90 are indicative of excellent reliability and reproducibility. [132, 133]

Plasma chemistry panel

Blood samples were collected from each animal immediately upon sacrifice, processed to isolate plasma, frozen in liquid nitrogen, and shipped on dry ice to Texas A&M Veterinary Medical Diagnostic Laboratory (TVMDL; College Station, TX, USA) for small animal serum chemistry analysis via standard protocols. TVMDL is accredited by the American Association of Veterinary Laboratory Diagnosticians and all results were confirmed with positive and negative controls. Complete plasma measures included hepatic panel (AST, ALT, ALP, GGT, GLDH, total bilirubin, albumin, globulin, AG ratio, total protein), renal panel (amylase, BUN, creatine kinase, calcium, phosphorus), amylase, electrolytes (sodium, potassium, and chloride), glucose, and cholesterol to validate systemic effects of repeated NNMTi treatment on major organ functions.

Differentiation of C2C12 myoblasts

C2C12 myoblast cells (CRL-1772, American Type Culture Collection; Manassas, VA, USA) were cultured with standard growth media (DMEM, 4.5 g/L glucose, L-glutamine, sodium pyruvate, 10% FBS, 1% penicillin/streptomycin) and grown to 70-80% confluency before initiating differentiation. To begin differentiation of myoblasts, growth media was replaced by differentiation media (DMEM, 4.5 g/L glucose, L-glutamine, sodium pyruvate, 2% Horse serum, 1% penicillin/streptomycin); low nutrient condition and increased cell-to-cell contact stimulated differentiation of myoblasts by inhibiting proliferation and promoting the formation of multi-nucleated myotubes. Differentiation media was replaced every other day to maintain myotubes in culture for 3-4 days, during which time experiments as described below were performed.

Immunocytochemical analysis of NNMT expression in C2C12 myoblasts and differentiated myotubes

C2C12 myoblasts and myotubes grown on glass cover slips were fixed in 4% PFA warmed to 37°C for 15 min, and then washed 3 times with PBS. Myoblasts and myotubes were permeabilized with a 10 min wash in PBS + 0.2% Triton-X100, and then blocked in 1% BSA made in PBS + 0.2% Triton-X100 for 1 hr. For myoblasts, cells were incubated in primary antibody (1:100, NMMT cat #ab119758, mouse IgG2b, Abcam) for 2 hr at room temp in 1% BSA, followed by PBS washing, and then secondary antibody (Gt anti-Ms IgG2b AF488, cat # A-21141, ThermoFisher) for 1 hr followed by a co-stain with DAPI and mounting. For myotubes, cells were incubated in primary antibody (NMMT, 1:100, cat #ab119758, mouse IgG2b, Abcam and myosin heavy chain, 1:200, cat #M4276, mouse IgG1, Sigma) for 2 hr at room temp in 1% BSA, followed by PBS washing, and then secondary antibody (Gt anti-Ms IgG2b AF488, cat # A-21141 and Gt anti-Ms IgG1 AF555, cat # A-21127, ThermoFisher) for 1 hr followed by a co-stain with DAPI and mounting. Images were captured at 200X total magnification.

Effect of NNMTi on C2C12 myoblast differentiation

To determine the effect of NNMTi on C2C12 myoblast differentiation, myoblasts were cultured to confluency as described above and stimulated to differentiate in the absence or presence of NNMTi (10 and 30 μM concentrations) in differentiation media for 96 h. Concentrations of NNMTi were chosen based on our previous published work in adipocytes, where significant phenotypic and metabolic changes were observed in the presence of the inhibitor relative to untreated conditions.[128] After 96 h of differentiation, media was removed and cells were fixed in 4% PFA pre-warmed to 37°C for 15 min. PFA was then removed and the cells were washed three times (3 min each wash) with PBS containing 0.2% Triton X-100. Cells were blocked for 1 h in 1% TSA (fTSA kit – compound D, Invitrogen ThermoFisher Scientific #T-30955) in PBS/Triton. Following

blocking, cells were incubated for 2 h at room temperature with anti-myosin heavy chain (MHC) primary antibody (Sigma #M4276 – from MY-32 clone) at 1:200 concentration made in TSA/PBS/Triton diluent. Cells were washed in PBS/Triton and incubated for 1 h at room temperature with goat anti-mouse secondary antibody (IgG1 AF488 conjugated; Invitrogen #A21121) at 1:500 concentration made in PBS/Triton. Cells were washed, incubated with DAPI (1:10,000 concentration; Invitrogen #D35471 in PBS) for 10 min to stain nuclei, and washed finally with PBS/Trition before imaging. Four random field of views were captured per well; total DAPI stained nuclei and MHC positive nuclei were counted to calculate %MHC positive nuclei. Control and NNMTi-treated conditions were run in duplicates with results averaged for each condition. %MHC positive nuclei analyzed were averaged and compared between control and NNMTi-treated myotubes with experiments repeated three times.

Effect of NNMTi treatment on NAD^+ and NADH levels in C2C12 myoblasts and myotubes.

C212 myoblasts were differentiated to myotubes using the protocol described above and maintained in culture for 4 days before NNMTi treatment. On day 3 of differentiation, media was removed and replaced with fresh differentiation media (control) or NNMTi (10 and 30 μM concentrations) made in differentiation media for 24 h. Similarly, C2C12 myoblasts were cultured to ~40% confluency and treated for 24 h with growth media alone (control) or in the presence of NNMTi (10 and 30 μM concentrations) in growth media for 24 h. Following 24 h of treatment with NNMTi, cells were treated with trypsin, centrifuged, and washed once in ice cold PBS. Cells were re-suspended in 300 μL of 75% ethanol / 25% 10 mM HEPES solution pre-heated to 80°C and extracted using a previously described protocol to obtain soluble NAD+ and NADH metabolites [44]. Levels of NAD+ and NADH in the extracted samples were assessed using a spectrophotometric enzymatic assay. Briefly, samples were re-suspended in distilled water

and treated with acid (0.1 M hydrochloric acid) or base (0.1 M sodium hydroxide) and heated at 75°C for 30 min to remove all the NADH and NAD+ in samples, respectively. Samples were then neutralized by appropriately adding acid (0.1 M HCl/0.5 M bicene) or base (0.1 M NaOH/0.5 M bicene) and treated with alcohol dehydrogenase (1x final; A3263–7, Sigma-Aldrich, St. Louis, MO, USA) for 15 min. Following incubation, 10 μL of WST-1 reagent (Roche Applied Science, Mannheim, Germany) to initiate the enzymatic reaction and the pink colored product formed over time was spectrophotometrically measured via absorbance detected at 450 nm wavelength and compared between control and treated samples.

Statistical analysis

Effects of NNMTi on satellite cell regeneration were expressed as incidence of activated satellite cells and fibers with myonuclei and analyzed using R statistical software (R Core Team, 2018, version 3.5.1) by mixed effect logistic regression as a function of dose group, adjusting for cohort (given that the experiments were conducted across separate cohorts), and controlling for repeated measures effect. Differences between dose groups were assessed by Tukey adjusted contrasts posthoc test. Fiber CSA data were log-transformed (for 1-week post-injury treatment data to better approximate normal distribution) or analyzed without transformation (3-week post-injury treatment data) by mixed effect analysis of variance (ANOVA) followed by Tukey multiple contrasts posthoc as a function of dose, adjusting for cohort (given that the experiments were conducted across separate cohorts), and controlling for repeated measures effect. Where applicable, statistical analysis for two-group comparisons was conducted using unpaired Student's t-test (serum chemistry results) or an appropriate non-parametric analysis (where datasets did not pass normality test) using Graphpad Prism (version 7.0). Two-way ANOVA with Sidak's multiple comparison posthoc test was used to compare frequency of fibers as a function of binned CSA/fiber size in controls versus NNMTi treated groups using

Graphpad Prism (version 7.0). One-way ANOVA with Dunnett's posthoc test was used to compare %MHC positive nuclei in NNMTi-treated myotubes versus control using Graphpad Prism (version 7.0). Absorbance data obtained at various timepoints for NAD^+ and NADH extracted control and NNMTi-treated C2C12 myotubes samples were transferred to Graphpad Prism (version 7.0) to perform linear regression analysis and obtain slopes from the linear reaction progress curves. Slopes for NAD^+ and NADH extracted samples and the ratio of NAD/NADH slopes were compared using unpaired Student's t-test between control and NNMTi treatment groups. All statistical analyses were performed with an experiment-wise error rate of $\alpha = 0.05$, for a 95% level of confidence.

RESULTS

NNMT expression increases in aged TA muscle

Immunolabeling of NNMT revealed NNMT-specific staining both in the TA muscle obtained from 24-month-old and 4-month-old mice (Fig. 4.1A, 4.1B). Expression of NNMT was qualitatively demonstrated to be relatively greater in aged muscle based on the immunohistochemical evaluations of the aged TA compared to young TA muscle tissues (Fig. 4.1A, 4.1B). To validate the qualitative findings using a semi-quantitative approach, NNMT immunoblots were established using aged and young mouse TA tissues (Fig. 4.1C). Consistent with the differential immunohistochemical NNMT results in aged versus young TA tissue, the expression level of NNMT protein in aged TA muscle was ~3-fold higher compared to the level of NNMT protein in young TA tissue (Fig. 4.1D; $p < 0.05$ vs. NNMT expression in young TA tissue). Taken together, these results support increased NNMT protein expression in the skeletal muscle as a function of age, suggesting likely enhanced NNMT activity in aged muscle tissue.

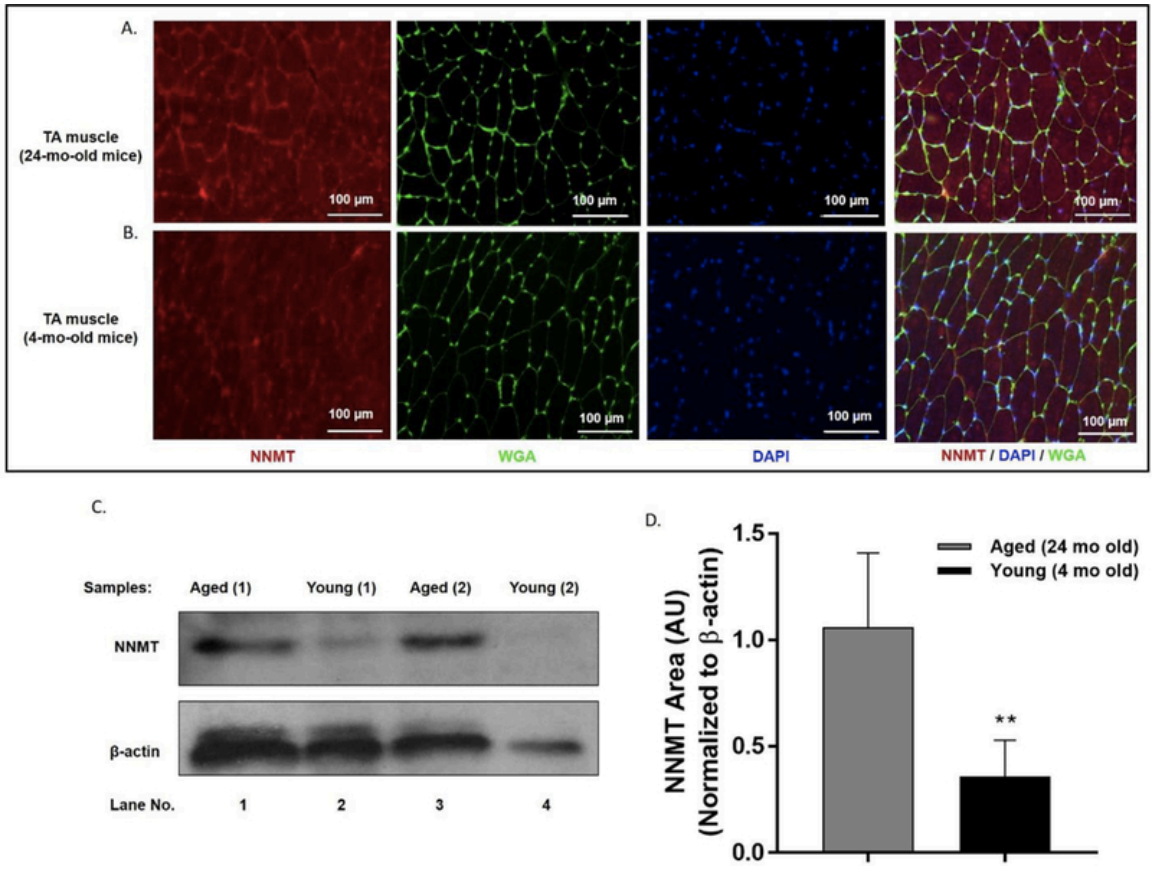

Figure 4.1: NNMT expression in aged (24 mo) and young (4 mo) TA muscle.

Representative images of (A) aged (top panels) and (B) young (bottom panels) TA muscle tissues immunolabeled for detection of NNMT protein (red), myofiber membrane border (marked by wheat germ agglutinin [WGA] in green), and nuclei (marked by DAPI in blue). (C) Representative immunoblots obtained from replicate aged and young TA mouse tissue samples. (D) NNMT protein expression normalized to the loading control β-actin in aged and young TA muscle tissues as analyzed using western blotting. **, $p < 0.01$ vs. aged TA muscle NNMT expression.

In vivo NNMT inhibition activates satellite cells and promotes aged muscle regeneration

Fig. 4.2A and 4.2B present representative images that highlight satellite cell proliferation and fusion into damaged myofibers of aged TA muscle in control and NNMTi (10 mg/kg, bid)-treated mice. As indicated by white arrowheads (rightmost panels, Fig. 4.2A, 4.2B), NNMT inhibition increased the number of proliferating satellite cells (measured by counting Pax7+/EdU+/DAPI+ cells per unit area); however, the total number

of satellite cells (i.e., Pax7+/DAPI+ cell counts per unit area) were unchanged in the control, low NNMTi dose, and high NNMTi dose groups, and averaged 209 ± 23, 213 ± 44, and 205 ± 9 satellite cells/mm2, respectively (Fig. 4.2A, 4.2B, representative panels showing Pax7+ positive cells indicated in green). Similarly, as indicated by yellow arrowheads (rightmost panel, Fig. 4.2A and 4.2B), NNMT inhibition promoted greater fusion of satellite cells into damaged myofibers (measured by newly acquired myonuclei; Pax7–/EdU+/DAPI+ within laminin border), suggesting improved muscle regeneration following injury.

Consistent with these results, extensive quantification of numerous images revealed a dose-related increase in the relative abundance of proliferating satellite cells (Fig. 4.2C) and fibers with integrated myonuclei via satellite cell fusion (Fig. 4.2D) following 1-week post-injury NNMTi treatment. The 5 mg/kg and 10 mg/kg doses of NNMTi tested resulted in 60% and 75% higher incidence of proliferating/active satellite cells, respectively, relative to control (Tukey adjusted P values: $p = 0.013$, 5 mg/kg dose vs. control; $p = 0.0007$, 10 mg/kg vs. control). The odds ratio of active satellite cells for control was 0.54 and 0.46 times the odds at the low and high doses, respectively. Although the higher treatment dose produced ~11% higher incidence of activated satellite cells compared to the lower treatment dose, this observed difference did not rise to the level of being statistically significant ($p > 0.05$, n.s.) (Fig. 4.2C). ICC for muSC abundance was 0.944 [95% CI (0.765,0.992)] and for proliferating satellite cells 0.754 [95% CI (–0.43,0.963)] indicating excellent reliability of the data recorded by independent experimenters in a blinded fashion.

Similarly, dose-dependent trends were observed with NNMTi treatment in the incidence of newly acquired myonuclei via satellite cell fusion into damaged myofibers (Fig. 4.2D). The relative numbers of fibers with an EdU+ myonucleus increased 40% and 48% with NNMTi treatment at 5 mg/kg and 10 mg/kg, respectively, relative to control. The odds ratio of fused myonuclei for control were 0.58 and 0.53 times the odds at the low and high NNMTi dose, respectively, and the Tukey adjusted P values bordered on the cutoff

generally considered statistically significant (p = 0.0686, 10 mg/kg dose vs. control). ICC for satellite cell fusion was 0.971 [95% CI (0.878,0.996)] indicating excellent reliability of data scored independently by blinded experimenters.

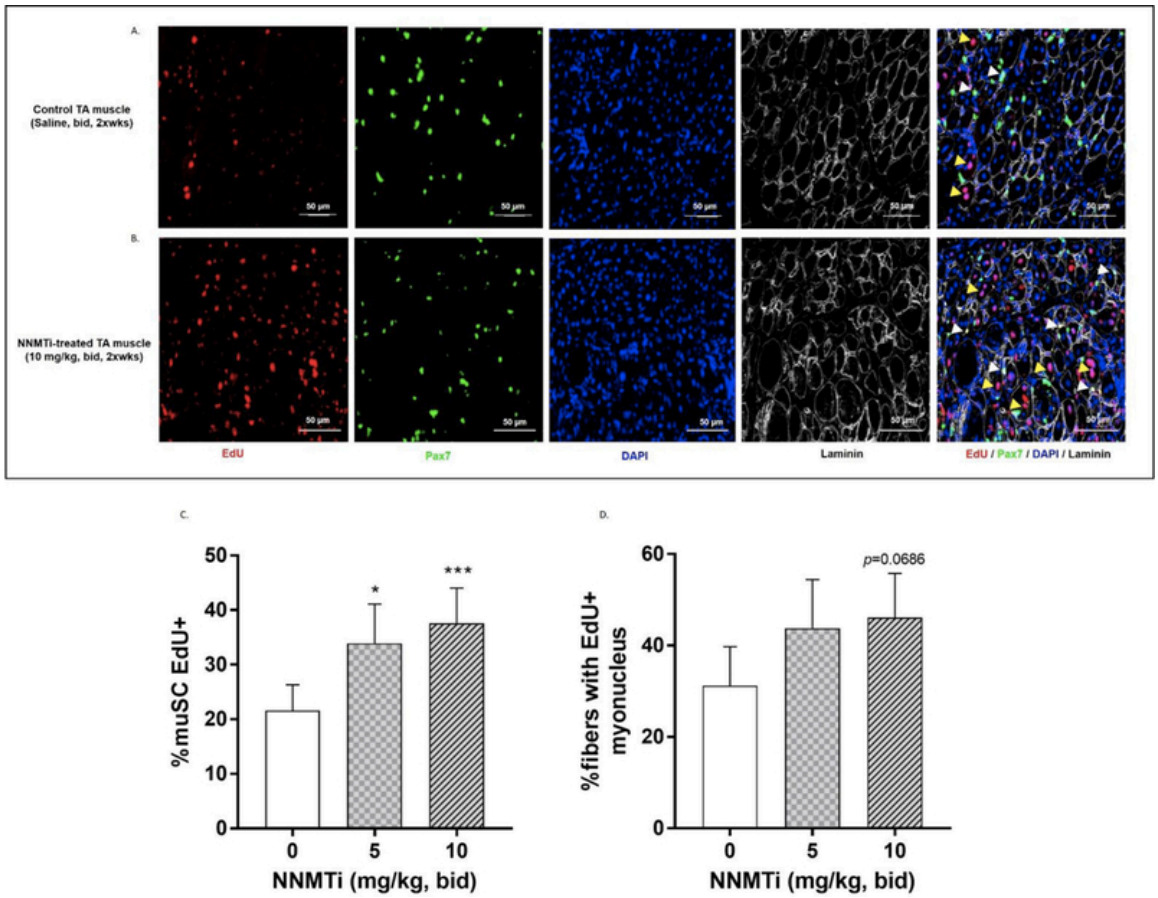

Figure 4.2: Effects of NNMTi on proliferation and fusion of muSCs into myofibers following injury of aged TA muscle.

(A) Representative image of control aged and injured TA muscle tissue immunolabeled to detect proliferation and fusion of muSCs using EdU (red), Pax7 (green), DAPI (blue), and laminin (white/gray) to trace myofibers.. (B) Representative image of aged and injured TA muscle tissue following 1-week post-injury treatment with NNMTi immunolabeled as in panel (A). White arrowheads denote muSCs that have proliferated post-injury (EdU+/Pax7+/DAPI+). Yellow arrowheads indicate myonuclei fused into damaged myofibers post-injury (EdU+/Pax7–/DAPI+). (C) Relative number of activated muSCs compared to total population of muSCs (% muSC EdU+) in NNMTi-treated and control aged TA muscle tissues following injury (n=10–12 per group). Data represent adjusted mean % muSC EdU+ ± 95% CI). *, $p < 0.05$ and ***, $p < 0.001$ vs. control as determined by Tukey-adjusted posthoc comparisons. (D) Percentage of myofibers containing EdU+ myonucleus (% fibers with EdU+ myonucleus) in NNMTi-treated and control aged TA

muscle tissues following injury (n=10–12 per group). Data represent adjusted mean % fibers with EdU+ myonucleus ± 95% CI. Consistent with % muSC EdU+ data (C), an increase in % fibers with EdU+ myonucleus trend was observed with NNMTi treatment relative to control, with the high dose of 10 mg/kg treatment showing a near statistically significant increase ($p = 0.069$) vs. control.

In vivo NNMT inhibition promotes muscle fiber growth after aged muscle injury

Damaged TA muscle tissues were immunolabeled with laminin to trace fibers, and the cross-sectional area (CSA) of the fibers was analyzed and compared between control and NNMTi-treated tissues. Representative laminin labeled, muscle fiber-traced images obtained from control (left panel) and NNMTi 10 mg/kg dose (right panel) treatment groups are shown in Fig. 4.3A. One-week post-injury treatment with NNMTi at the high dose (10 mg/kg) produced a significant 1.8-fold increase in the mean CSA of damaged TA muscle fibers relative to control (Tukey adjusted P values: $p = 0.0052$, 10 mg/kg dose vs. control) (Fig. 4.3B). A similar (1.6-fold) dose-dependent increase was observed at the high dose of NNMTi treatment compared to the low dose tested (Tukey adjusted P values: $p = 0.023$, 10 mg/kg dose vs. 5 mg/kg), while the low dose of NNMTi treatment did not significantly alter the muscle fiber mean CSA compared to control (Tukey adjusted $p > 0.05$) (Fig. 4.3B). These results demonstrate that small molecule-mediated in vivo NNMT inhibition improves muscle regeneration and growth, consistent with the enhanced satellite cell activation and fusion observed following injury of the aged muscle (Fig. 4.2).

The dramatic increase in muscle fiber size following a brief treatment with NNMTi supported the testing of high dose NNMTi in a separate cohort of aged mice to assess the impact of longer-term treatment on complete muscle recovery following injury. As shown in Fig. 4.3C, the mean CSA of damaged muscle fibers from aged mice was significantly (2-to 3-fold) larger at 3-weeks post-injury compared to 1-week post-injury (Fig. 4.3C vs. vs. 4.3B), indicating progressive longitudinal recovery of damaged muscle in aged mice. Consistent with CSA results observed with 1-week post-injury treatment, three-week post-injury treatment with 10 mg/kg NNMTi produced a statistically significant and

physiologically relevant 1.5-fold increase in the mean CSA of damaged TA muscle fibers relative to control (Tukey adjusted $p = 0.039$). As noted in the Methods section, a single aged mouse that showed unusually low CSA (included for completeness and indicated by filled diamond scatter point in Fig. 4.3C) due to unaccountable factors (i.e., lower CSA than control CSA in even the 1-week post-injury data) was excluded from analysis. Taken together, these results suggest that in vivo NNMT inhibition not only increases the rate of recovery by early activation of satellite cells, but also increases the overall magnitude of recovery following injury to aged muscle (Tukey adjusted $p > 0.05$).

Further, binned analysis of the muscle fiber CSA size distribution demonstrated a significant interaction between fiber size and NNMTi treatment ($F(17, 396) = 3.315$; $p < 0.0001$) as analyzed by a two-way ANOVA (Fig. 4.3D). Particularly, a significant downward shift in the frequency of smaller sized myofibers (Fig. 3D; $p = 0.03$, NNMTi treatment vs. control in the frequency of fibers up to 100 μm2 CSA; $p = 0.0002$, NNMTi treatment vs. control for 200 μm2 CSA bin) and prominent rightward and upward shifts toward larger sized fibers ($p = 0.07$, NNMTi treatment vs. control in the frequency of fibers at sizes greater than 1600 μm2 CSA) were noted in the damaged myofibers of aged mice treated with the high dose NNMTi (Fig. 4.3D).

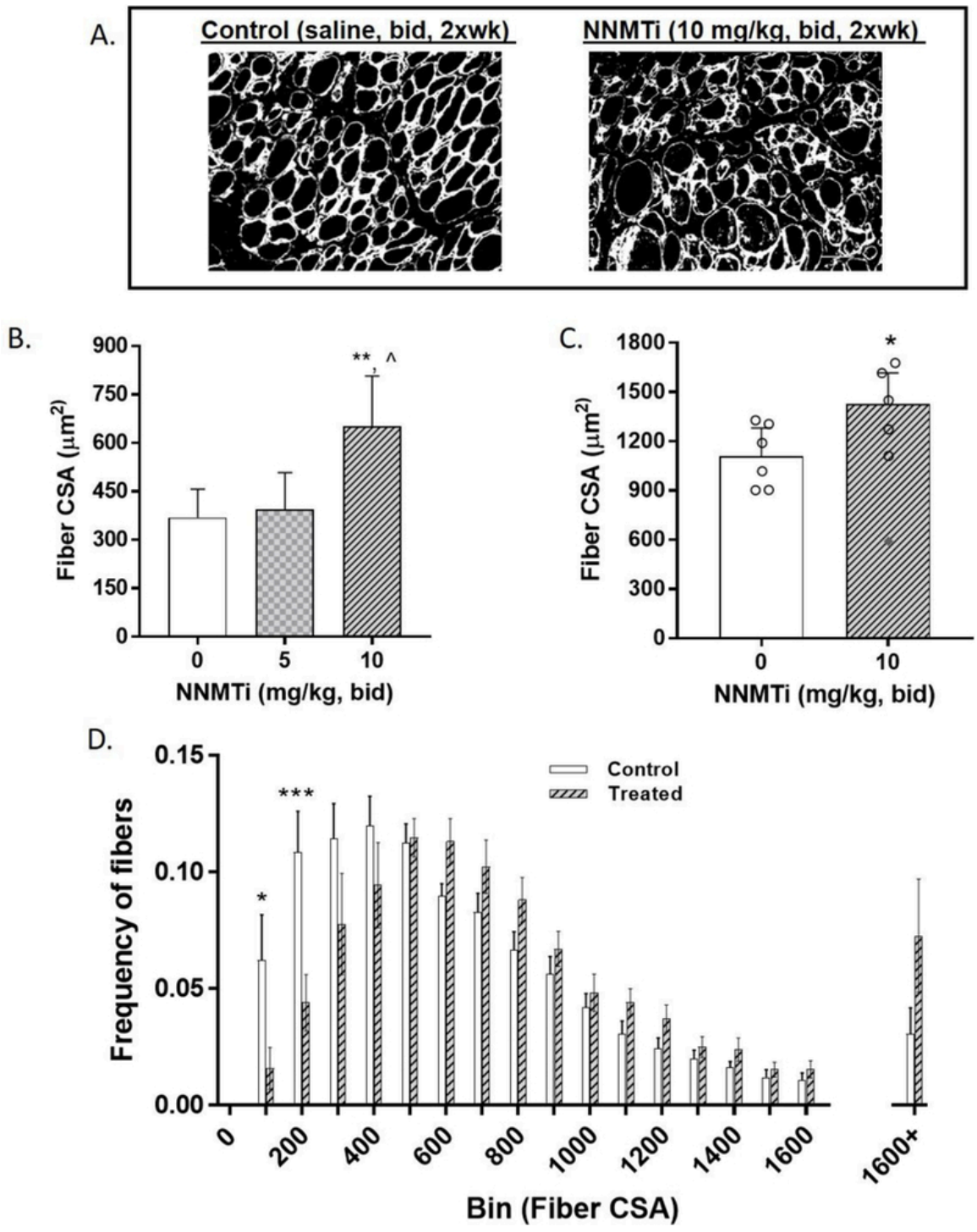

Figure 4.3: Effect of NNMTi on damaged TA muscle fiber cross-sectional area (CSA).

(A) Representative images of aged and injured TA muscle tissue following 1-week post-injury in control (left panel) NNMTi-treated (right panel); immunolabeled with laminin (indicated in white) to quantify CSA. (B) Mean CSA of damaged TA muscle fibers analyzed in aged control and NNMTi-treated mice (n=10–12 per group). Data represent adjusted mean CSA (μm2) ± 95% CI. **, $p < 0.01$ vs. control; ^, $p < 0.05$ vs. 5 mg/kg. (C)

Mean CSA of damaged TA muscle fibers analyzed in aged control and treated (10 mg/kg) mice following longer-term (3-week post-injury) treatment to assess more complete recovery (n=6 per group). Data represent adjusted mean CSA (μM2) ± 95% CI with individual datapoints represented as a scatter plot. *, $p < 0.05$ vs. control, with one datapoint (indicated in filled diamond) in the treated group eliminated from analysis on the basis of an unusually low (i.e., below threshold) CSA value for complete recovery analysis ($p > 0.05$, n.s. with this data point included). (D) Frequency of fibers binned as a function of CSA area in aged control and NNMTi (high dose, 10 mg/kg)-treated mice (n=12/group). Data represent mean frequency of fibers per bin ± SEM. *, $p < 0.05$ vs. control and ***, $p < 0.001$ vs. control.

In vivo NNMT inhibition improves aged TA muscle contractile force

In vivo dorsiflexor torque measurements were conducted 1-week post-injury on the damaged TA muscle of control and NNMTi treated aged mice to assess muscle contractile function properties at maximum applied force conditions. Peak torque output of the damaged TA muscle, when normalized to body weight of each animal, was 67% higher in NNMTi-treated group compared to control group. This increase that was functionally and statistically significant ($p = 0.033$ vs. control; Fig. 4.4A), and consistent with the increased fiber size observed in the treated cohort. In contrast, peak torque output when normalized to the muscle fiber size (i.e, normalized to regenerating TA myofiber CSA and presented as torque per unit area, Fig. 4.4B) showed no difference between the treated and control groups ($p > 0.05$; Fig. 4.4B); this lack of difference was largely driven by the significantly larger muscle fiber mean CSA in the NNMTi-treated mice relative to controls. These data clearly provide support for greatly improved functional strength in aged muscle with in vivo NNMTi treatment, in addition to the improved muscle regeneration response observed following injury.

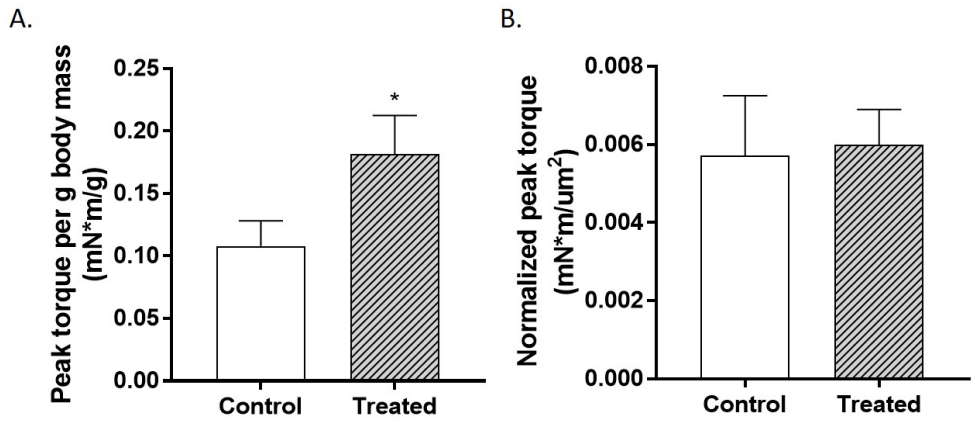

Figure 4.4: Effect of NNMTi on TA muscle contractile force in aged mice following TA muscle injury.

(A) Maximum torque measured per g of body mass *in vivo* in response to maximum force delivered via minimal electric stimulation of the TA muscle in aged control and NNMT-treated mice (n=6-7 per group). Data represent mean peak torque per g of body mass (mN*m/g) ± SEM. *, $p < 0.05$ vs. control. (B) Maximum torque measured normalized to fiber CSA analyzed per animal in aged control and NNMT-treated mice (n=6-7 per group). Data represent mean normalized peak torque (mN*m/um^2) ± SEM.

Chronic administration of NNMTi produces no systemic toxicity

As shown in Table 4.1, a complete plasma chemistry panel including major organ enzymes (liver, pancreas, gastrointestinal, renal, endocrine), total lipid, plasma proteins, and major electrolytes were profiled and compared between control and high dose (10 mg/kg) NNMTi-treated plasma samples. No significant differences were noted in the levels of the tested enzymes, glucose, cholesterol, plasma proteins, and electrolytes between control and NNMTi-treated samples (Table 4.1). Amylase levels were noted to be higher in all aged animals (regardless of control/treatment conditions) relative to young animals, likely indicative of general age-related dysfunctions (Table 4.1). Moreover, control and treated cohorts had similar body weight changes in all studies, suggesting similar feeding patterns (data not shown). Taken together, 1-week post-injury daily repeat-dosing of NNMTi was well tolerated with no untoward systemic toxicity or behavioral implications in aged mice.

Table 4.1: Serum chemistry panel from control and NNMTi-treated (10 mg/kg) aged mice.

Serum marker	Control	Treated	p-value*
Creatine kinase (U/L)	648 ± 229	419 ±88	0.39
AST(U/L)	280 ± 84	248 ± 81	0.79
ALT(U/L)	142 ± 61	110 ± 44	0.69
ALP (U/L)	85 ± 15	75 ± 8	0.55
GGT (U/L)	< 3	< 3	
GLDH (U/L)	73 ± 46	103 ± 43	0.66
Amylase(U/L)^	1365 ± 748	1344 ± 554	0.77
Total bilirubin (mg/dL)	0.18 ± 0.03	0.18 ± 0.03	>0.99
BUN (mg/dL)	23 ± 2	43 ± 12	0.17
Glucose (mg/dL)	194 ± 23	173 ± 10	0.43
Cholesterol (mg/dL)	81 ± 3	94 ± 12	0.36
Total protein (g/dL)	4.4 ± 0.2	4.4 ± 0.1	0.91
Albumin (g/dL)	2.4 ± 0.063	2.4 ± 0.048	0.25
Globulin (g/dL)	1.9 ± 0.2	2.2 ± 0.075	0.29
Calcium (mg/dL)	8.7 ± 0.3	8.7 ± 0.2	0.94
Phosphorous (mg/dL)	6.7 ± 0.8	5.6 ± 0.5	0.29
Sodium (mEq/L)	147.5 ± 1.7	153.8 ± 2.8	0.10
Potassium (mEq/L)	5.6 ± 0.5	5.0 ± 0.2	0.30
Chloride (mEq/L)	114.5 ± 1.1	119.5 ± 2.4	0.10

p-value calculated using 2-tailed Student's t-test with Welch's correction (populations not assumed to have same standard deviations). Data represent mean ± SEM;n=4/group. *, *p*

> 0.05; no significant difference. ^, elevated levels in both cohorts suggesting age-related dysfunctions.

NNMTi treatment promotes differentiation of C2C12 myoblasts and alters NAD^+/NADH redox cofactors in differentiated C2C12 myotubes

In vitro experiments were conducted to probe phenotypic and metabolic implications of NNMT inhibition in C2C12 cells that capture many characteristics of satellite cells. Prior to determining the effects of NNMTi treatment in C2C12 cells, presence of NNMT target protein was qualitatively confirmed both in C2C12 myoblasts and differentiated myotubes using immunocytochemistry (Fig. 4.5A, 4.5B). NNMT expression was observed in C2C12 myoblast cells (Fig. 4.5A), differentiating myoblasts that were myogenic committed precursor cells (Fig. 4.5B, elongated, MHC-expressing cells indicated by yellow arrowheads), as well as in fully developed myotubes, which was confirmed by co-expression of NNMT with MHC (marker for myotubes/myofibers; Fig. 5B). Addition of NNMTi to confluent myoblasts under differentiation conditions produced a concentration-related increase in myoblast differentiation (Fig. 4.5C; $F(2, 21) = 10.27$, $p = 0.0008$ for NNMTi treatment factor). 30 μM NNMTi resulted in 18 ± 0.03% MHC-positive myotube nuclei, representing a 45% increase in the extent of myoblast differentiation (expressed as %MHC positive myotube nuclei) compared to untreated differentiating myoblasts that only produced 12 ± 0.4 % MHC-positive myotube nuclei (Fig.4. 5C; $p = 0.0004$ versus control).

C2C12 myoblasts and differentiating myotubes were treated with NNMTi for 24 h to determine the effects of NNMTi treatment on NAD+ and NADH levels and the metabolic redox states. NNMTi treatment did not significantly alter NAD+ (Fig. 4.5D; $H(2) = 4.57$, $p = 0.067$) and NADH (Fig. 4.5E; $H(2) = 3.71$, $p = 0.2$) levels or the redox state (NAD+/NADH ratio; Fig. 4.5F) in C2C12 myoblasts. Similarly, NNMTi treatment produced no significant change in the NAD+ levels (Fig. 4.5G, $F(2, 8) < 1.0$, $p > 0.05$, n.s.) in differentiated C2C12 myotubes. However, NNMTi treatment produced concentration-

dependent increases in NADH levels (Fig. 4.5H; $F(2, 8) = 7.059$, $p = 0.0171$), as indicated by 50% higher slopes generated from reaction progress curves for NADH extracted samples with 30 μM NNMTi treatment suggesting 50% higher NADH concentrations compared to control untreated myotubes (Fig. 4.5H; $p = 0.0118$ versus control). Given the observed NAD+ and NADH responses to NNMTi treatment, NAD+/NADH ratios decreased in a concentration-related manner with NNMTi treatment of myotubes (Fig. 4.5I; $F(2, 8) = 11.65$, $p = 0.0043$). The NAD+/NADH ratio was 25% lower with 10 μM NNMTi (Fig. 4.5I; $p = 0.0443$ versus control) and 40% lower with 30 μM NNMTi (Fig. 4.5I; $p = 0.0024$ versus control) compared to control.

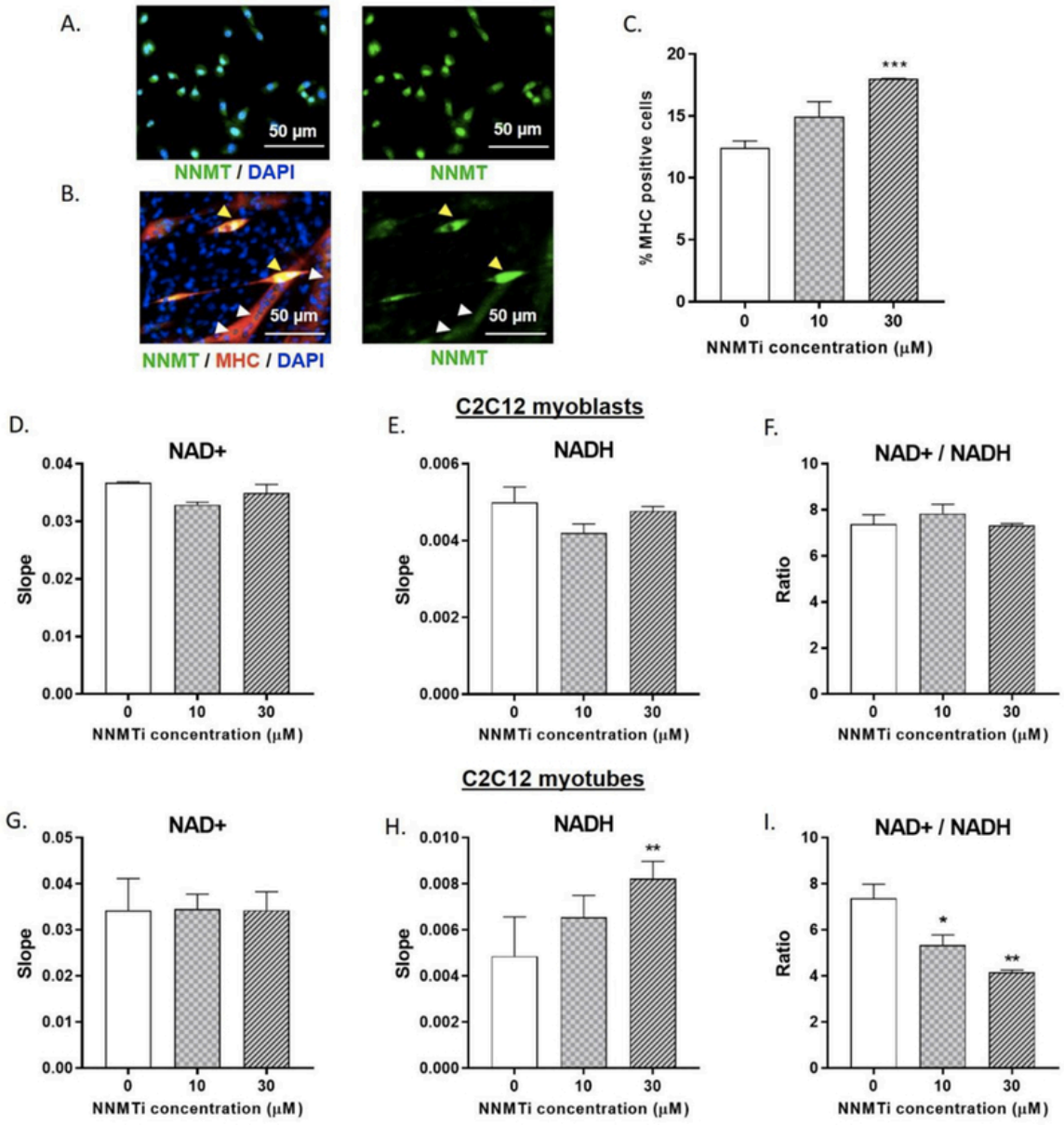

Figure 4.5: Effects of NNMTi on C2C12 myoblast differentiation and NAD+ salvage pathway metabolites in C2C12 myoblasts and myotubes.

(A) Representative image of C2C12 myoblasts immunolabeled to highlight NNMT (green) and nuclei (blue). All myoblast cells appear to express NNMT. (B) Representative image of C2C12 differentiated myotubes immunolabeled to highlight NNMT (green), myosin heavy chain (MHC; red), and nuclei (blue). Yellow arrowheads represent NNMT expression in elongated, differentiation-committed myogenic precursor cells (co-labeled with MHC) and white arrowheads indicate NNMT expression in fully-differentiated myotubes (co-labeled with MHC marking myofibers). (C) Relative frequency of MHC positive cells in control and NNMTi -treated myoblasts at 96 h post-treatment in culture and under differentiation conditions. Data represent mean % MHC positive cells ± SEM measured in duplicates per condition. ***, $p < 0.001$ vs. control. (D) NAD+ levels, (E)

NADH levels, and (F) NAD+/NADH ratio in control and NNMTi-treated (24 hr) C2C12 myoblasts. (G) NAD+levels, (H) NADH levels, and (I) NAD+/NADH ratio in control and NNMTi-treated (24 hr) differentiated C2C12 myotubes. Data represent mean slopes calculated from reaction progress curves (D, E, G, H) or ratios of slopes (F, I) obtained from spectrophotometric enzyme assays, where the slope is proportional to NAD+ and NADH concentrations (performed in duplicates across two experiments). *, $p < 0.05$ and **, $p < 0.01$ vs. control.

DISCUSSION

To our knowledge, this is the first study to demonstrate that systemic treatment of aged animals with a small molecule drug-like NNMT inhibitor[128, 129] can rejuvenate satellite cells, thereby robustly promoting satellite cell activation and fusion which are critical to support de novo myofiber regeneration and repair following injury.[26, 27, 115] At 1-week post-injury, control aged mice showed poor myofiber growth, minimal satellite cell activity, and a compromised skeletal muscle repair profile; these observations were consistent with impaired satellite cell regenerative capacity previously reported in skeletal muscles from aged mice.[134, 135] In contrast, aged mice treated with NNMTi dramatically increased the frequency of activated satellite cells and greatly enhanced muscle repair via satellite cell fusion and subsequent myonuclear accrual. Both the number of activated satellite cells and the average size of regenerating myofibers on the injured limb had nearly doubled at 1-week post-injury with treatment facilitating the development of myofibers with much larger cross-sectional areas, similar to youthful myogenic growth response.[134, 135] Consistent with increased muscle fiber growth, NNMTi treatment nearly doubled peak dorsiflexor torque output on the injured limb, suggesting clinically meaningful overall improvements in muscle strength and function. Additionally, at 3-weeks post-injury, when the damaged muscles of the control animals had undergone additional recovery, we observed that prolonged NNMTi treatment resulted in further enhancement of myofiber growth compared to controls. These results suggest that prolonged NNMTi treatment enables a more complete recovery of the injured aged muscles, as average myofiber sizes were

comparable between injured TA muscles of the treated aged mice and uninjured TA muscles of similar aged (24-mo-old) mice.[55]

Consistent with our findings, Zhang and colleagues recently observed that 6-8 week treatment of 22-24-mo-old mice with high levels of NR (an NAD^+ precursor agent) accelerated muscle regeneration following cardiotoxin-induced injury to the TA muscle.[70] Interestingly, we observed that NNMTi treatment did not alter the pool of muSCs from the TA muscle of aged mice, whereas Zhang et al. observed that NR treatment increased the absolute number of muSCs pooled from numerous (e.g., gastrocnemius, soleus, quadriceps, TA) aged muscle tissues.[70] This difference may be due to the shorter (2-week) treatment regimen used in the current study compared to the longer (6-8 week) treatment regimen employed with NR,[70] or to the different skeletal muscle groups examined in these studies since it has been observed that only a few mouse muscle groups (e.g., gastrocnemius, soleus) experience age-related declines in satellite cell abundance.[51]

The molecular mechanisms by which NNMT inhibition promotes satellite cell activation and myogenic response are currently unknown, but potentially associates with NNMT's central role in regulating the NAD+ salvage pathway, which in turn affects intracellular NAD+ levels and SIRT1 (NAD-dependent deacetylase sirtuin 1) activity that modulate a cell's metabolic and transcriptional responses.[120, 124] Since satellite cells represent only about 3–5% of adult muscle fiber nuclei and a small proportion of the cells within the whole muscle tissue,[64, 70] we performed additional experiments in cultured C2C12 myoblasts undergoing programmed differentiation, a system that recapitulates many of the features of satellite cell activation and thus can serve as a model to better understand how NNMTi treatment rejuvenates aged satellite cell and alters metabolic states of cells during differentiation.[64, 136] NNMTi treatment enhanced C2C12 myoblast differentiation and promoted myotube formation, selectivity increasing NADH levels and reducing NAD+/NADH ratio in differentiating myotubes, without impacting the metabolic states of myoblasts. These in vitro results suggest that NNMT inhibition enables satellite

cells to become increasingly activated and committed to muscle precursor cells with increased potential to differentiate, which is consistent with the increased differentiation and fusion of activated satellite cells observed in NNMTi-treated aged mice following muscle injury.

Satellite cell differentiation-dependent metabolic reprogramming has been previously demonstrated by Ryall and colleagues.[64] Specifically, activated and differentiation-committed C2C12 myoblasts were shown to switch to glycolytic metabolism with marked reductions in NAD+/NADH ratio (mediated by increased NADH levels and reduced NAD+ levels) and SIRT-1 histone deacetylase activity, and accompanied by myogenic stimulation and increased MyoD expression (muscle-specific transcription factor routinely used to denote activated satellite cells). In contrast, oxidation-dependent metabolism marked by higher NAD+ levels and SIRT-1 activity predominate in C2C12 myoblasts that are more equivalent to quiescent satellite cells.[64, 70, 137] Thus, our findings that NNMTi treatment selectively increased NADH levels and reduced NAD+/NADH ratio in differentiating myotubes, without impacting metabolic states in quiescent myoblasts are consistent with results from Ryall et al., favoring a switch towards glycolytic metabolism reprogramming (i.e., increased NAD+ substrate utilization in glycolysis for meeting muSC differentiation energy demands) that supports enhanced myoblast differentiation. Taken together, our working model regarding the molecular mechanisms whereby NNMT inhibition promotes satellite cell activation and increases myogenic response is illustrated schematically in Figure 4.6. As muscles age, NNMT expression and activity increases in the skeletal muscles, which impairs NAD+ flux through the salvage pathway and dysregulates SIRT-1 activity, thereby interfering with the capacity of satellite cells to maintain quiescence as well as the efficiency to proliferate, differentiate, and promote efficient muscle regeneration following injury.[64, 70] Given that NNMT appears to be uniformly expressed in skeletal muscles independent of fiber type distribution (i.e., type I, IIa, IIb) as previously demonstrated,[125] suggests its dynamic

involvement in the regulation of both oxidative and glycolytic metabolism. Future studies will investigate if similar metabolic changes are observed in satellite cells isolated from NNMTi-treated skeletal muscle ex-vivo, and subsequently investigate the effects of NNMTi treatment on mitochondrial biogenesis and epigenetic modulations (both via SIRT-1 and SAM in the methionine pathways) in aged muscles.

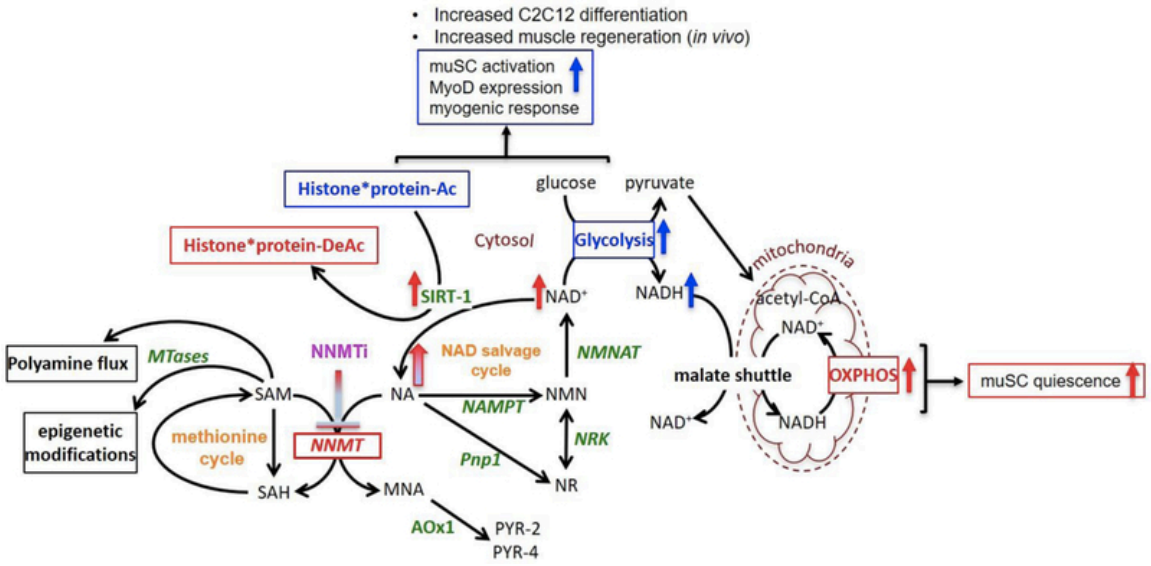

Figure 4.6: Schematic illustration of pathways regulated by NNMT and proposed working model of mechanisms of action of NNMT inhibition as it relates to muSC activation and metabolic state in aged muscle tissue.

Maintenance of flux through the NAD salvage pathway by NNMTi is indicated by gradient blue/red arrow; (i) increase flux of NAD+, activated SIRT-1, and oxidative metabolism that support quiescent muSCs are indicated by red arrows; (ii) increased NADH (i.e., increased NAD+ utilization in glycolysis), enhanced glycolysis, and reduced SIRT-1 mediated histone deacetylation that support muSC activation and differentiation are indicated by blue arrows. Pathway abbreviations include AOx1 (aldehyde oxidase), NA (nicotinamide), MNA (1-methylnicotinmaide), NAMPT (nicotinamide phosphoribosyltransferase), NMN (nicotinamide mononucleoside), NMNAT (nicotinamide adenylyltransferase), NNMT (nicotinamide N-methyltransferase), NR (nicotinamide riboside), NRK (nicotinamide riboside kinase), PNP1 (purine nucleoside phosphorylase), PYR-2/4 (1-methyl-2/4-pyridone-5-carboxamide), SAH (S-adenosyl-L-homocysteine), SAM (S-adenosylmethionine), MTases (methyl transferases), SIRT1 (NAD-dependent deacetylase sirtuin 1), NAD+/NADH (oxidized Nicotinamide adenine dinucleotide/reduced form of NAD+), OXPHOS (oxidative phosphorylation), Histone*protein-Ac/DeAc (Acetylated/deacetylated histones).

In conclusion, the present findings convincingly demonstrate that NNMT inhibition provides a viable, safe, and non-invasive therapeutic approach to rejuvenate dysregulated satellite cells and restore their regenerative capacity in aged skeletal muscles, as well as their intrinsic quiescent properties, to support dynamic muscle repair mechanisms after injury. Significantly, NNMT inhibition enhanced myofiber regeneration and growth following injury and dramatically improved the strength of the injured muscle, suggesting overall functional improvements to aged skeletal muscles. These results support NNMT inhibitors as novel therapeutics to restore a healthy myogenic response in injured aging skeletal muscle through rejuvenation of satellite cell activity, translating into improved muscle function and potentially mitigating the functional decline which sarcopenic older adults typically experience following muscular injury. Evaluations on the longitudinal effects of NNMTi treatment on muscle functional outputs (including measures of strength and endurance), safety/toxicology, and mechanistic implications of NNMT inhibition on aged muscle physiology will be continued to validate the clinical translational benefits of NNMTi therapeutics.

CHAPTER 5:

General Conclusion and Future Directions

Satellite cells are important regulators of plasticity of skeletal muscle adapting to stimuli—such as exercise and injury. However, age-associated satellite cell dysfunction mediated by intrinsic and extrinsic factors impairs optimal responsiveness and subsequent adaptation to these stimuli, resulting in impeded overload-induced hypertrophy and regeneration of muscle after injury.[25, 29, 30, 35]

The studies included in this dissertation demonstrate that satellite cells of aged skeletal muscle are activated by overload stimuli (synergist ablation and PoWeR). However, with surgical overload via synergist ablation, hypertrophy is not achieved in plantaris muscles from old mice, regardless of satellite cell availability. This finding highlights impaired overload-induced hypertrophy in the plantaris muscles of old mice compared to young mice also subjected to surgically induced mechanical overload of the same duration.[41] Furthermore, the lack of overload-induced hypertrophy in plantaris muscles resultant from synergist ablation surgery in old mice calls into question this common murine model to study muscle hypertrophy, underscoring the need for an alternative overload model to investigate hypertrophy specifically in old mice. Results presented in Chapter 3 indicate that PoWeR is a more translatable murine overload model to induce hypertrophy of the intact plantar complex, similar to the growth response observed in older adult exercise training studies (resistance exercise training and cycle ergometer training).[18, 77, 92]

PoWeR appears to be a superior model to study mechanisms contributing to exercise adaptations in aging skeletal muscle as compared to surgical overload, by eliciting expansion of the satellite cell pool with myonuclear accrual, fiber type adaptations, and improved contractile function—possibly mediated by a robust angiogenic response in

skeletal muscle with PoWeR that is absent from surgical overload.[86] Capillary density is documented to decrease with age as CD31+ endothelial cells undergo age-associated apoptosis.[102] Increased capillary density has been reported in response to surgical overload in young mice concurrent with myofiber hypertrophy, with no increase in capillary density occurring in old mice given the same surgical overload stimulus.[86] The inability of surgical overload to elicit an angiogenic response in skeletal muscle of old mice may explain impeded overload-induced hypertrophy, as capillaries are integral to supply oxygen, nutrients, hormones, and other signaling molecules and remove waste products in skeletal muscle myofibers and satellite cells[138-140]—which supports optimal tissue turnover and responsiveness to anabolic stimuli. Ongoing studies aim to assess this idea by preceding synergist ablation in old mice with a period of aerobic exercise (unweighted wheel running) to promote angiogenesis and increased capillary density prior to surgical overload to ascertain the role of increased muscle capillarization to at least partially restore a youthful hypertrophic response to synergist ablation in old mice.

Additionally, the final study included in this dissertation explores satellite cells as a mediator of muscle plasticity with injury and demonstrates that inhibition of NNMT enhances the impaired activity of satellite cells in aging muscle after injury, resulting in improved muscle plasticity and recovery that supports superior functional performance. Future studies will examine the addition of pharmacological NNMT inhibition to PoWeR in old mice to optimize satellite cell activity and potentially augment overload-induced hypertrophy of aging muscle, determining if NNMTi not only attenuates sarcopenia through restoration of muscle recovery after acute injury but also as a conjunctive therapy to resistance exercise.

References

1. Lieber RL, Roberts TJ, Blemker SS, Lee SSM, Herzog W. Skeletal muscle mechanics, energetics and plasticity. *J Neuroeng Rehabil*. Oct 23 2017;14(1):108. doi:10.1186/s12984-017-0318-y

2. Deer RR, Volpi E. Protein intake and muscle function in older adults. *Curr Opin Clin Nutr Metab Care*. May 2015;18(3):248-53. doi:10.1097/mco.0000000000000162

3. Cruz-Jentoft AJ, Baeyens JP, Bauer JM, et al. Sarcopenia: European consensus on definition and diagnosis: Report of the European Working Group on Sarcopenia in Older People. *Age Ageing*. Jul 2010;39(4):412-23. doi:10.1093/ageing/afq034

4. Kim T, Choi K. Sarcopenia: Definition, Epidemiology, and Pathophysiology. *Journal of Bone Metabolism*. 2013;20(1):1-10.

5. Kramer IF, Snijders T, Smeets JSJ, et al. Extensive Type II Muscle Fiber Atrophy in Elderly Female Hip Fracture Patients. *J Gerontol A Biol Sci Med Sci*. Oct 1 2017;72(10):1369-1375. doi:10.1093/gerona/glw253

6. Nilwik R, Snijders T, Leenders M, et al. The decline in skeletal muscle mass with aging is mainly attributed to a reduction in type II muscle fiber size. *Exp Gerontol*. May 2013;48(5):492-8. doi:10.1016/j.exger.2013.02.012

7. Grounds MD. Age-associated changes in the response of skeletal muscle cells to exercise and regeneration. *Ann N Y Acad Sci*. Nov 20 1998;854:78-91.

8. Goodpaster BH, Park SW, Harris TB, et al. The loss of skeletal muscle strength, mass, and quality in older adults: the health, aging and body composition study. *J Gerontol A Biol Sci Med Sci*. Oct 2006;61(10):1059-64.

9. Brown JC, Harhay MO, Harhay MN. Sarcopenia and mortality among a population-based sample of community-dwelling older adults. *J Cachexia Sarcopenia Muscle*. Jun 2016;7(3):290-8. doi:10.1002/jcsm.12073

10. Shafiee G, Keshtkar A, Soltani A, Ahadi Z, Larijani B, Heshmat R. Prevalence of sarcopenia in the world: a systematic review and meta- analysis of general population studies. *J Diabetes Metab Disord*. 2017;16:21. doi:10.1186/s40200-017-0302-x

11. Baumgartner RN, Koehler KM, Gallagher D, et al. Epidemiology of sarcopenia among the elderly in New Mexico. *Am J Epidemiol*. Apr 15 1998;147(8):755-63.

12. Janssen I, Heymsfield SB, Wang ZM, Ross R. Skeletal muscle mass and distribution in 468 men and women aged 18-88 yr. *J Appl Physiol (1985)*. Jul 2000;89(1):81-8. doi:10.1152/jappl.2000.89.1.81

13. Hunter GR, McCarthy JP, Bamman MM. Effects of resistance training on older adults. *Sports Med*. 2004;34(5):329-48.

14. Janssen I, Shepard DS, Katzmarzyk PT, Roubenoff R. The healthcare costs of sarcopenia in the United States. *J Am Geriatr Soc*. Jan 2004;52(1):80-5.

15. Paul AC, Rosenthal N. Different modes of hypertrophy in skeletal muscle fibers. *J Cell Biol*. Feb 18 2002;156(4):751-60. doi:10.1083/jcb.200105147

16. Candow DG, Forbes SC, Little JP, Cornish SM, Pinkoski C, Chilibeck PD. Effect of nutritional interventions and resistance exercise on aging muscle mass and strength. *Biogerontology*. Aug 2012;13(4):345-58. doi:10.1007/s10522-012-9385-4

17. Fry C, Drummond M, Glynn E, et al. Aging impairs contraction-induced human skeletal muscle mTORC1 signaling and protein synthesis. *Skeletal Muscle*. 2011;1(11)

18. Kosek DJ, Kim JS, Petrella JK, Cross JM, Bamman MM. Efficacy of 3 days/wk resistance training on myofiber hypertrophy and myogenic mechanisms in young vs. older adults. *J Appl Physiol (1985)*. Aug 2006;101(2):531-44. doi:10.1152/japplphysiol.01474.2005

19. Karlsen A, Bechshøft RL, Malmgaard-Clausen NM, et al. Lack of muscle fibre hypertrophy, myonuclear addition, and satellite cell pool expansion with resistance training in 83-94-year-old men and women. *Acta Physiol (Oxf)*. Sep 2019;227(1):e13271. doi:10.1111/apha.13271

20. Snijders T, Nederveen JP, McKay BR, et al. Satellite cells in human skeletal muscle plasticity. *Front Physiol*. 2015;6:283. doi:10.3389/fphys.2015.00283

21. Ballak SB, Jaspers RT, Deldicque L, et al. Blunted hypertrophic response in old mouse muscle is associated with a lower satellite cell density and is not alleviated by resveratrol. *Exp Gerontol*. Feb 2015;62:23-31. doi:10.1016/j.exger.2014.12.020

22. McCarthy JJ, Dupont-Versteegden EE, Fry CS, Murach KA, Peterson CA. Methodological issues limit interpretation of negative effects of satellite cell depletion on adult muscle hypertrophy. *Development*. 2017:1363-1365. vol. 8.

23. Egner IM, Bruusgaard JC, Gundersen K. An apparent lack of effect of satellite cell depletion on hypertrophy could be due to methodological limitations. Response to 'Methodological issues limit interpretation of negative effects of satellite cell depletion on adult muscle hypertrophy'. *Development*. 2017:1365-1367. vol. 8.

24. Brack AS, Conboy MJ, Roy S, et al. Increased Wnt signaling during aging alters muscle stem cell fate and increases fibrosis. *Science*. Aug 10 2007;317(5839):807-10. doi:10.1126/science.1144090

25. Conboy IM, Rando TA. Aging, stem cells and tissue regeneration: lessons from muscle. *Cell Cycle*. Mar 2005;4(3):407-10. doi:10.4161/cc.4.3.1518

26. Lepper C, Partridge TA, Fan CM. An absolute requirement for Pax7-positive satellite cells in acute injury-induced skeletal muscle regeneration. *Development*. Sep 2011;138(17):3639-46. doi:10.1242/dev.067595

27. Murphy MM, Lawson JA, Mathew SJ, Hutcheson DA, Kardon G. Satellite cells, connective tissue fibroblasts and their interactions are crucial for muscle regeneration. *Development*. Sep 2011;138(17):3625-37. doi:10.1242/dev.064162

28. Sambasivan R, Yao R, Kissenpfennig A, et al. Pax7-expressing satellite cells are indispensable for adult skeletal muscle regeneration. *Development*. Sep 2011;138(17):3647-56. doi:10.1242/dev.067587

29. Conboy IM, Conboy MJ, Wagers AJ, Girma ER, Weissman IL, Rando TA. Rejuvenation of aged progenitor cells by exposure to a young systemic environment. *Nature*. Feb 17 2005;433(7027):760-4. doi:10.1038/nature03260

30. Conboy IM, Conboy MJ, Smythe GM, Rando TA. Notch-mediated restoration of regenerative potential to aged muscle. *Science*. Nov 28 2003;302(5650):1575-7. doi:10.1126/science.1087573

31. Zammit PS, Heslop L, Hudon V, et al. Kinetics of myoblast proliferation show that resident satellite cells are competent to fully regenerate skeletal muscle fibers. *Exp Cell Res*. Nov 15 2002;281(1):39-49.

32. Fry CS, Lee JD, Jackson JR, et al. Regulation of the muscle fiber microenvironment by activated satellite cells during hypertrophy. *Faseb j*. Apr 2014;28(4):1654-65. doi:10.1096/fj.13-239426

33. Zammit PS, Partridge TA, Yablonka-Reuveni Z. The skeletal muscle satellite cell: the stem cell that came in from the cold. *J Histochem Cytochem*. Nov 2006;54(11):1177-91. doi:10.1369/jhc.6R6995.2006

34. Kuang S, Kuroda K, Le Grand F, Rudnicki MA. Asymmetric self-renewal and commitment of satellite stem cells in muscle. *Cell*. Jun 1 2007;129(5):999-1010. doi:10.1016/j.cell.2007.03.044

35. Sousa-Victor P, Garcia-Prat L, Serrano AL, Perdiguero E, Munoz-Canoves P. Muscle stem cell aging: regulation and rejuvenation. *Trends Endocrinol Metab*. Jun 2015;26(6):287-96. doi:10.1016/j.tem.2015.03.006

36. Fry CS, Kirby TJ, Kosmac K, McCarthy JJ, Peterson CA. Myogenic Progenitor Cells Control Extracellular Matrix Production by Fibroblasts during Skeletal Muscle Hypertrophy. *Cell Stem Cell*. Jan 5 2017;20(1):56-69. doi:10.1016/j.stem.2016.09.010

37. Schiaffino S, Bormioli SP, Aloisi M. The fate of newly formed satellite cells during compensatory muscle hypertrophy. *Virchows Arch B Cell Pathol*. Aug 11 1976;21(2):113-8.

38. Rosenblatt JD, Parry DJ. Gamma irradiation prevents compensatory hypertrophy of overloaded mouse extensor digitorum longus muscle. *J Appl Physiol (1985)*. Dec 1992;73(6):2538-43. doi:10.1152/jappl.1992.73.6.2538

39. Rosenblatt JD, Yong D, Parry DJ. Satellite cell activity is required for hypertrophy of overloaded adult rat muscle. *Muscle Nerve*. Jun 1994;17(6):608-13. doi:10.1002/mus.880170607

40. Cheek DB, Powell GK, Scott RE. GROWTH OF MUSCLE MASS AND SKELETAL COLLAGEN IN THE RAT. II. THE EFFECT OF ABLATION OF PITUITARY, THYROID OR TESTES. *Bull Johns Hopkins Hosp*. Jun 1965;116:387-95.

41. McCarthy JJ, Mula J, Miyazaki M, et al. Effective fiber hypertrophy in satellite cell-depleted skeletal muscle. *Development*. Sep 2011;138(17):3657-66. doi:10.1242/dev.068858

42. Goh Q, Millay DP. Requirement of myomaker-mediated stem cell fusion for skeletal muscle hypertrophy. *Elife*. Feb 10 2017;6doi:10.7554/eLife.20007

43. Egner IM, Bruusgaard JC, Gundersen K. Satellite cell depletion prevents fiber hypertrophy in skeletal muscle. *Development*. Aug 15 2016;143(16):2898-906. doi:10.1242/dev.134411

44. Lee JD, Fry CS, Mula J, et al. Aged Muscle Demonstrates Fiber-Type Adaptations in Response to Mechanical Overload, in the Absence of Myofiber Hypertrophy, Independent of Satellite Cell Abundance. *J Gerontol A Biol Sci Med Sci*. Apr 2016;71(4):461-7. doi:10.1093/gerona/glv033

45. Englund DA, Figueiredo VC, Dungan CM, et al. Satellite cell depletion disrupts transcriptional coordination and muscle adaptation to exercise. *Function*. 2021;2(1)

46. Dungan CM, Murach KA, Frick KK, et al. Elevated myonuclear density during skeletal muscle hypertrophy in response to training is reversed during detraining. *Am J Physiol Cell Physiol*. May 1 2019;316(5):C649-c654. doi:10.1152/ajpcell.00050.2019

47. Tatsumi R, Anderson JE, Nevoret CJ, Halevy O, Allen RE. HGF/SF is present in normal adult skeletal muscle and is capable of activating satellite cells. *Dev Biol*. Feb 1 1998;194(1):114-28. doi:10.1006/dbio.1997.8803

48. Wozniak AC, Anderson JE. Nitric oxide-dependence of satellite stem cell activation and quiescence on normal skeletal muscle fibers. *Dev Dyn*. Jan 2007;236(1):240-50. doi:10.1002/dvdy.21012

49. Hara M, Tabata K, Suzuki T, et al. Calcium influx through a possible coupling of cation channels impacts skeletal muscle satellite cell activation in response to mechanical stretch. *Am J Physiol Cell Physiol*. Jun 15 2012;302(12):C1741-50. doi:10.1152/ajpcell.00068.2012

50. Tatsumi R, Hattori A, Ikeuchi Y, Anderson JE, Allen RE. Release of hepatocyte growth factor from mechanically stretched skeletal muscle satellite cells and role of pH and nitric oxide. *Mol Biol Cell*. Aug 2002;13(8):2909-18. doi:10.1091/mbc.e02-01-0062

51. Keefe AC, Lawson JA, Flygare SD, et al. Muscle stem cells contribute to myofibres in sedentary adult mice. *Nat Commun*. May 14 2015;6:7087. doi:10.1038/ncomms8087

52. Verdijk LB, Koopman R, Schaart G, Meijer K, Savelberg HH, van Loon LJ. Satellite cell content is specifically reduced in type II skeletal muscle fibers in the elderly. *Am J Physiol Endocrinol Metab*. Jan 2007;292(1):E151-7. doi:10.1152/ajpendo.00278.2006

53. Sousa-Victor P, Gutarra S, Garcia-Prat L, et al. Geriatric muscle stem cells switch reversible quiescence into senescence. *Nature*. Feb 20 2014;506(7488):316-21. doi:10.1038/nature13013

54. Dumont NA, Wang YX, Rudnicki MA. Intrinsic and extrinsic mechanisms regulating satellite cell function. *Development*. May 1 2015;142(9):1572-81. doi:10.1242/dev.114223

55. Fry CS, Lee JD, Mula J, et al. Inducible depletion of satellite cells in adult, sedentary mice impairs muscle regenerative capacity without affecting sarcopenia. *Nat Med*. Jan 2015;21(1):76-80. doi:10.1038/nm.3710

56. Englund DA, Murach KA, Dungan CM, et al. Depletion of resident muscle stem cells negatively impacts running volume, physical function, and muscle fiber hypertrophy in response to lifelong physical activity. *Am J Physiol Cell Physiol*. Jun 1 2020;318(6):C1178-c1188. doi:10.1152/ajpcell.00090.2020

57. Schultz E, Lipton BH. Skeletal muscle satellite cells: changes in proliferation potential as a function of age. *Mech Ageing Dev*. Dec 1982;20(4):377-83.

58. Neelakantan H, Vance V, Wetzel MD, et al. Selective and membrane-permeable small molecule inhibitors of nicotinamide N-methyltransferase reverse high fat diet-induced obesity in mice. *Biochem Pharmacol*. Jan 2018;147:141-152. doi:10.1016/j.bcp.2017.11.007

59. McCroskery S, Thomas M, Maxwell L, Sharma M, Kambadur R. Myostatin negatively regulates satellite cell activation and self-renewal. *J Cell Biol*. Sep 15 2003;162(6):1135-47. doi:10.1083/jcb.200207056

60. Giresi PG, Stevenson EJ, Theilhaber J, et al. Identification of a molecular signature of sarcopenia. *Physiol Genomics*. Apr 14 2005;21(2):253-63. doi:10.1152/physiolgenomics.00249.2004

61. Imai S, Armstrong CM, Kaeberlein M, Guarente L. Transcriptional silencing and longevity protein Sir2 is an NAD-dependent histone deacetylase. *Nature*. Feb 17 2000;403(6771):795-800. doi:10.1038/35001622

62. Ramsey KM, Mills KF, Satoh A, Imai S. Age-associated loss of Sirt1-mediated enhancement of glucose-stimulated insulin secretion in beta cell-specific Sirt1-overexpressing (BESTO) mice. *Aging Cell*. Jan 2008;7(1):78-88. doi:10.1111/j.1474-9726.2007.00355.x

63. Imai S, Guarente L. NAD+ and sirtuins in aging and disease. *Trends Cell Biol*. Aug 2014;24(8):464-71. doi:10.1016/j.tcb.2014.04.002

64. Ryall JG, Dell'Orso S, Derfoul A, et al. The NAD(+)-dependent SIRT1 deacetylase translates a metabolic switch into regulatory epigenetics in skeletal muscle stem cells. *Cell Stem Cell*. Feb 5 2015;16(2):171-83. doi:10.1016/j.stem.2014.12.004

65. Covarrubias AJ, Perrone R, Grozio A, Verdin E. NAD(+) metabolism and its roles in cellular processes during ageing. *Nat Rev Mol Cell Biol*. Dec 22 2020;doi:10.1038/s41580-020-00313-x

66. Pala F, Di Girolamo D, Mella S, et al. Distinct metabolic states govern skeletal muscle stem cell fates during prenatal and postnatal myogenesis. *J Cell Sci*. Jul 27 2018;131(14)doi:10.1242/jcs.212977

67. Fang EF, Scheibye-Knudsen M, Brace LE, et al. Defective mitophagy in XPA via PARP-1 hyperactivation and NAD(+)/SIRT1 reduction. *Cell*. May 8 2014;157(4):882-896. doi:10.1016/j.cell.2014.03.026

68. Mills KF, Yoshida S, Stein LR, et al. Long-term administration of nicotinamide mononucleotide mitigates age-associated physiological decline in mice. *Cell Metab*. Dec 13 2016;24(6):795-806. doi:10.1016/j.cmet.2016.09.013

69. van de Weijer T, Phielix E, Bilet L, et al. Evidence for a direct effect of the NAD+ precursor acipimox on muscle mitochondrial function in humans. *Diabetes*. Apr 2015;64(4):1193-201. doi:10.2337/db14-0667

70. Zhang H, Ryu D, Wu Y, et al. NAD(+) repletion improves mitochondrial and stem cell function and enhances life span in mice. *Science*. Jun 17 2016;352(6292):1436-43. doi:10.1126/science.aaf2693

71. Abellan van Kan G. Epidemiology and consequences of sarcopenia. *Journal of Nutrition Health and Aging*. 2009;13(8):708-712.

72. Cruz-Jentoft AJ, Landi F, Schneider SM, et al. Prevalence of and interventions for sarcopenia in ageing adults: a systematic review. Report of the International Sarcopenia Initiative (EWGSOP and IWGS). *Age Ageing*. Nov 2014;43(6):748-59. doi:10.1093/ageing/afu115

73. von Haehling S, Morley J, Anker S. An overview of sarcopenia: facts and numbers on prevalence and clinical impact. *Journal of Cachexia Sarcopenia and Muscle*. 2010;1(2):129-133.

74. Tolea MI, Galvin JE. Sarcopenia and impairment in cognitive and physical performance. *Clin Interv Aging*. 2015;10:663-71. doi:10.2147/cia.s76275

75. Liguori I, Russo G, Aran L, et al. Sarcopenia: assessment of disease burden and strategies to improve outcomes. *Clin Interv Aging*. 2018;13:913-927. doi:10.2147/CIA.S149232

76. McGlory C, Phillips SM. Exercise and the Regulation of Skeletal Muscle Hypertrophy. *Progress in Molecular Biology and Translational Science*. Elsevier Inc. ; 2015:153-173:chap 7.

77. Moro T, Brightwell CR, Deer RR, et al. Muscle Protein Anabolic Resistance to Essential Amino Acids Does Not Occur in Healthy Older Adults Before or After

Resistance Exercise Training. *J Nutr*. Jun 1 2018;148(6):900-909. doi:10.1093/jn/nxy064

78. Murach KA, Fry CS, Kirby TJ, et al. Starring or Supporting Role? Satellite Cells and Skeletal Muscle Fiber Size Regulation. *Physiology (Bethesda)*. Jan 1 2018;33(1):26-38. doi:10.1152/physiol.00019.2017

79. Petrella JK, Kim JS, Mayhew DL, Cross JM, Bamman MM. Potent myofiber hypertrophy during resistance training in humans is associated with satellite cell-mediated myonuclear addition: a cluster analysis. *J Appl Physiol (1985)*. Jun 2008;104(6):1736-42. doi:10.1152/japplphysiol.01215.2007

80. Petrella JK, Kim JS, Cross JM, Kosek DJ, Bamman MM. Efficacy of myonuclear addition may explain differential myofiber growth among resistance-trained young and older men and women. *Am J Physiol Endocrinol Metab*. Nov 2006;291(5):E937-46. doi:10.1152/ajpendo.00190.2006

81. Murach KA, Englund DA, Dupont-Versteegden EE, McCarthy JJ, Peterson CA. Myonuclear Domain Flexibility Challenges Rigid Assumptions on Satellite Cell Contribution to Skeletal Muscle Fiber Hypertrophy. *Front Physiol*. 2018;9:635. doi:10.3389/fphys.2018.00635

82. Nishijo K, Hosoyama T, Bjornson CR, et al. Biomarker system for studying muscle, stem cells, and cancer in vivo. *Faseb j*. Aug 2009;23(8):2681-90. doi:10.1096/fj.08-128116

83. Kirby TJ, McCarthy JJ, Peterson CA, Fry CS. Synergist Ablation as a Rodent Model to Study Satellite Cell Dynamics in Adult Skeletal Muscle. *Methods Mol Biol*. 2016;1460:43-52. doi:10.1007/978-1-4939-3810-0_4

84. Wen Y, Murach KA, Vechetti IJ, Jr., et al. MyoVision: software for automated high-content analysis of skeletal muscle immunohistochemistry. *J Appl Physiol (1985)*. Jan 1 2018;124(1):40-51. doi:10.1152/japplphysiol.00762.2017

85. Murach KA, Dungan CM, Peterson CA, McCarthy JJ. Muscle Fiber Splitting Is a Physiological Response to Extreme Loading in Animals. *Exerc Sport Sci Rev*. Apr 2019;47(2):108-115. doi:10.1249/jes.0000000000000181

86. Hendrickse PW, Krusnauskas R, Hodson-Tole E, Venckunas T, Degens H. Regular endurance exercise of overloaded muscle of young and old male mice does not attenuate hypertrophy and improves fatigue resistance. *Geroscience*. Jul 8 2020;doi:10.1007/s11357-020-00224-x

87. Moro T, Brightwell CR, Phalen DE, et al. Low skeletal muscle capillarization limits muscle adaptation to resistance exercise training in older adults. *Exp Gerontol*. Sep 10 2019;127:110723. doi:10.1016/j.exger.2019.110723

88. Macaluso A, De Vito G. Muscle strength, power and adaptations to resistance training in older people. *Eur J Appl Physiol*. Apr 2004;91(4):450-72. doi:10.1007/s00421-003-0991-3

89. Murach KA, McCarthy JJ, Peterson CA, Dungan CM. Making Mice Mighty: recent advances in translational models of load-induced muscle hypertrophy. *J Appl Physiol (1985)*. Sep 1 2020;129(3):516-521. doi:10.1152/japplphysiol.00319.2020

90. Olesen AT, Malchow-Møller L, Bendixen RD, et al. Age-related myofiber atrophy in old mice is reversed by ten weeks voluntary high-resistance wheel running. *Exp Gerontol*. Nov 9 2020:111150. doi:10.1016/j.exger.2020.111150

91. Kurtys K, Gonera B, Olewnik Ł, Karauda P, Tubbs RS, Polguj M. Is the plantaris muscle the most undefined human skeletal muscle? *Anat Sci Int*. Nov 7 2020;doi:10.1007/s12565-020-00586-4

92. Harber MP, Konopka AR, Douglass MD, et al. Aerobic exercise training improves whole muscle and single myofiber size and function in older women. *Am J Physiol Regul Integr Comp Physiol*. Nov 2009;297(5):R1452-9. doi:10.1152/ajpregu.00354.2009

93. Harber MP, Konopka AR, Undem MK, et al. Aerobic exercise training induces skeletal muscle hypertrophy and age-dependent adaptations in myofiber function in young and older men. *J Appl Physiol (1985)*. Nov 2012;113(9):1495-504. doi:10.1152/japplphysiol.00786.2012

94. Izquierdo M, Ibañez J, K HA, Kraemer WJ, Larrión JL, Gorostiaga EM. Once weekly combined resistance and cardiovascular training in healthy older men. *Med Sci Sports Exerc*. Mar 2004;36(3):435-43. doi:10.1249/01.mss.0000117897.55226.9a

95. Ferrari R, Kruel LF, Cadore EL, et al. Efficiency of twice weekly concurrent training in trained elderly men. *Exp Gerontol*. Nov 2013;48(11):1236-42. doi:10.1016/j.exger.2013.07.016

96. Cadore EL, Pinto RS, Bottaro M, Izquierdo M. Strength and endurance training prescription in healthy and frail elderly. *Aging Dis*. Jun 2014;5(3):183-95. doi:10.14336/ad.2014.0500183

97. Murach KA, Mobley CB, Zdunek CJ, et al. Muscle memory: myonuclear accretion, maintenance, morphology, and miRNA levels with training and detraining in adult mice. *J Cachexia Sarcopenia Muscle*. Dec 2020;11(6):1705-1722. doi:10.1002/jcsm.12617

98. Konhilas JP, Widegren U, Allen DL, Paul AC, Cleary A, Leinwand LA. Loaded wheel running and muscle adaptation in the mouse. *Am J Physiol Heart Circ Physiol*. Jul 2005;289(1):H455-65. doi:10.1152/ajpheart.00085.2005

99. Soffe Z, Radley-Crabb HG, McMahon C, Grounds MD, Shavlakadze T. Effects of loaded voluntary wheel exercise on performance and muscle hypertrophy in young and old male C57Bl/6J mice. *Scand J Med Sci Sports*. Feb 2016;26(2):172-88. doi:10.1111/sms.12416

100. Jang YC, Sinha M, Cerletti M, Dall'Osso C, Wagers AJ. Skeletal muscle stem cells: effects of aging and metabolism on muscle regenerative function. *Cold Spring Harb Symp Quant Biol*. 2011;76:101-11. doi:10.1101/sqb.2011.76.010652

101. Moro T, Brightwell CR, Volpi E, Rasmussen BB, Fry CS. Resistance exercise training promotes fiber type-specific myonuclear adaptations in older adults. *J Appl Physiol (1985)*. Apr 1 2020;128(4):795-804. doi:10.1152/japplphysiol.00723.2019

102. Wang H, Listrat A, Meunier B, et al. Apoptosis in capillary endothelial cells in ageing skeletal muscle. *Aging Cell*. Apr 2014;13(2):254-62. doi:10.1111/acel.12169

103. Gavin TP, Kraus RM, Carrithers JA, Garry JP, Hickner RC. Aging and the Skeletal Muscle Angiogenic Response to Exercise in Women. *J Gerontol A Biol Sci Med Sci*. Oct 2015;70(10):1189-97. doi:10.1093/gerona/glu138

104. Prior SJ, Blumenthal JB, Katzel LI, Goldberg AP, Ryan AS. Increased skeletal muscle capillarization after aerobic exercise training and weight loss improves insulin sensitivity in adults with IGT. *Diabetes Care*. May 2014;37(5):1469-75. doi:10.2337/dc13-2358

105. Murach KA, Bagley JR. Skeletal Muscle Hypertrophy with Concurrent Exercise Training: Contrary Evidence for an Interference Effect. *Sports Med*. 2016:1029-39. vol. 8.

106. Hendrickse PW, Krusnauskas R, Hodson-Tole E, Venckunas T, Degens H. Endurance exercise plus overload induces fatigue resistance and similar hypertrophy in mice irrespective of muscle mass. *Exp Physiol*. Nov 2 2020;doi:10.1113/ep089096

107. Shirai T, Obara T, Takemasa T. Effect of endurance exercise duration on muscle hypertrophy induced by functional overload. *FEBS Open Bio*. Nov 6 2020;doi:10.1002/2211-5463.13028

108. Neelakantan H, Brightwell CR, Graber TG, et al. Small molecule nicotinamide N-methyltransferase inhibitor activates senescent muscle stem cells and improves regenerative capacity of aged skeletal muscle. *Biochem Pharmacol*. May 2019;163:481-492. doi:10.1016/j.bcp.2019.02.008

109. Health, United States, 2014: With special feature on adults aged 55–64. (US Government Printing Office) 1-473 (2015).

110. Abe T, Thiebaud RS, Loenneke JP. Age-related change in handgrip strength in men and women: is muscle quality a contributing factor? *Age (Dordr)*. Feb 2016;38(1):28. doi:10.1007/s11357-016-9891-4

111. Cawthon PM, Fox KM, Gandra SR, et al. Do muscle mass, muscle density, strength, and physical function similarly influence risk of hospitalization in older adults? *J Am Geriatr Soc*. Aug 2009;57(8):1411-9. doi:10.1111/j.1532-5415.2009.02366.x

112. Studenski SA, Peters KW, Alley DE, et al. The FNIH sarcopenia project: Rationale, study description, conference recommendations, and final estimates. *J Gerontol A Biol Sci Med Sci*. 2014;69:547-558.

113. Burns ER, Stevens JA, Lee R. The direct costs of fatal and non-fatal falls among older adults - United States. *J Safety Res*. Sep 2016;58:99-103. doi:10.1016/j.jsr.2016.05.001

114. Newman AB, Kupelian V, Visser M, et al. Strength, but not muscle mass, is associated with mortality in the health, aging and body composition study cohort. *J Gerontol A Biol Sci Med Sci*. Jan 2006;61(1):72-7.

115. Shadrach JL, Wagers AJ. Stem cells for skeletal muscle repair. *Philos Trans R Soc Lond B Biol Sci*. Aug 12 2011;366(1575):2297-306. doi:10.1098/rstb.2011.0027

116. Cosgrove BD, Gilbert PM, Porpiglia E, et al. Rejuvenation of the muscle stem cell population restores strength to injured aged muscles. *Nat Med*. Mar 2014;20(3):255-64. doi:10.1038/nm.3464

117. Goody MF, Henry CA. A need for NAD+ in muscle development, homeostasis, and aging. *Skelet Muscle*. Mar 7 2018;8(1):9. doi:10.1186/s13395-018-0154-1

118. Canto C, Menzies KJ, Auwerx J. NAD(+) metabolism and the control of energy homeostasis: A balancing act between mitochondria and the nucleus. *Cell Metab*. Jul 07 2015;22(1):31-53. doi:10.1016/j.cmet.2015.05.023

119. Braidy N, Guillemin GJ, Mansour H, Chan-Ling T, Poljak A, Grant R. Age related changes in NAD+ metabolism oxidative stress and Sirt1 activity in wistar rats. *PLoS One*. Apr 26 2011;6(4):e19194. doi:10.1371/journal.pone.0019194

120. Gomes AP, Price NL, Ling AJ, et al. Declining NAD(+) induces a pseudohypoxic state disrupting nuclear-mitochondrial communication during aging. *Cell*. Dec 19 2013;155(7):1624-38. doi:10.1016/j.cell.2013.11.037

121. Prolla TA, Denu JM. NAD+ deficiency in age-related mitochondrial dysfunction. *Cell Metab*. Feb 4 2014;19(2):178-80. doi:10.1016/j.cmet.2014.01.005

122. Frederick DW, Loro E, Liu L, et al. Loss of NAD homeostasis leads to progressive and reversible degeneration of skeletal muscle. *Cell Metab* 2016;24:269-282.

123. Fang EF, Lautrup S, Hou Y, et al. NAD(+) in aging: Molecular mechanisms and translational implications. *Trends Mol Med*. Oct 2017;23(10):899-916. doi:10.1016/j.molmed.2017.08.001

124. Pissios P. Nicotinamide N-methyltransferase: More than a vitamin B3 clearance enzyme. *Trends Endocrinol Metab*. May 2017;28(5):340-353. doi:10.1016/j.tem.2017.02.004

125. Kim HC, Mofarrahi M, Vassilakopoulos T, et al. Expression and functional significance of nicotinamide N-methyl transferase in skeletal muscles of patients with chronic obstructive pulmonary disease. *Am J Respir Crit Care Med*. Apr 15 2010;181(8):797-805. doi:10.1164/rccm.200906-0936OC

126. Rudolphi B, Zapp B, Kraus NA, Ehebauer F, Kraus BJ, Kraus D. Body weight predicts nicotinamide N-methyltransferase activity in mouse fat. *Endocr Res*. Oct 16 2017:1-9. doi:10.1080/07435800.2017.1381972

127. Kraus D, Yang Q, Kong D, et al. Nicotinamide N-methyltransferase knockdown protects against diet-induced obesity. *Nature*. Apr 10 2014;508(7495):258-62.

128. Neelakantan H, Vance V, Wetzel M, et al. Selective and membrane permeable small molecule inhibitor of nicotinamide N-methyltransferase reverses diet-induced obesity in mice. *Biochemical Pharmacology*. 2018;147:141-152. doi:10.1016/j.bcp.2017.11.007

129. Neelakantan H, Wang HY, Vance V, Hommel JD, McHardy SF, Watowich SJ. Structure-activity relationship for small molecule inhibitors of nicotinamide N-methyltransferase. *J Med Chem*. Jun 22 2017;60(12):5015-5028. doi:10.1021/acs.jmedchem.7b00389

130. Iyer SR, Valencia AP, Hernandez-Ochoa EO, Lovering RM. In vivo assessment of muscle contractility in animal studies. *Methods Mol Biol*. 2016;1460:293-307. doi:10.1007/978-1-4939-3810-0_20

131. Call JA, Eckhoff MD, Baltgalvis KA, Warren GL, Lowe DA. Adaptive strength gains in dystrophic muscle exposed to repeated bouts of eccentric contraction. *J Appl Physiol (1985)*. Dec 2011;111(6):1768-77. doi:10.1152/japplphysiol.00942.2011

132. Erratum to "A Guideline of Selecting and Reporting Intraclass Correlation Coefficients for Reliability Research" [J Chiropr Med 2016;15(2):155-163]. *J Chiropr Med*. Dec 2017;16(4):346. doi:10.1016/j.jcm.2017.10.001

133. Koo TK, Li MY. A Guideline of Selecting and Reporting Intraclass Correlation Coefficients for Reliability Research. *J Chiropr Med*. Jun 2016;15(2):155-63. doi:10.1016/j.jcm.2016.02.012

134. Choi JY, Hwang CY, Lee B, et al. Age-associated repression of type 1 inositol 1, 4, 5-triphosphate receptor impairs muscle regeneration. *Aging (Albany NY)*. Sep 21 2016;8(9):2062-2080. doi:10.18632/aging.101039

135. Cousin W, Ho ML, Desai R, et al. Regenerative capacity of old muscle stem cells declines without significant accumulation of DNA damage. *PLoS One*. 2013;8(5):e63528. doi:10.1371/journal.pone.0063528

136. Ryall JG. Metabolic reprogramming as a novel regulator of skeletal muscle development and regeneration. *Febs j*. Sep 2013;280(17):4004-13. doi:10.1111/febs.12189

137. Repele A, Lupi R, Eaton S, Urbani L, De Coppi P, Campanella M. Cell metabolism sets the differences between subpopulations of satellite cells (SCs). *BMC Cell Biol*. May 3 2013;14:24. doi:10.1186/1471-2121-14-24

138. Christov C, Chretien F, Abou-Khalil R, et al. Muscle satellite cells and endothelial cells: close neighbors and privileged partners. *Mol Biol Cell*. Apr 2007;18(4):1397-409. doi:10.1091/mbc.e06-08-0693

139. Nederveen JP, Joanisse S, Snijders T, Thomas ACQ, Kumbhare D, Parise G. The influence of capillarization on satellite cell pool expansion and activation following

exercise-induced muscle damage in healthy young men. *J Physiol*. Mar 15 2018;596(6):1063-1078. doi:10.1113/jp275155

140. Verma M, Asakura Y, Murakonda BSR, et al. Muscle Satellite Cell Cross-Talk with a Vascular Niche Maintains Quiescence via VEGF and Notch Signaling. *Cell Stem Cell*. Oct 4 2018;23(4):530-543.e9. doi:10.1016/j.stem.2018.09.007

Vita

NAME: Camille Brightwell

PRESENT POSITION: PhD Candidate/Graduate Research Assistant
Cell Biology Graduate Program
University of Texas Medical Branch/University of Kentucky

CONTACT INFORMATION: Email: Camille.brightwell@uky.edu
Phone: 979-900-6171

EDUCATION: 2016, M.S. University of Houston- Clear Lake. Exercise and Health Sciences.
2011, B.S. Texas A&M University- Corpus Christi. Kinesiology- Exercise Science.

RESEARCH INTERESTS: Skeletal muscle and exercise physiology; Cellular mechanisms of skeletal muscle remodeling in exercise and injury

PUBLICATIONS IN PEER-REVIEWED JOURNALS:

1. Finnerty CC, McKenna CF, Cambias LA, Brightwell CR., Prasai A, Wang Y, El Ayadi A, Herndon DN, Suman OE and Fry CS. Inducible satellite cell depletion attenuates skeletal muscle regrowth following a scald-burn injury. Journal of Physiology. 2017. doi: 10.1113/JP274841.

2. Graber TG, Rawls BL, Tian B, Durham WJ, Brightwell CR, Brasier AR, Rasmussen BB, Fry CS. Repetitive TLR3 activation in the lung induces skeletal muscle adaptations and cachexia. Experimental Gerontology. 2018. doi: 10.1016/j.exger.2018.02.002.

3. Moro T, Brightwell CR, Deer RR, Graber TG, Galvan E, Fry CS, Volpi E, Rasmussen BB. Muscle Protein Anabolic Resistance to Essential Amino Acids Does Not Occur in Healthy Older Adults Before or After Resistance Exercise Training. Journal of Nutrition. 2018. doi: 10.1093/jn/nxy064.

4. Abramowitz M, Paredes W, Zhang K, Brightwell CR, Newsom J, Kwon H, Custodio M, Buttar R, Farooq H, Zaidi B, Pai R, Pessin J, Hawkins M, Fry CS. Skeletal muscle fibrosis is associated with decreased muscle inflammation and weakness in patients with chronic kidney disease. American Journal of Physiology- Renal Physiology. 2018. doi: 10.1152/ajprenal.00314.2018.

5. Graber TG, Fry CS, Brightwell CR, Moro T, Maroto R, Bhattari N, Porter C, Wakamiya M, Rasmussen BB. Skeletal Muscle Specific Knockout of DEP Domain-Containing 5 Increases mTORC1 Signaling, Muscle Cell Hypertrophy, and Mitochondrial Respiration. Journal of Biological Chemistry. 2019. doi: 10.1074/jbc.RA118.005970.

6. Neelakantan H*, Brightwell CR*, Graber TG, Maroto R, Wang HL, McHardy SF, Papaconstantinou J, Fry CS, Watowich SJ. Small molecule nicotinamide N-methyltransferase inhibitor activates senescent muscle stem cells and improves regenerative capacity of aged skeletal muscle. Biochemical Pharmacology. 2019. doi: 10.1016/j.bcp.2019.02.008.

7. *Co-first authors.

8. D'Lugos A, Fry CS, Ormsby J, Sweeney K, Brightwell CR, Hale T, Gonzales R, Angadi S, Carroll C, Dickinson J. Chronic doxorubicin administration impacts satellite cell and capillary abundance in a muscle-specific manner. Physiological Reports. 2019. doi: 10.14814/phy2.14052.

9. Peck BD, Brightwell CR, Johnson DL, Ireland ML, Noehren B, Fry CS. Anterior Cruciate Ligament Tear Promotes Skeletal Muscle Myostatin Expression, Fibrogenic Cell Expansion, and a Decline in Muscle Quality. American Journal of Sports Medicine. 2019. doi: 10.1177/0363546519832864.

10. Moro T, Brightwell CR, Velarde B, Fry CS, Nakayama K, Sanbongi C, Volpi E, Rasmussen BB. Whey Protein Hydrolysate Increases Amino Acid Uptake, mTORC1 Signaling, and Protein Synthesis in Skeletal Muscle of Healthy Young Men in a Randomized Crossover Trial. Journal of Nutrition. 2019. doi: 10.1093/jn/nxz053.

11. Brightwell CR, Markofski MM, Moro T, Fry CS, Porter C, Volpi E, Rasmussen BB. Moderate Intensity Aerobic Exercise Improves Skeletal Muscle Quality in Older Adults. Translational Sports Medicine. 2019. doi.org/10.1002/tsm2.70.

12. Moro T, Brightwell CR, Phalen D, McKenna CF, Lane S, Porter C, Volpi E, Rasmussen BB, Fry CS. Low skeletal muscle capillarization limits muscle adaptation to resistance exercise training in older adults. Experimental Gerontology. 2019. doi: 10.1016/j.exger.2019.110723.

13. Moro T, Brightwell CR, Volpi E, Rasmussen BB, Fry CS. Resistance exercise training promotes fiber type-specific myonuclear adaptions in older adults. Journal of Applied Physiology. 2020. doi: 10.1152/japplphysiol.00723.2019.

14. Brightwell CR, Hanson ME, El Ayadi A, Prasai A, Wang Y, Finnerty CC, Fry CS. Thermal injury initiates pervasive fibrogenesis in skeletal muscle. American Journal of Physiology- Cell Physiology. 2019. doi: 10.1152/ajpcell.00337.2019.

15. Graber TG, Maroto R, Fry CS, Brightwell CR, Rasmussen BB. Measuring Exercise Capacity and Physical Function in Adult and Older Mice. The Journals of Gerontology. Series A, Biological Sciences and Medical Sciences. 2020. doi: 10.1093/gerona/glaa205.

16. Mikovic J, Brightwell CR, Lindsay A, Wen Y, Kowalski G, Russell AP, Fry CS, Lamon S. An obesogenic maternal environment impairs growth patterns, satellite cell activation and markers of post-natal myogenesis. American Journal of Physiology- Endocrinology and Metabolism. 2020. doi: 10.1152/ajpendo.00398.2020.

17. Englund DA, Figueiredo VC, Dungan CM, Murach KA, Peck BD, Petrosino JM, Brightwell CR, Dupont AM, Neal AC, Fry CS, Accornero F, McCarthy JJ, Peterson CA. Satellite cell depletion disrupts transcriptional coordination and muscle adaptation to exercise. Function. 2020. https://doi.org/10.1093/function/zqaa033.

PUBLICATIONS- SUBMITED/IN PEER REVIEW:

1. Brightwell CR, Graber TG, Brightwell BD, Borkowski M, Noehren B, Fry CS. In vivo measurement of knee extensor muscle function in mice. Journal of Visualized Experiments.

2. Murach KA, Peck BD, Policastro RA, Vechetti IJ, Van Pelt DW, Dungan CM, Denes LT, Fu X, Brightwell CR, Zentner GE, Dupont-Versteegden EE, Richards CI, Wang ET, Smith JJ, Fry CS, McCarthy JJ, Peterson CA. Early satellite cell communication creates a permissive environment for long-term hypertrophic growth. Cell Reports.

ABSTRACTS/POSTER/PODIUM PRESENTATIONS:

1. Brightwell CR, Graber TG, Maroto R, Noehren B, Fry CS. Myostatin mediates quadriceps muscle atrophy and fibrosis rapidly after ACL transection in novel murine model. American College of Sports Medicine Annual Meeting, 2020. (published abstract)

2. Brightwell CR, Neelakantan H, Graber TG, Maroto R, Wang HL, McHardy SF, Papaconstantinou J, Fry CS, Watowich SJ. Small molecule Nicotinamide N-methyltransferase inhibitor enhances satellite cell dynamics and plasticity of aging skeletal muscle. 6th Annual Cell Biology Student Symposium, 2019. (poster)

3. Brightwell CR, Neelakantan H, Graber TG, Maroto R, Wang HL, McHardy SF, Papaconstantinou J, Fry CS, Watowich SJ. Small molecule Nicotinamide N-

methyltransferase inhibitor enhances satellite cell dynamics and plasticity of aging skeletal muscle. Muscle Biology Conference, 2019. (poster)

4. Brightwell CR, Neelakantan H, Graber TG, Faaitiiti K, Ferris C, Watowich SJ, Fry CS. A novel inhibitor promotes satellite cell activity and enhances regeneration of aging skeletal muscle after injury. 22nd Annual Forum on Aging, 2018. (poster)

5. Brightwell CR, Markofski MM, Moro T, Fry CS, Volpi E, Rasmussen BB. Aerobic Exercise Training Improves Myofibrillar Protein Synthesis, Capillarization, and Muscle Quality in Older Adults. American College of Sports Medicine Annual Meeting, 2018. (thematic poster and published abstract)

6. Brightwell CR, Markofski MM, Moro T, Fry CS, Volpi E, Rasmussen BB. Aerobic Exercise Training Improves Myofibrillar Protein Synthesis, Capillarization, and Muscle Quality in Older Adults. 5th Annual Cell Biology Student Symposium, 2018. (poster)

7. Brightwell CR, Moro T, Fry CS, Volpi E, Rasmussen BB. Moderate Intensity Aerobic Exercise Training Improves Myofibrillar Protein Synthesis, Capillarization, and Quadriceps Strength in Older Adults. 21st Annual Forum on Aging, 2017. (poster)

8. Brightwell CR, Karmarkar A. Diabetes Is Associated with Lower Limb Strength Decline in Hispanic Older Adults. 21st Annual Forum on Aging, 2017. (poster)

9. Brightwell CR, Karmarkar A. Diabetes Is Associated with Lower Limb Strength Decline in Hispanic Older Adults. American Congress of Rehabilitation Medicine 2017 Annual Congress. (podium presentation)

10. Brightwell CR, Brightwell BD, McDonald G, Amonette WE. Comparison of Vertical Jump Scores Measured Using Center of Mass Displacement and Jump Height with Different Standing Reach Techniques. National Strength and Conditioning Association National Conference, 2016. (poster and published abstract)

AWARDS:

Doctoral Student Research Grant. American College of Sports Medicine. $5000. "Anterior cruciate ligament injury stimulates cytokine activation and morphological maladaptations in patellar tendon", 2020.

Sigma Xi Award- Overall Best Presentation. 6th Annual Cell Biology Student Symposium, April 2019.

First Place- Poster Session: Frontiers in Cell Biology. 6th Annual Cell Biology Student Symposium, April 2019.

Outstanding Leadership: Society of Cell Biology. 6th Annual Cell Biology Student Symposium, April 2019.

Leadership Award- Graduate School of Biomedical Sciences. University of Texas Medical Branch Student Government Association, January 2019.

Sigma Xi Award- Overall Best Presentation. 5th Annual Cell Biology Student Symposium, May 2018.

First Place- Poster Session: Frontiers in Cell Biology. 5th Annual Cell Biology Student Symposium, May 2018.

Gail E. Butterfield Nutrition Travel Award. 2018 American College of Sports Medicine Annual Meeting, June 2018.

Excellence in Student Research- Clinical Physiology Research/Clinical Trial. Sealy Center on Aging, 21st Annual Forum on Aging, October 2017.

Excellence in Student Research- Rehabilitation Sciences Research. Sealy Center on Aging, 21st Annual Forum on Aging, October 2017.

Category 3 Travel Award for Secondary Data Analysis of Archived Studies. Center for Large Data Research and Data Sharing in Rehabilitation, August 2017.

CERTIFICATIONS:

2011-Current	Certified Strength and Conditioning Specialist, National Strength and Conditioning Association

LEADERSHIP & MEMBERSHIPS:

2018-2019	Vice President, Society of Cell Biology at University of Texas Medical Branch
2018-Current	Member, Sigma Xi
2017-Current	Member, American College of Sports Medicine

PROFESSIONAL EXPERIENCE: (academic, non-academic)

5/2016-12/2016	Muscle Research Exercise Trainer and Muscle Biology Lab Intern, University of Texas Medical Branch, Department of Nutrition and Metabolism
10/2013-12/2016	Certified Strength and Conditioning Specialist, Urban Health and Fitness, Galveston, Texas
8/2013-5/2014	Muscle Research Exercise Trainer, University of Texas Medical Branch, Department of Nutrition and Metabolism
11/2011-5/2013	Clinical Exercise Physiologist, Christus Spohn Cardiac Rehabilitation, Corpus Christi, Texas